NTNU

Norwegian University of
Science and Technology

Polyethyleneimine-coated magnetic iron oxide nanoparticles for improvement of flow assurance

Regina Lopez Fyllingsnes

Chemical Engineering and Biotechnology
Submission date: October 2017
Supervisor: Johan Sjöblom, IKP
Co-supervisor: Galina Rodionova, IKP

Norwegian University of Science and Technology
Department of Chemical Engineering

Preface

The objective of this thesis has been provided by my main supervisor Professor Johan Sjöblom. The research has been carried out at the Ugelstad Laboratory at Department of Chemical Engineering at the Norwegian University of Science and Technology as part of fulfilling the five-year-master's degree program in Chemical Engineering and Biotechnology. The literature review related to the thesis was mainly done during the autumn of 2016 under the supervision of the initial co-supervisor Dr. Galina Rodionova. The experimental work has been conducted during the spring and summer of 2017, supervised by Sebastien Simon.

The report has been written in LaTex where the figures drawn have been created in Tikz and converted to png format using Ktikz.

I declare that this is an independent work in consistency with the exam regulations of the Norwegian University of Science and Technology (NTNU).

Trondheim, October 23, 2017

Regina Lopez Fyllingsnes

Abstract

This thesis aims to gain further insight into how the naphthenic acids (NA), which cause different problems with respect to flow assurance, can be removed from the water phase. The main objective has been to test how effective the polyethyleneimine functionalized magnetic iron oxide nanoparticles are to remove phenylacetic acid, which functioned as model naphthenic acid from water.

The first part of the experimental work was concerned with the adsorption of polyethyleneimine onto the nanoparticle surface. The zeta potentials as function of pH were determined for both the iron oxide nanoparticles and the polymer. From superimposing the isoelectric points for both synthesised and purchased iron oxide nanoparticles and comparing them to the zeta potentials for polyethyleneimine, pH 8 was chosen.

Since the confidence for the true mean of the zeta potential was low for the functionalized iron (II, III) oxide core, using shaking overnight, the functionalization was done again with iron (III) oxide as core. In a new approach the polyethyleneimine was added to the supernatant of iron (III) oxide after centrifugation followed by sonication.

The new functionalized nanoparticles gave a high confidence for the zeta potentials and were attracted to an external magnetic field. The specific surface area for the functionalized iron (III) oxide nanoparticles was

determined to be 62.5 ± 0.2 with 95% confidence, using gas adsorption. The composition with respect to mass was determined to be 6 wt% from running a thermogravimetric analysis. Hence, the surface excess of polyethyleneimine was calculated to be 0.9 mg/m^2.

In the second part of the experiments, test adsorptions of the model acid were conducted using the polyethyleneimine coated iron (III) oxide nanoparticles. At pH 8 the adsorption of the phenylacetic acid was negligible. A new calibration curve was made at pH 4.5. Two different values for the surface excess were obtained. When concentration of the bulk acid prior to the adsorption was estimated from the calibration curve, the surface excess was calculated to be 0.16 mg/m^2, whereas 0.28 mg/m^2 was procured using the value from the balance.

Since previous research has indicated that the chain length of the polymer determines the adsorption and the surface excess is independent of the chain length, it was concluded to continue using polyethyleneimine in the functionalization of iron (III) oxide, but with a lower average molecular weight.

Sammendrag

Hensikten med denne masteroppgaven har vært å skaffe et bedre innblikk i hvordan naftenske syrer (NA), som forårsaker ulike problemer med hensyn til drift av anlegg, kan fjernes fra vannfasen. Hovedmålet har vært å sjekke hvor effektive polyethyleneimine-funksjonaliserte magnetiske jernoksid nanopartikler er til å fjerne 2-fenyl-etan syre (PAA), som fungerte som modellsyre, fra vann.

I den første delen av det eksperimentelle arbeidet skulle polyethyleneimine bli adsorbert på overflaten av nanopartiklene. Zetapotensialene som funksjon av pH ble bestemt for både nanopartiklene og polymeren for å kunne finne en optimal pH for adsorpsjonen.

Ved å sammenligne det isoelektriske punktet for både de syntetiserte og de kjøpte nanopartiklene, samt ved å bruke zetapotensialene for polyethyleneimine, ble pH 8 bestemt.

På grunn av lav tillitt til zetapotensialene for de polyethyleneimine-funksjonaliserte jern (II, III) oksid partiklene, som hadde vært ristet over natten, ble funksjonaliseringen gjort igjen med jern (III) oksid som kjerne.

En ny fremgangsmåte ble brukt hvor polyethyleneimine tilsatt supernatanten etter å ha sentrifugert de dispergerte nanopartiklene. For å adsorbere polymeren ble sonikering brukt som metode.

De nye funsjonaliserte nanopartiklene gav høy tillitt til zetapotensia-

lene, og de ble tiltrukket et ytre magnetisk felt. Det spesifikke overflatearealet for de funksjonaliserte jern (III) oksid nanopartiklene ble bestemt ved gassadsorpsjon til å være 62.5 ± 0.2 med 95% sikkerhet. Sammensetningen med hensyn til masse ble estimert til å være 6 wt% ved termogravimetrisk analyse. Følgelig ble surface excess beregnet til å være 0.9 mg/m^2.

I den andre delen av eksperimentene ble det gjort forsøk på å adsorbere modellsyren ved å bruke det polyethyleneimine-funksjonaliserte jern (III) oksid nanopartiklene. For pH 8 vas adsorpsjonen ubetydelig.

En ny kalibreringskurve ble laget ved pH 4.5. To ulike verdier for surface excess ble beregnet. Ved å bruke kalibreringskurven til å finne konsentrasjonen til modellsyren før adsorpsjon, ble surface excess regnet ut til å være 0.16 mg/m^2. Derimot ved å bruke konsentrasjonsverdien fra vekten, ble resultatet 0.28 mg/m^2.

Siden tidligere forskning har indikert at det er lengden på polymeren som bestemmer adsorpsjonen, og siden surface excess er uavhengig av kjedelengden, ble det konkludert å forsette med å bruke polyethyleneimine til å funksjonalisere jern (III) oksid, men med en lavere gjennomsnittlig molarmasse.

Abbreviations

API	=	American Petroleum Institute
BET	=	Brunauer-Emmett-Teller
CaNA	=	Calcium naphthenate
CMC	=	Critical Micelle Concentration
CPP	=	Critical Packing Parameter
DVM	=	Digital Video Microscope
EBA	=	4-ethylbenzoic acid
FABS	=	Fast Atom Bombardment Spectrometry
Fe_2O_3/PEI	=	Polyethyleneimine coated iron (III) oxide
Fe_3O_4/PEI	=	Polyethyleneimine coated iron (II, III) oxide
HSE	=	Health, Environment and Safety
MNP	=	Magnetic Nanoparticles
MQ	=	Milli-Q water
NA	=	Naphthenic Acids
PAA	=	Phenylacetic acid
PEI	=	Polyethyleneimine
TAN	=	Total Acid Number
TGA	=	Thermogravimetric Analysis
TLC	=	Thin-Layer-Chromatography
UV	=	Ultra Violet

vdW	=	van der Waal
VPO	=	Vapour Pressure Osmometry
WAT	=	Wax Appearance Temperature

List of Symbols

In the case of one symbol having two separate meanings, black is used the first time and either red or blue when related to magnetism or statistics.

T	=	Temperature
S	=	Entropy
G	=	Gibbs free energy
H	=	Enthalpy
Ω	=	Number of conformations
S	=	Amphiphatic species
S_n	=	Micelle
n	=	Degree of aggregation
V_t	=	Volume of the hydrophobic chain of the surfactant
a_h	=	Optimal area of the hydrophilic head of the surfactant
$l_{c,t}$	=	Length of the hydrophobic chain of the surfactant
κ	=	Debye-H ückel parameter
N_{A}	=	Avogadro constant
ϵ	=	Permittivity
k_{B}=k	=	Boltzmann constant
e	=	Charge of electron
z	=	Valence number of ions
M	=	Molar concentration
m	=	Magnetic moment
θ	=	Angle

H	=	External magnetic field
p	=	Strength of a magnetic pole
l	=	Length of separating two magnetic poles
F	=	Force
T_{B}	=	Blocking temperature
K_{eff}	=	Anistropy constant
E	=	Energy
E_{e}x	=	Energy of exchange
E_{m}s	=	Magnetostatic energy
E_{k}	=	Anistropy energy
E_{z}	=	Zeeman energy
W_{Az}	=	Molar flux of A
D_{AB}	=	Diffusivity of A in B
$\tilde{k_c}$	=	Local mass-transfer coefficient
p_0	=	Saturation pressure
m	=	Mass
Mm	=	Molar mass
$\bar{x}$	=	Mean
s	=	Sample standard deviation
σ	=	Standard deviation for parallels
n	=	Number of measurements
m	=	Number of samples
θ	=	Surface coverage
c	=	Concentration
p	=	Pressure

k_{ads}	=	Adsorption rate constant
k_{des}	=	Desorption rate constant
ε	=	Energy of adsorption
ε_v	=	Energy of vaporization
V_{m}	=	Volume of gas adsorbed, monolayer
D	=	Diffusion coefficient
η	=	Solvent viscosity
R_h	=	Hydrodynamic radius
ζ	=	Zeta potential
A	=	Absorbance
I_0	=	Intensity of the reference beam
I	=	Transmitted intensity
q_e	=	Equilibrium concentration of adsorbate adsorbed
c_0	=	Initial concentration of adsorbate
c_e	=	Equilibrium concentration of the adsorbate in solution
Γ	=	Surface excess
A_{sp}	=	Specific surface area
σ^0	=	Radius of a sphere
δ	=	Area or surface occupied per molecule
Rs	=	Thickness of the diffusional film
ρ	=	Density
$\mathrm{M_x}$	=	Molecular weight of a molecule, degree of polymerisation x
$\mathrm{N_x}$	=	Number of chains with repeating units

Table of Contents

Chapter 1

Introduction

There are different problems related to the occurence of naphthenic acids in the crude oil, such as the formation of calcium naphthenate deposits caused by ARN acids and corrosion in the refinery plant as well as affecting the health of mammals. A continued research is of interest in order to gain further insight into the handling of these acids.

The main objective of this thesis has been to test how effective the polyethyleneimine coated magnetic iron oxide nanoparticles are to remove the model naphthenic acid from the water phase. Hence, the adsorption of polyethyleneimine onto the nanoparticle surface and the amount of adsorption sites are important.

Chapter 2

Theoretical Background

Crude oil

Crude oil is a complex mixture of hydrocarbons with the presence of impurities such as metals and salt in addition to the heteroatoms: oxygen, nitrogen and sulphur. The main components consist of both linear and branched alkanes (paraffins), cycloalkanes and aromatics. As the amount of polycyclic aromatic compounds increases, the crude oil becomes heavier or dense. This composition depends upon the geographic origin of the crude. Even within a well the composition may be different with respect to the depth of the well.

Of the mentioned heteroatoms, sulphur, has to be removed as it causes corrosion and poisons catalysts as well as being harmful for the environment. Nitrogen also has to be dealt with as it can influence catalytic processes. The metals, even though they are present in trace amounts, can deposit on catalysts and hence deactivate them. [pp. 25-27] [1]

Initially both desalting and dehydration take place. Then both atmospheric and vacuum distillation are performed as part of the initial treatment process, where the separation is done based on the volatility of the compounds, before further thermal or catalytic processing. The atmospheric distillation plant has its limitations since hydrocarbons, if heated above approximately 630 K (357 °C), can suffer thermal decomposition. As result a carbonaceous material known as coke can deposit on the tube walls. The vacuum distillation is then needed in order to treat the residue from the atmospheric distillation plant. The tendency of the formation of coke can be reduced by removing large aromatic compounds, which can be done by using extraction where propane is recycled. These compounds, also known as asphaltenes, are soluble in propane, but not in pentane. [pp. 42-45] [1]

The classification of the crude oil can be based on the content of sulphur, naphthenes, aromatics and paraffins in addition to the density measured in the American Petroleum Institute (API) gravity scale. For instance a sweet crude oil has a content of sulphur of 0.5 percent or less [2][1]. For a crude oil to be regarded as acidic, the total acid number (TAN) has to exceed 0.5 mg of potassium hydroxide (KOH) per gram of crude oil by titration, where the base neutralises the acidic components [p. 4177] [3].

Another classification, which is based on the solubility of the molecules or their polarity, indicates the components of the crude oil as: saturates, asphaltenes, resins and aromatics or in other words SARA. The saturated fraction consists of the nonpolar hydrocarbons (linear and branched alkanes as well as cycloalkanes), the aromatics are polarisable due to the pres-

[1] No date given. Online access the 10th of January

ence of at least one aromatic ring and the two last fractions contain polar substituents (heteroatom). The resins are miscible with pentane, whereas asphaltenes are not as previously mentioned. [p.1] [4]

Wax consists of long chain paraffins that occur as natural components of crude oil, thus belonging to the saturates. London van der Waal (vdW) forces, also known as dispersion forces, are always present between molecules as neither permanent polarity nor induced polarity is necessary for affinity to occur. These forces are always attractive and the particles will bind to each other [p. 464] [5].

This affinity causes a volume-spanning network of crystals, which entraps the liquid oil phase and forms a gel as depicted in figure 2.1:

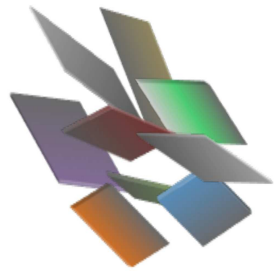

Figure 2.1: Physical gel

Wax does not only cause deposition on the inside wall of a pipeline and rheological gelling during shut-in below wax appearance temperature (WAT) [pp. 2-9] [6], but can form stable emulsions in the presence of asphaltenes [p.7] [7]. However, [8] found that neither the asphaltenes nor the naphthenic acids affect WAT [p. 352].

Naphthenic acids chemistry

Naphthenic acids (NA) define a complex mix of different organic acids present in the crude oil, with the general formula, RCOOH, where the R depicts any cycloaliphatic[2] structure. These acids occur naturally in crude oils and vary both with respect to structure and molecular weight.

Experimental work done by [9] using Fast Atom Bombardment Spectrometry (FABS) shows that the carbon number for NA ranges from C_{10} to C_{50}, which varies depending upon the feedstock [pp. 373-375]. It is pointed out by [10], that both naphthenic rings can fuse together as well as naphthenic and aromatic rings [pp. 183-185], although highly aromatic acids may not be very common [p.372] [9]. It is suggested in [8] that these acids may be regarded as a subfraction of the resins [p. 350].

To further add to the complexity of the NA, [11] found that the acids responsible for precipitation of calcium naphthenates (CaNA), which is further illustrated in section 2.3, do not contain only one carboxylic acid per molecule. Using vapour pressure osometry (VPO), the NA were determined to have four carboxylic groups separated by four or more CH_2-groups in addition to four to eight unsaturated rings in the hydrocarbon skeleton, however, not aromatics. This group of acids was named ARN acids. It was also discovered that the average molecular weight of the naphthenic acids from the CaNA deposits was higher than what TAN titration indicates. It was thus concluded that the TAN was not the correct indicator of a possible reaction between calcium ions and naphthenic acid ions. In

[2]Hydrocarbon chains with the presence of a ring structure

stead the content of ARN acids was deduced to be a better indicator.

A different way to depict the formula of NA is: $C_nH_{2n+z}O_2$, where z is the hydrogen deficiency[3] due to the ring formation. For a saturated aliphatic carboxylic acid, z=0. Possible structures of NA are shown in figure 2.2.

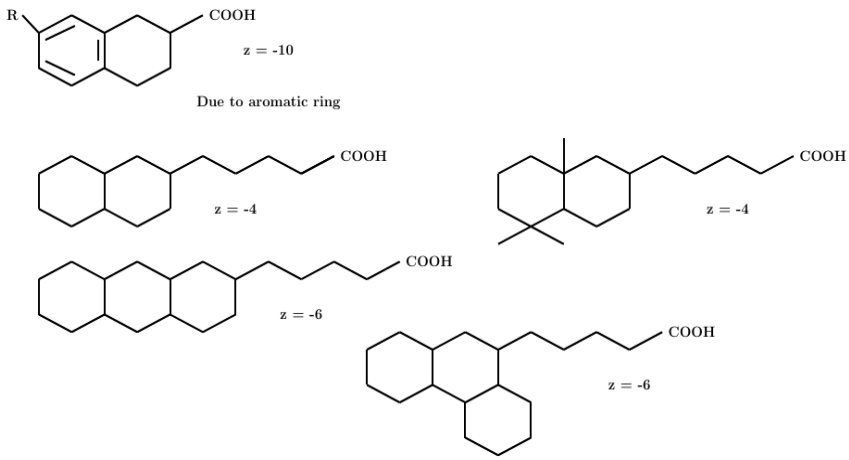

Figure 2.2: Proposed structures of naphthenic acids

The carboxyl group has an affinity for water, which gives the carboxylic acid an amphiphilic nature as the hydrocarbons have an affinity for the oil phase. The NA can in other words be regarded as surfactants, which indicates surface-active agents, as illustrated in figure 2.3:

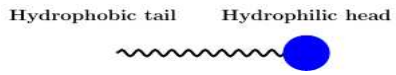

Figure 2.3: Surfactant

The attractive forces acting on the molecules at the interface, which is a layer of finite thickness between the two phases, are anistropic[4]. In

[3]Hydrogen atoms lost due to ring formation or the formation of double bonds

[4] The physical properties are different depending on the direction [12]

other words the net force for the water phase is then oriented towards the water bulk. The interfacial tension then arises from the water phase, which attempts to reduce its surface area [pp. 248-249] [5].

The distribution of the undissociated NA in the water and oil phase depends upon the size or the length of the hydrocarbon skeleton. As the system is dynamic this distribution can be represented according to equation (2.1), where the $[RCOOH]_w$ and the $[RCOOH]_o$ represent the water phase and the oil phase respectively .

$$[RCOOH]_w \rightleftarrows [RCOOH]_o \tag{2.1}$$

The interface can become negatively charged due to the dissociation of a proton from a carboxylic group as indicated in equation (2.2) [p. 502] [5]:

$$RCOOH + H_2O \rightleftarrows RCOO^- + H_3O^+ \tag{2.2}$$

Experimental work conducted by [13] found that the partition coefficient for the acids studied, defined in equation (2.3), generally decreases as the pH increases. This led to the conclusion that below a pH of 5, a significant quantity of the NA was dissolved in the oil phase, but as the pH increases more acids became dissolved in the water phase. An interpretation in other words, may be that the dissociation of an organic acid increases with the increasing pH (2.4).

The affinity for the water phase changes due to the charged functional group. However, not all naphthenic acids will be hydrated (dissolved). As a result the critical micelle concentration (CMC), which is further explained

in section 2.2.3, reduces with an increase in pH.

$$\mathrm{K} = \frac{[\mathrm{NA}]_{\mathrm{o}}}{[\mathrm{NA}]_{\mathrm{w}}} \tag{2.3}$$

$$\mathrm{pH} = -\log(\mathrm{H_3O^+}) \tag{2.4}$$

The negative surface excess will cause the interface to become a negatively charged electrical double layer, or in other words a negatively charged interface. The interfacial tension, which is a bulk property, is affected. The dissociated form of an amphiphilic molecule behaves like a bridge between the two phases, thus reducing the interfacial tension.

Formation of aggregates

Amphiphilic molecules have the ability to self-assembly and form different shaped aggregates, depending upon the volume of the hydrophobic part and the effective area occupied by the polar heads, which is affected by parameters such as pH and electrolyte concentration. The structure can be indicated by the critical packing parameter (CPP), which is determined from equation (2.5):

$$P = \frac{V_t}{a_h l_{c,t}} \tag{2.5}$$

where P denotes CPP, V_t indicates the volume of the hydrophobic chain, a_h is the optimal area of the hydrophilic head of the surfactant and $l_{c,t}$ represents the length of the chain. Spherical micelles are formed when P <1/3, whereas reverse micelles are obtained at P >1. [pp.367-371] [5]

Gibbs free energy, which is used to explain the formation of aggregates, has the symbol G and is procured from equation (2.6) where H is the enthalpy and S is the entropy. For a thermodynamically stable system, Gibbs free energy is reduced.

$$\Delta G = \Delta H - T\Delta S \tag{2.6}$$

The entropy is defined as the number of conformations[5] available, Ω as shown in equation (2.7) [p. 266] [14]. The constant k is the Boltzmann constant.

[5] Arrangements of the entire chain

$$S = klnΩ \tag{2.7}$$

Formation of micelles and reverse micelles

In the water phase the surfactants will self-assembly into micelles, which are often called association colloids [p. 11] [5]. The hydrophobic tails of the surfactants affect the entropy of the water as the number of configurations (arrangements) for the water molecules is reduced, the surfactants are forced to form a core where the polar heads point towards the water phase. This core forms a cavity in the water structure and hydrogen bonds are broken causing an enthalpic loss. However, as the water molecules in the vicinity of the micelle are capable of rearranging themselves and form hydrogen bonds, it is the entropy that primarily is affected and not the enthalpy [p. 375] [5].

The formation of reverse micelles is not caused by the hydrophobic effect, but the hydrogen bonds between the water molecules [p. 386] [5]. Thus the hydrophilic heads form a core to prevent contact with the oil. The solvation of the surfactants are optimised [p. 90] [15]. Even though there can be steric repulsion between the hydrophobic tails, Gibbs free energy (2.6) will be reduced.

Critical Micelle Concentration

The critical concentration at which micelles start to form is known as the critical micelle concentration (CMC). Above this concentration, further surfactants will contribute to the formation of more micelles. There are different factors that have an impact on the CMC, such as the presence of electrolytes, the valency of counterions and the hydrophobic skeleton size. The latter mentioned factor, will reduce the CMC as the system will try to oppose a decrease in the entropy of the water. Counterions shield the repulsion between the polar heads, reducing the effective area occupied as illustrated in figure 2.4. The shielding effect becomes stronger when the valency increases.

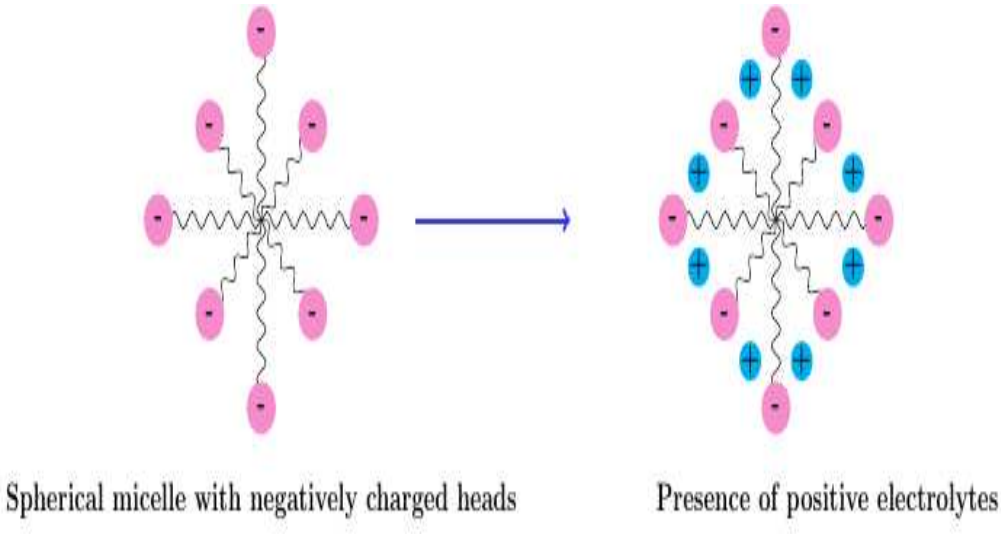

Figure 2.4: A simplified illustration of how the CMC can be affected due to added electrolytes

The equilibrium between the aggregates and the monomeric surfactants for an aqueous medium is depicted in equation (2.8), where the amphiphatic species is represented by S, n is the degree of aggregation and the micelle is given as S_n.

$$nS \leftrightarrow S_n \tag{2.8}$$

([pp. 355- 376] [5], [p. 44] [16])

Flow assurance issues in general

The NA present in the crude oil can cause various problems in refinery processes. Some of the problems with respect to flow assurance[6] are presented in the following subsections.

Formation of stable emulsions

Emulsions are classified as water-in oil, oil-in-water and multiple emulsions. For water-in-oil emulsions, which are the most common emulsions in the petroleum industry, the water droplets are dispersed in oil. The oil-in-water emulsions on the other hand, are defined as oil drops dispersed in water. The medium in which the particles are dispersed, is the continuous phase also known as the bulk. An illustration of a colloidal system is given in figure 2.5, where the presented dimension of the colloid is in the range of 1 nm - 1 µm. The size of the dispersed particles in oildfield emulsions are in general larger and may even exceed 50 µm.

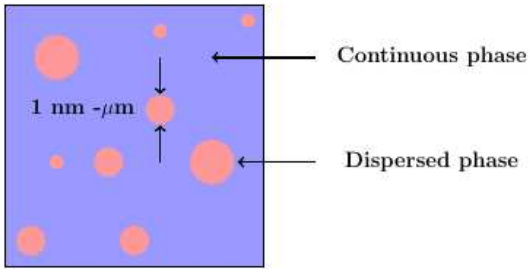

Figure 2.5: Colloidal dispersion

Emulsions can be kinetically stable, which indicates that they are stable

[6]The design and strategies that attempt to ensure an uninterrupted flow of crude oil from the reservoir until the point of sale.

over a period of time, even though they do not possess thermodynamic stability. This kinetic stability is caused by the small size of the dispersed particles and the interfacial film surrounding them. Hence, the stability of the colloidal system depends upon the film between the two phases.

Indigenous emulsifiers in the crude oil are surface active components such as asphaltenes, resins, solid particles in general and naphthenic acids. These molecules migrate and form interfacial films, hence creating a steric or electrostatic barrier that prevents separation of the phases. In other words, with respect to flow assurance it is of importance to prevent or destabilise the emulsions.

([pp. 1-15] [5] , [pp. 5-6] [7])

Demulsification

Demulsification is defined as the process of breaking an emulsion into water and oil, or in other words destabilisation. There are two coarsening processes for kinetically stable emulsions. The primary step is aggregation, also known as coagulation, which does not change the total surface area, as the colloidal dispersed particles form clusters. For particles to fuse together, coalesce, the interfacial film cannot be very viscous and strong. If the viscosity, which is a measurement of friction between molecules, of the interface is high, there will be a mechanical barrier preventing coalescence and there will be no reduction in the total surface area.
([p. 412] [14], [p. 9] [7], [p. 15] [5])

According to [7], the separation of the two phases can be achieved by adding chemical demulsifiers, increasing the temperature of the emulsion

and the application of an electrical field [pp.9-10]. Another possibility is to reduce the velocity of the flow to allow gravity to separate oil, water and gas. By increasing the temperature, the dispersed particles move faster [p. 426] [14], hence colliding at a higher frequency [p. 8] [7]. In other words, as the temperature increases, the forces between the molecules at the interface cannot withstand the increased thermal energy as they are classified as weak. The molecules then break apart from each other causing the film to become thinner.

A side-effect of this thermal method, however, as pointed out by [7], is the increased potential for both corrosion and CaNA deposition [p.10]. To heat up the emulsion is also expensive. The application of the electrical field is then often used in addition. If the field is applied perpendicular to the direction of flow, the water molecules at the interface may be rearranged, which weakens the interfacial film. Since the electrical field causes the water droplets to move rapidly, they collide easier. Hence, the coalescence rate will increase. An illustration of the effect of the electrical field on the individual water drops is provided in figure 2.6, where the field causes the water drops to deform.

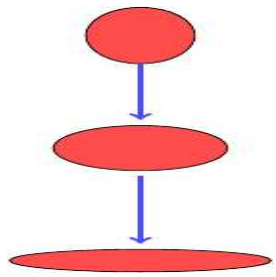

Figure 2.6: Change of the water droplets caused by the electrical field

Demulsifiers are interfacially active chemicals such as dodecylbenzene sulphonic acid, toluene, benzene, alcohols with short chains and surfactants. Polar components that stabilise the interface can then be adsorbed. As a result there will be less molecules to "rub" against each other, thus reducing the friction and hence the viscosity of the film. However, as the feedstock will be different, an added demulsifier may not necessarily work since demulsifiers are usually specific for a given emulsion. An expensive shut-down can be the only solution. [pp.10-11] [7]

Flow assurance with respect to naphthenic acids

Formation of calcium naphthenate deposits

The formation of CaNA, which may precipitate in pipelines and separators is another problem of concern. The build-up of CaNA deposits in a hydroclone is given in figure 2.7 [17].

Figure 2.7: Calcium naphthenate deposits

The crude oil is transported in the subsea environment by means of pipelines from the high pressure and high temperature reservoirs. Downstream the crude oil will be affected by the surroundings. Carbon dioxide (CO_2) will be degassed from the coproduced water, which occurs naturally within the pores of the reservoir rock, as the pressure decreases [p. 668] [18]. When CO_2 is removed, the pH can increase in accordance with Le Châtelier's principle. The process is indicated in equation (2.9), where H_2CO_3 is the formula for carbonic acid.

$$CO_2 + H_2O \rightleftharpoons H_2CO_3 \tag{2.9}$$

As a result the NA dissociates, as mentioned in section 2.2. The metal cations that are present in the produced water, shield the negatively charged heads of the carboxylate groups of ARN acids (section 2.2) in the oil phase. Calcium has a higher valency than sodium and can screen the electrostatic repulsion better. Since it is divalent it also associates with two carboxylate groups. Thus CaNA will be less hydrated and will preferentially go to the oil phase or to the interface [p.2] [19]. This is consistent with an increased CPP (section 2.2.1) due to the decreased effective area. The water cut[7] may then be of importance in the formation of CaNA.

Preventing calcium naphthenate deposits

A possible solution to prevent the formation of CaNA scale is to add hydrochloric acid (HCl), due to both efficiency in reducing the pH and low cost. However, such a solution will add to already existing corrosion problems downstream and may cause corrosion at the point of injection. An organic acid with an affinity for water, such as acetic acid (CH_3COOH) or formic acid (HCOOH), can be used instead in order to impede an increase in pH. It may be of interest to note that acetic acid in addition to impeding the formation of CaNA, also dissolves existing naphthenates. Nonetheless, the bicarbonate buffer in the formation water has to be taken into consideration.

The carbonic acid is a diprotic acid capable of donating one proton or two protons, as illustrated in equation (2.10). If one proton is donated, the bicarbonate ion (HCO_3^-) is obtained, whereas the carbonate ion (CO_3^{2-})

[7] The ratio of produced water to the volume of all produced liquids [20]

is the result of two donated protons. When acid is added, the buffer will neutralise it within the limits of its capacity. Batch injection is hence preferred. This is also one of the main problems with respect to health, safty and environment (HSE) issues, as about 1000 to 2000 ppm acid per water phase may be needed. ([p. 4] [19], [p. 6] [21])

$$H_2CO_3 \rightleftharpoons H^+ + HCO_3^- \rightleftharpoons 2\,H^+ + CO_3^{2-} \text{ buffer system} \tag{2.10}$$

Chemicals known as sequestering agents, can be added in order to form complex structures with the divalent calcium ion. The cations are then prevented from reacting with the ARN-acids, which are resposible for causing CaNA as mentioned in section 2.2. However, a large volume of sequestering agents is needed, since the amount of these acids can be high. This implicates large storage tanks, which will be expensive.

Inhibitors, which are also interfacially active compounds, can control the formation of CaNA through different mechanisms. These chemicals then suppress the reaction between the calcium ions and the acids, though the choice of the inhibitor is dependent on the concentration of acids, the pH and the temperature.

Finally, if none of the methods mentioned can improve the flow assurance with respect to CaNA formation, it may be necessary to disperse the formed naphthenates to halt the accumulation or to attempt the removal of the NA before they can react. [pp. 669-674] [18]

Corrosion

Crude oil cannot be used unless it is treated as mentioned in section 2.1. Corrosion can occur downstream due to the presence of acids. Plant experience indicates that the corrosion occurs when the temperature exceeds 200 °C, due to the diffusion of acids towards a metallic surface, and stops at approximately 400 °C, presumably due to decomposition of the NA.

The distillation units are then exposed to corrosion caused by NA due to the high processing temperature, as well as other units in the refinery such as heat exchangers. The vacuum distillation plant is the most vulnerable unit with respect to corrosion caused by these acids as the vacuum gas oil, which is residue from the atmospheric distillation plant, has the highest TAN.

The corrosion due to naphthenic acids is illustrated by equation (2.11) and yields a complex, which is soluble in the oil phase.

$$\mathrm{Fe} + 2\mathrm{RCOOH} \rightarrow \mathrm{Fe(RCOO)_2} + \mathrm{H_2} \tag{2.11}$$

Whether the corrosion will take place or not, is not only dependent upon the NA, represented by the TAN. Different sulphur compounds are present with a various affinity for iron. A protective layer can be formed as depicted in equation (2.12):

$$\mathrm{Fe} + \mathrm{H_2S} \rightarrow \mathrm{FeS} + \mathrm{H_2} \tag{2.12}$$

([pp.1403-1404] [22], [23][8])

[8]No date given, located the 2nd of November 2016

However, experimental work conducted by [24], concludes that if a sulphur compound such as sulphoxide is present the situation is different. The produced water, as illustrated in equation (2.13), enhances the dissociation of the NA, thus increasing the corrosion.

$$R_2SO + H_2 \rightarrow R_2S + H_2O \tag{2.13}$$

A preventive action with respect to flow assurance could then be to separate streams containing sulphoxides and NA.

Removal of naphthenic acids

The removal of NA before they can cause flow assurance problems is of importance. For instance 20 % 2-methylimidazole in ethanol at 30 $^{\circ}C$ was found to have the best positive effect on the removal rate of NA from Bejiiang crude oil of the imidazole derivatives used in studies performed by [3].

Another compound of interest is the magnesium oxide (MgO) catalyst, which has a strong basicity that can react with the naphthenic acids through acid-base neutralisation. In the experiments conducted by [25], the MgO catalyst was used in catalytic decarboxylation, which is defined as the removal of a carboxyl group. The effectivity of the catalyst was tested both in model organic solvents as well as directly in crude oil.

A competing reaction is the formation of ketones (RCOR), as reported in the work of [26], where MgO was used to obtain 2-propanone. However, the possibility of ketonization reaction, given in equation (2.15), can be low due to the estimated negative value of the catalytic decarboxylation reaction of acetic acid (CH_3COOH) (2.14).

$$2\,CH_3COOH \rightarrow CH_3COOCH_3 + CO_2 + H_2O \quad \text{(-5.4 kcal/mol)} \quad (2.14)$$

$$2RCOOH \rightarrow RCOR + CO_2 + H_2O \quad (2.15)$$

The catalytic decarboxylation is regarded to be the dominant reaction.

Moreover, it was suggested that this catalyst is promising for large-scale industrial application since the effectiveness it was not found to be dependent on the structure of the NA in addition to a low reaction temperature.
[pp. 106-109] [25]

Environmental issues with respect to naphthenic acids

Studies have been performed in order to gather information regarding the effects of the NA which enter the aquatic environment. For instance [27] found that a repeated exposure to NA from the environment, affect the health of mammals where the liver is the main target organ.

Application of naphthenic acids

Even though NA are a source to problems as explained in section 2.3, they also have their areas of use. The metallic soaps, with the following chemical formula: $(RCOO)_2M$, are produced by means of precipitation of a soluble salt and soluble sodium naphthenate as indicated in equation (2.16) or the fusion method. The metallic cation can for instance be aluminum, calcium, magnesium or zink.

$$MSO_4 + 2\,RCOONa \rightarrow (RCOO)_2M + Na_2SO_4 \tag{2.16}$$

The metallic soap is not soluble in water and can be used in waterproof materials, leather dressing and cosmetics. Soaps of sodium and potassium can be used as detergents as they are soluble in water. Due to the cation present in the naphthenates other areas where they can be applied are: paint driers, catalysis and ceramics.
([pp. 11-14] [28], [p. 1] [11])

Magnetism of magnetic nanoparticles

Nanoparticles are particles ranging from 1 nm to 100 nm [p. 390] [5]. Both the chemical and the physical properties can be unique for these particles. Magnetic nanoparticles (MNP) are nanoparticles that exhibit a response to an applied magnetic field. In ferromagnetic materials such as iron, nickel and cobalt, an atom has unpaired electrons that cause a net magnetic moment. These materials have domains where the magnetic moments are randomly distributed, which cause the net magnetic moment to be zero. However, when an external magnetic field is used, there will be a large magnetism [p. 21266] [29].

The magnetic moment, m , can be defined as the strength of the poles, p, times the length, l, separating them as given in equation (2.17). If a magnet is placed at an angle, θ , to a uniform field, H , then there will be a torque that acts on the magnet tending to turn the magnet parallel to the applied field. Moreover, the magnetisation is the amount of magnetic moments per volume.

$$m = pl \tag{2.17}$$

In figure 2.8, the plus and the minus signs represent the north and the south poles respectively. The magnetic poles give rise to a magnetic field. This field produces a force, F, on a second pole in the vicinity.
[pp. 3-6] [30]

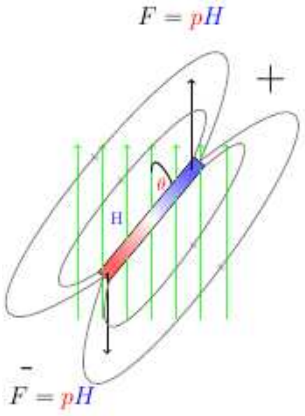

Figure 2.8: Magnetic field of a magnetic dipole

Depending upon the material, nanoparticles give the best magnetic performance when their size is about 10-20 nm ,when they turn into one single magnetic domain[9] from a multiple magnetic domain[10]. This transition is a result of the cost energy to sustain the domain walls, becomes larger than the cost of magnetostatic energy[11]. [pp. 1223-1224] [32]

As the diameter of the particle decreases, the thermal energy becomes larger than the energy barrier caused by the anistropy of the particle. With respect to magnetism, the anistropy is the energy related to the orientation of the magnetic vector field. In other words a certain energy is acquired to change the direction of the electronic spin. This energy is referred to as a blocking temperature, T_{B}, and indicates the transition between ferromagnetism[12] and superparamagnetism [p. 181] [33]. The temperature is subject to the effective anistropy constant, K_{eff}, the size of the particles, V, and

[9]The spin of the electrons are all aligned in the same direction
[10]Regions of uniform magnetisation are separated with interfaces
[11]Dipolar energy [p.30] [31]
[12]The magnetism remains after the applied field is removed [12]

Boltzmann constant, k_{B} as illustrated in equation (2.18) [p. 1225] [32]:

$$T_{\mathrm{B}} = \frac{K_{eff}\ V}{30 k_{\mathrm{B}}} \tag{2.18}$$

In the case of ferromagnetism, which is the magnetic behaviour of the larger particles, the thermal energy is not sufficient to overcome the energy barrier. However, once the particles are small enough the thermal energy flips the spin direction from spin-down to spin-up, or the opposite situation state change. The sketch given in figure 2.9 depicts the relation between the size and the thermal energy.

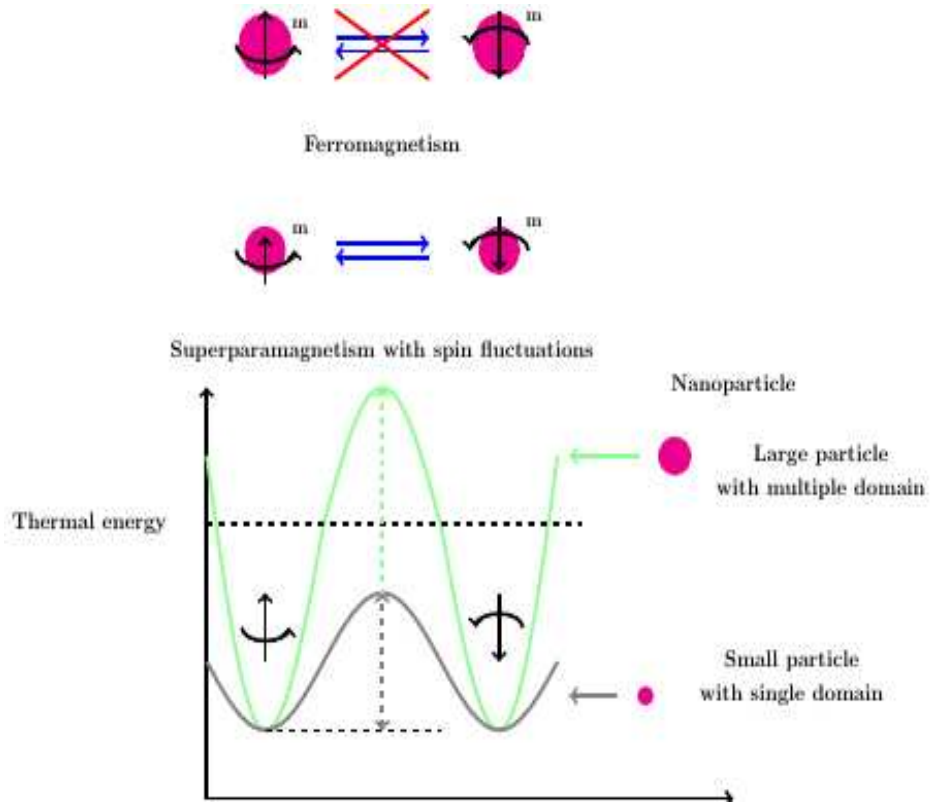

Figure 2.9: Schematic representation of ferromagnetism and superparamagnetism

This size-dependent magnetic behaviour, where the net magnetisation is zero, is known as superparamagnetism. [p. 181] [33]

In other words, the magnetic moments become more random. The system then behaves like one paramagnet and the residual magentism is negligible [pp. 1225-1226] [32]. The γ-Fe_2O_3 (maghemite) nanoparticles are ferrimagnetic at room temperature and superparamagnetic at an elevated temperature, as indicated in figure 2.9.

It may be of interest that for a ferromagnetic particle the formation of the magnetic domains is the consequence of minimising the total energy, E_{tot}, which is estimated from equation (2.19):

$$E_{\mathrm{tot}} = E_{\mathrm{ex}} + E_{\mathrm{ms}} + E_{\mathrm{k}} + E_{\mathrm{z}} \tag{2.19}$$

where E_{ex} represents the energy of exchange, E_{ms} is the magnetostatic energy, E_{k} presents the anistropy energy and E_{z} symbolises the Zeeman energy, which occurs when there is an external field. It is further pointed out that these energies are compared to the thermal energy. Moreover, the large magnetism of the ferromagnetic particle is caused by the coupling of atomic moments, when placed in a magnetic field, or in other words the interaction between electron spins.
[p. 408] [34]

According to [33], the thermal energy of the MNP is not enough to overcome this spin-spin exchange energy [p. 181].

A single-domain particle behaves like one paramagnetic atom. Since the MNP do not have domain walls, spin rotation will change the magnetism. When a magnetic field is applied, the MNP will respond fast and

align themselves with the direction of the external field. [pp. 1223-1225] [32]

Based on this magnetism the magnetic iron oxide nanoparticles can be separated from its solvent using an external magnet. They can also be reused once the undesirable compounds have been adsorbed.

Synthesis of magnetic nanoparticles

Various materials can be used to synthesise MNP including iron oxides γ-Fe_2O_3, α-Fe_2O_3 (hematite) and Fe_3O_4 (magnetite) ([35], [36], [37]) and ferromagnents such as $CoFe_2O_4$ ([38], [32]) as well as alloys like $CoPt_3$ [39]. However, pure magnetic metals such as Fe, Ni and Co can be preferred for the synthesis of MNP due to their superior magnetic properties [40].

There are different methods that can be used to produce MNP, such as microemulsion, thermal decomposition, co-precipitation, thermal synthesis and hydrothermal synthesis. The three last mentioned methods provide high-quality MNP. Using microemulsions to obtain MNP is also less efficient than for instance thermal decomposition, as the operating window is narrow and the amount of nanoparticles is low. [pp. 1228-1231] [32]

The different methods can be used to affect the shape and the size of the nanoparticles as well as the colloidal and magnetic properties. Some of these synthesis methods are described in the following subsections.

Co-precipitation

Co-percipitation may be regarded as a simple method for producing MNP. Magnetite can be produced from aqueous salt solutions containing iron ions by adding a base, usually NaOH, at either room temperature or higher keeping the atmosphere inert ([p. 1228] [32], [p. 8204] [37]). A potential chemical reaction is presented in (2.20):

$$FeCl_2 + 2\,FeCl_3 + 8\,NaOH \rightarrow Fe_3O_4 + 4\,H_2O + 8NaCl \tag{2.20}$$

In order to obtain maghemite the co-precipitated MNP can be oxidized in air [32].

Cobalt ferrite($CoFe_2O_4$) can also be co-precipitated by adding $FeCl_3$ and $CoCl_2$ into a boiling aqueous solution of NaOH as done by [38]. A possible chemical reaction is given in equation (2.21):

$$2\,FeCl_3 + CoCl_2 + 8\,NaOH \rightarrow CoFe_2O_4 + 4\,H_2O + 8\,NaCl \tag{2.21}$$

MNP prepared from this method have a tendency to vary in sizes and shapes. Hence, the magnetic behaviour might not be ideal as polydispersity gives raise to different blocking temperatures. This temperature does not only depend on polydispersity, but also the effective anisotropy constant, the applied magnetic field, and the experimental measuring time. [pp.1225-1228] [32]

Thermal decomposition

In order to achieve monodisperse nanoparticles, thermal decomposition of organometallic compounds can be performed in boiling organic solvents using surfactants as stabilizators [p. 1228] [32]. An illustration of synthesising maghemite from iron pentacarbonyl using this method, is given in figure 2.10 [pp. 12798-12799] [35].

According to [32], the synthesis is done in two steps in order to prevent the formation of the metal itself, since a metal attached to carbonyls is zerovalent [p. 1228].

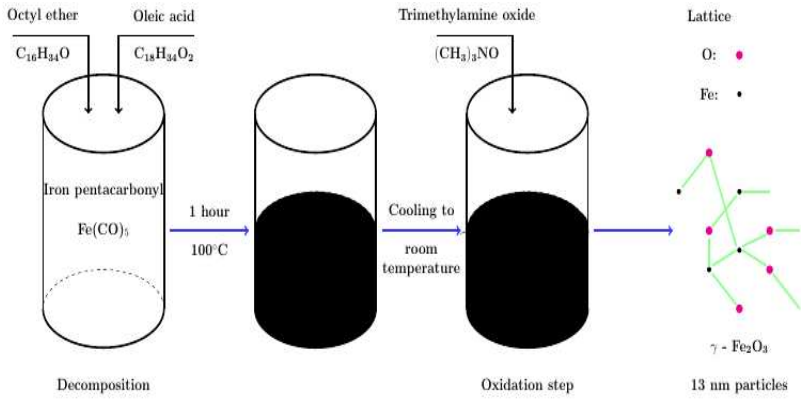

Figure 2.10: Thermal decomposition synthesis to obtain monodisperse nanoparticles

A proposed chemical reaction, where RCOOH represent the oleic acid:

$$Fe(CO)_5 + RCOOH + (C_{16}H_{34}O \rightarrow Fe_3O_4 \overset{(CH_3)NO}{\rightarrow} \gamma - Fe_2O_3 \qquad (2.22)$$

Microemulsion

A water-in-oil microemulsion (reverse micelle) is a thermodynamically stable system (section 2.2.1), that can be used as a reactor in order to obtain MNP [p. 1230] [32]. A microemulsion itself is clear and the particles are between 10^{-8} m and 10^{-7} m [pp. 1, 390] [5].

When electrolytes are added, the core of the reverse micelle will be changed due to the electrolytes affinity for water. As a result the interfacial region or the double layer will be affected. Using the Debye - Hükel approximation [p. 512] [5], which assumes low potentials, the relationship between the electrolytes and the extension of the double layer given as, κ^{-1}, is depicted in equations (2.23, 2.24).

$$\kappa = \sqrt{\frac{1000e^2 N_A}{\epsilon k_B T} \sum_i z_i^2 M_i} \tag{2.23}$$

where κ is the Debye-Hükel parameter, N_{A} represents the Avogadro constant, ϵ indicates the permittivity, k_{B} illustrates the Boltzmann constant, e is the charge of the electron. The ionic strength is also part of the Debye-Hükel model and is the sum of the molar concentration, M multiplied by the valence number of ions squared, z^2.

$$\text{Debye-length} = \frac{1}{\kappa} \tag{2.24}$$

The added electrolytes decrease the Debye - length, which allows particles to come closer together. When the effect from the attractive forces becomes stronger than the steric repulsion, which initially masked the vdW

forces, the particles will coalesce. When the particles are large enough they will precipitate and a solvent such as ethanol can be used to extract the MNP, however, the particles can be polydisperse [pp. 1230-1231] [32].

Synthesis of cobalt ferrite using microemulsion as method

In the experimental work done by [41] cobalt ferrite ($CoFe_2O_4$) was synthesised using microemulsion as method. Sodium dodecyl sulfate was added to a mixture of $CoCl_2 \cdot 6\,H_2O$ and $FeCl_2 \cdot 4\,H_2O$ in order to obtain a mixed micellar solution. A potential chemical reaction is given in equation (2.25), where SDS denotes $NaC_{12}H_{25}SO_4$ and DS indicates $(C_{12}H_{25}SO_4)^-$.

$$\begin{aligned} CoCl_2 \cdot 6\,H_2O + FeCl_2 \cdot 4\,H_2O + 4\,SDS \rightarrow \\ Co(DS)_2 + Fe(DS)_2 + 4\,NaCl + 10\,H_2O \end{aligned} \tag{2.25}$$

After heating the solution methylamine (CH_3NH_2) was added. The solution was stirred in order to allow the precipitation of $CoFe_2O_4$ to be completed.

Surface properties of magnetic nanoparticles

Interfacial properties such as the interfacial tension and the contact angle are important as they determine the coating processes, since these properties determine whether a liquid will spread on the surface or break into small droplets. The affinity between a surface and a liquid can be controlled through the formation of monolayers on the surface with desirable properties. When the particles decrease in size, more atoms become surface atoms. For colloidal particles the surface is large as well as the energy of the surface, which results in different properties for the colloidal particles compared to the bulk. [pp. 8, 249] [5]

Nanoparticles are even smaller than the colloidal particles, hence the surface is also larger. Magnetization is one property that can occur for some nanoparticles as described in section 2.7. The properties of the monolayer that is grafted onto the nanoparticle surface also help determine the properties of the nanoparticle. Some metal nanoparticles can posses optical properties, such as gold and silver. In the studies done by Sosa et al. [42] it was noticed that the spectra obtained for particles with less symmetry was more complex than for more symmetric particles, which suggested that the properties of a nanoparticle is not only dependent upon the size, but the shape as well.

Surface charge of magnetite

The structure of magnetite can be represented by its unit cell as for other salts. When there are two cations present, one tetrahedral and one octahedral, they will occupy fixed positions and the distance between them is only defined by the dimension of the unit cell. The combination of iron as tetrahedral cation and iron as octahedral cation, the inversion parameter is one. In other words the structure is an inverse binary spinel, where the structure might be depicted in general as $B[AB]X_4$ or $[Fe^{3+}]_A[Fe^{3+}Fe^{2+}]_BO_4$ for magnetite where the tetrahedral sites are occupied by ferric ions and the octahedral sites are occupied by an equal amount of ferric and ferrous ions.

Within the unit cell both oxygen and the iron cations are present. The amount of oxonium ions $[H_3O^+]$ present in the bulk depends on the pH. At low pH protons will bind to the oxygen in the unit cell, causing the unit cell to become positively charged. Depending on the current pH the surface reactions may be given as shown in equation (2.26).

$$\mathrm{Fe(II,III)OH_2^+} \overset{-\mathrm{H^+}}{\rightarrow} \mathrm{Fe(II,III)OH} \overset{-\mathrm{H^+}}{\rightarrow} \mathrm{Fe(II,III)O^-} \tag{2.26}$$

([pp. 318-329] [43], [p. 4] [44], [p. 155] [45])

Surface charge of ferric oxide

Commercial ferric oxide consists of mainly γ-Fe_2O_3, though some α-Fe_2O_3 will be present. Hematite has a centered hexagonal structure, whereas maghemite has a cubic unit cell of inverse spinel type. Maghemite is both ferromagnetic and superparamagnetic.

Within the unit cell both Fe^{3+} and O^{2-} are represented. Distinct crystal structures have different physical properties. ([46], [47])

Based on the crystal structures of magnetite and maghemite the oxonium ions [H_3O^+] present in the bulk will bind to the oxygen at low pH and there will be no negative charge for the unit cell.

Measurement of the surface charge, an introduction to the zeta potential

At the particle surface the fluid is stagnant, however, after a certain distance the fluid becomes mobile. That particular perimeter is known as the surface of shear and the potential there is the zeta potential, ζ. Although it is stated that the exact location of the surface of shear is unknown, its position is believed to be within the length of the double layer, which has been depicted in section (2.8.3). [pp. 541-542] [5]

Measuring the zeta potential provides information about the stability of dispersed nanoparticles as this potential determines their effective surface charge [48]. The zeta potential is an experimental determined value [p. 534] [5], which is of interest if the stability of the particles is due to electrostatic repulsion. If the potential is lower than the vdW attractive forces, then the particles will coalesce. If the zeta potential is in the range of +30 mV and -30 mV, the suspension is considered unstable. Furthermore, the system is the least stable at the point where the charge reversal can be observed, which is known as the Isoelectric point [pp. 15.2-15.3] [49].

In order to achieve the zeta potential from experiments electrokinetic measurements have to be performed, which is a combination of motion and electricity. Amongst the electrokinetic methods are: electrophoresis, electroosmosis and streaming potential. In electrophoresis the particle will move relative to a stationary fluid while an electrical field is applied. With respect to electroosmosis an electrolytic solution will move past a charged surface, as the applied electric field induces flow. If an electrolytic solution

is forced, however, to flow past the charged surface, an electric field will be created and a phenomenon known as the streaming potential is obtained. [p. 534][5]

In electrophoresis the particles with a zeta potential will move towards an electrode when an electric field is applied. There are viscous forces in the solvent which opposes the particles movement. The velocity at which the particles travel depends on the viscosity and the dielectric constant of the solvent in addition to being proportional to the field strength and the zeta potential ([p. 6] [50], [p. 15.4] [49]).

Using either the Hükel approximation (2.27) or the Helmholtz-Smoluchowski approximation (2.28), depending on whether the radius of the particle is regarded as small compared to the extension of the double layer or not, the zeta potential can be calculated.

$$u = \frac{2}{3}\frac{\epsilon\zeta}{\eta} \tag{2.27}$$

$$u = \frac{\epsilon\zeta}{\eta} \tag{2.28}$$

In equations (2.27) and (2.28), the electrophoretic mobility is denoted u, the permittivity is ϵ and η is the viscosity.

No assumptions are made with respect to the actual extension of the double layer in the derivation of the Helmholtz-
Smoluchowski equation besides the Poisson equation (2.29) and the bulk values of both the permittivity and the viscosity being valid also at the shear surface.

$$\zeta = \frac{q}{4\pi\epsilon R_{\mathrm{s}}} \tag{2.29}$$

Experiments have shown that the model is valid for $\kappa R_s > 100$ for spherical particles. If the particle size is intermediate, then the relation between the electrophoretic mobility and the zeta potential is more complex. [pp. 543-550] [5]

Coating of nanoparticles and functionalization

It is of importance to stabilise the nanoparticles once they have been obtained in order to prevent them from degradation and coalescence. As the magnetic nanoparticles have a very large surface area, they strive to minimise their surface energy. Particularly pure metals such as Fe, Co and Ni as well as their metal alloys need a protective layer due to oxidation.

The MNP can for instance be coated with inorganic components such as silica or carbon, other metals such as gold and silver or organic components such as surfactants, depicted in figure 2.3, or polymers in addition to metal oxides. Steric repulsion or electrostatic stability provide stabilisation of the nanoparticles after the synthesis, depending upon the coating material. Polymers as coating material and applications with respect to the removal of acids will be described in section 2.11.

The protective shell can also be used for further functionalization of the nanoparticles, for instance specific binding sites or catalytically active species. Due to the characteristics of the surface of a functionalized iron oxide MNP they can have an affinity for water or oil or be amphiphilic if small molecules or surfactants are used in the functionalization.
([pp. 401-411] [51], [pp. 1232-1237] [32])

Silica coating and application of modified surface

Using silica to coat iron oxide MNP has several advantages: the particles become more stable due to the shielding of the magnetic dipoles, prevents interactions between particles and agglomeration. The most widespread choices for coating iron oxide MNP with silica are the Stöber method, sol-gel processes and aerosol[13] pyrolysis[14]. Moreover, if the coating is done through hydroxyl groups (-OH) in an aqueous environment, the aggregation control of the MNP may increase [p. 407] [51].

The sol-gel processes are based upon the conversion of the precursor[15] into a sol or a gel, which then is converted into the oxide compound [p.8] [52]. There are three different sol-gel technologies: colloidal sol-gel, inorganic polymeric gel derived from organometallic compounds and gel routes which involve the formation of organic polymeric glass [p. 11] [52]. Once the magnetic nanoparticles have been coated, they become negatively charged and can be re-dispersed in water without the use of additional surfactants [p. 1234] [32].

According to experimental work done by [53], using a sol-gel process based on hydrolysis[16] of tetraetyl orthosilicate (TEOS), the thickness of the silica layer can be controlled through the variation of the concentration of the sol-gel precursor. An increase in the silica coating layer gave more monodisperse magnetic nanoparticles [pp. 184-185] [53]. Different pa-

[13] Colloidal dispersion of solid or liquid in a gas [12]
[14] Chemical decomposition due to high temperature [12]
[15] A compound that will lead to another compound through a series of chemical reactions [12]
[16] A chemical reaction of a compound with water [12]

rameters can affect the sol-gel process. If the amount of 25 wt% ammonia aqueous (NH_3), which acted as catalyst was too high, magnetite became dispersed without silica coating. A simplified illustration of the coating process using TEOS is presented in figure 2.11.
[pp. 89-92] [54]

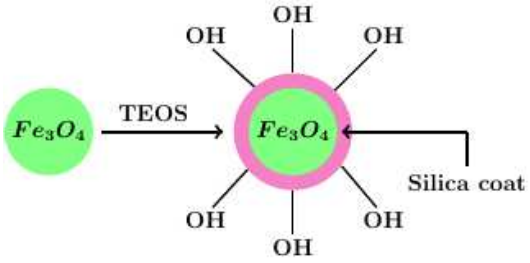

Figure 2.11: Silica coating of iron oxide nanoparticles

Once the MNP have been coated with silica they can be further functionalized and modified using different ligands, as in the experimental work conducted by [55]. The functionalization of the silica coated iron oxide nanoparticle, is depicted underneath in figure 2.12:

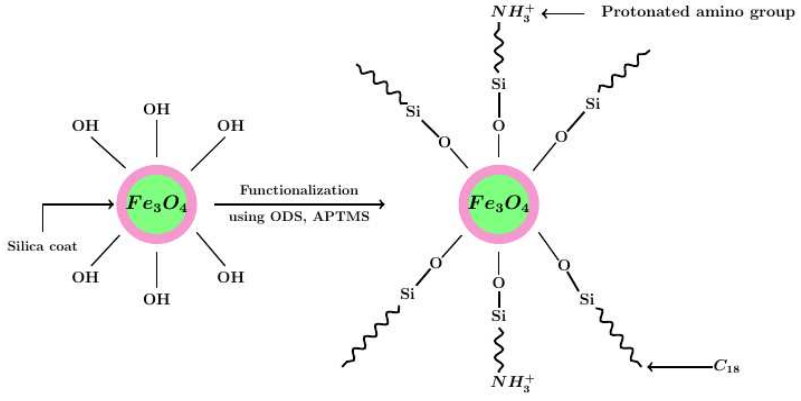

Figure 2.12: Modification of a silica coated iron oxide nanoparticle

The use of different ligands increases the possibility of adsorbing undesirable compounds with different functional groups due to hydrophobic attraction caused by the C_{18} - groups and the electrostatic attraction provoked by the protonated amino group. It was concluded that the modification using mixed groups effectively extracted anionic organic pollutants in an acidic environment. [pp. 107-112] [55]

Gold coating and application of the modified surface

Gold can be used to coat iron oxide MNP in order to prevent oxidation. The coating can be performed either through a direct reduction of the single-metal ions on the surface of the iron oxide nanoparticle or by reducing a single-metal ion on the surface of the small molecule, polymer or silica which functionalize the iron oxide nanoparticle [p. 409] [51]. An application of gold as coating material has for instance been used in the experimental work conducted by [36]. In the experiment a water-soluble fluorescent polyethylene glycol (PEG) and thiol (SH) compounds were used to modify spindle-shaped gold coated iron oxide MNP in order to easier observe the cells treated in magnetolysis therapy. The functionalization of the polymer polyethylene glycol was done through the substitution of terminal hydroxyl groups [p. 223] [36]. The synthesis is illustrated in a simplified model in figure 2.13:

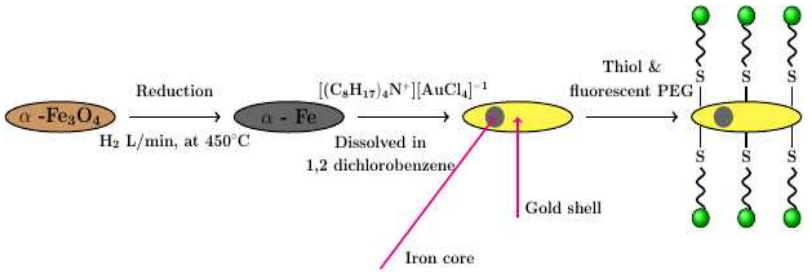

Figure 2.13: Modification of a gold coated iron oxide nanoparticle

Adsorption of naphthenic acids and interfacial kinetics

Adsorption can be regarded as the formation of a layer on a solid or liquid surface. The substance that is adsorbed on the surface is the adsorbate and the substance of which the adsorbate is adsorbed is the adsorbent. The adsorption can be classified as either physisorption or chemisorption [12]. For the NA to be removed from the oil phase using the modified iron oxide nanoparticles, they have to be adsorbed onto the functionalized nanoparticle.

There are different factors that can affect the adsorption such as the surface of the adsorbent, the affinity of the adsorbate towards the solvent and the chemical structure of the adsorbate.

Physisorption and chemisorption

If the NA is not able to share electrons with the surface, the adsorption is classified as
physisorption or physical adsorption. The interaction regarded as physisorption involves the weak intermolecular vdW forces caused by the positive nucleus. The physical adsorption can hence be multilayered. When chemical bonds are formed between the adsorbate and the adsorbent due to shared electrons, the adsorption is known as chemisorption. Strong intramolecular bonds have to be broken, which implies an activation energy (pairing energy), which is not the case for physical adsorption. In the case of

chemisorption only a monolayer is formed. The chemisorption can be either associative or dissociative as indicated in figure 2.14.

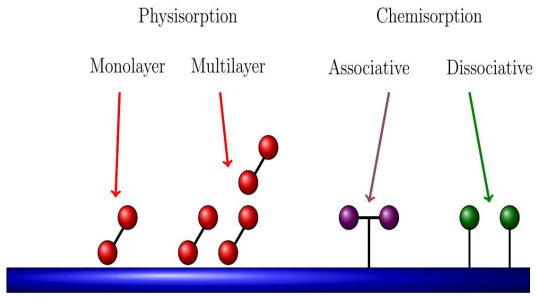

Figure 2.14: Illustration of potentially formed layers on the adsorbent surface

As the particle approaches the surface the positive nucleus will affect the electrons of the adsorbate. The vdW forces will be felt first, yielding physical adsorption. This can be regarded as a precursor state. When the adsorbate approaches the surface of the adsorbent even more, the kinetic energy of the electrons of the adsorbate increases due to the Pauli principle, which basically states that the spin has to be in opposite directions as all four quantum numbers cannot be identical for electrons within the same atom. Electrons with opposite spins have a higher energy state as there is a finite possibility that they can occupy the same space, which indicates that there has to be a pairing energy that is greater than the repulsion between the electrons. In other words when the adsorbate approached the surface of the adsorbent, it experiences repulsion.

If the particle can rearrange its electronic configuration and gain enough energy to overcome the small activation barrier indicated after the physisorption, associative chemisorption is possible. At a very short distance, the repulsion is high as indicated by E_a. If electron structure can be changed

more and enough energy is gained to overcome this activation barrier, the result is dissociative adsorption. Two adjacent vacant and active sites on the surface are then necessary for dissociative adsorption, where there are two chemisorbed atoms. E_d indicates the energy that is necessary in order to desorb the dissociated atoms. A simplified potential energy diagram of a particle approaching the surface from the right is shown in figure 2.15.

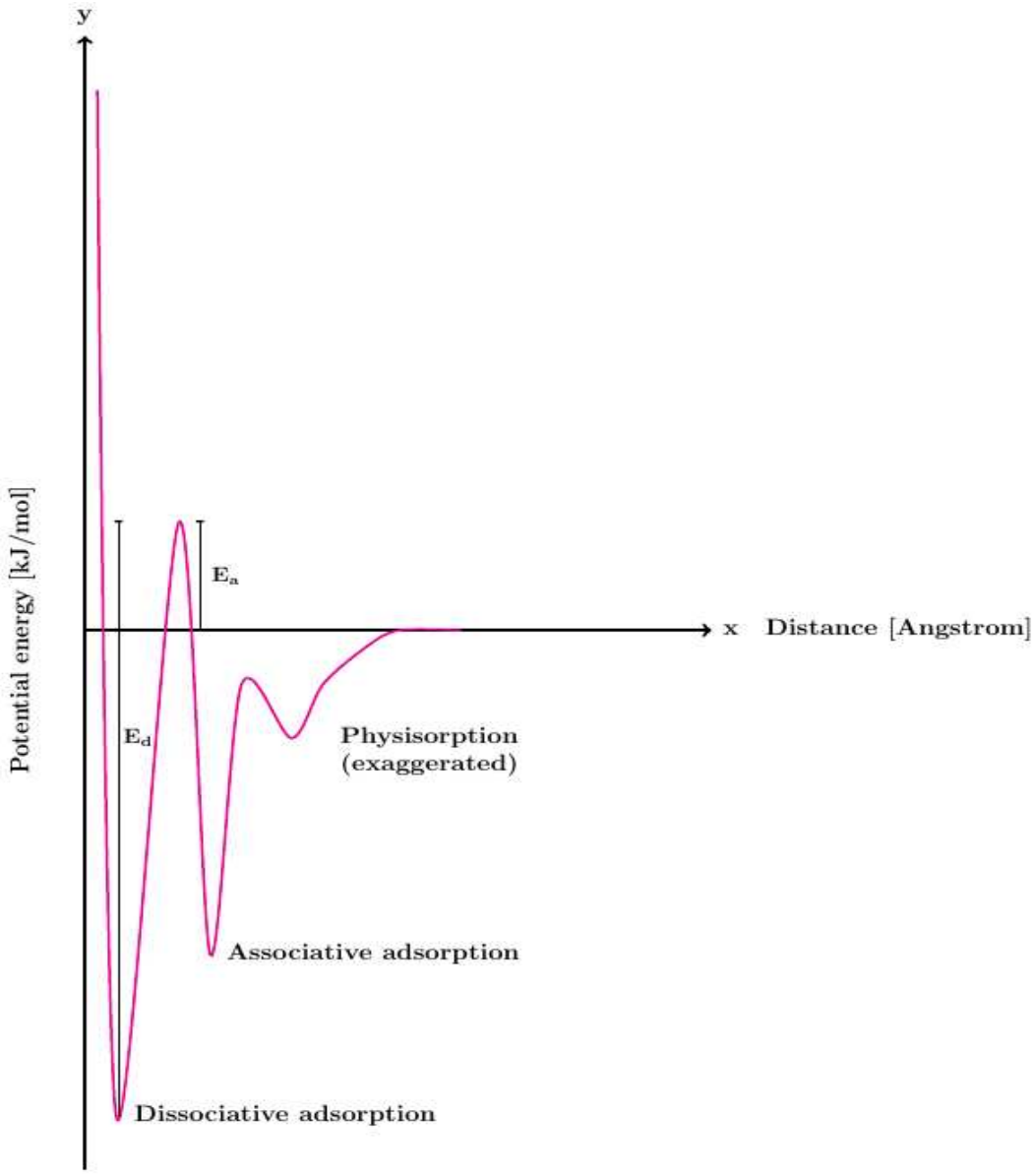

Figure 2.15: Potential energy curve for the different types of adsorption

([pp. 9-10] [56], [p. 90] [57], [119, 215-218, 254-255] [58], [p. 253] [59])

Molecular orbital theory and adsorption onto nanoparticles

Shared electrons between the adsorbate and the adsorbent is the result of overlapping molecular orbitals. One of the molecular orbitals is bonding and the other one anti-bonding. The bonding orbital is the region with the highest electron density and is located between the two nuclei, thus the molecule becomes stabilized. [pp. A-18 -A-23] [60]

For heteronuclear diatomic molecules the energy levels are asymmetric as the different atoms have different screening effects[17]. The molecular orbitals are then derived primarily from the 2s atomic orbitals of one element which overlap significantly in energy with those derived from the 2p atomic orbitals of the other element, as opposed to homonuclear diatomic molecules.

Perhaps there will be delocalised electrons or in other words hybridisation of s and p orbitals for the adsorption of the adsorbate onto the surface. The covalent character of the gold-sulphur bond, formed when adsorbing p-aminothiophenol onto gold nanoparticles, provides an example where hydbridization occurs [p. 735][61].

It may be mentioned that if the the s-orbital and the bonding p-orbital are orthogonal, the number of bonding orbitals and the number antibonding orbitals cancel each other
[p. 90] [57]. There will then not be any Pauli repulsion or molecular orbital.

[17]The higher energy level electrons are shielded from the full attraction of the protons by the electrons in the lower energy levels [p. 28] [56].

Kinetics

Kinetics relates macroscopic processes such as concentration, pressure and temperature to the reaction rate. In other words kinetics indicates the reaction mechanism or the main steps involved in the reaction. For the individual molecules, kinetics is viewed as reaction dynamics [pp. 23 - 24] [58].

For the adsorption process there are two prior steps: external and internal diffusion, which is defined as the spontaneous mixing of atoms or molecules by random thermal motion. The external diffusion is regarded as the transport from the bulk fluid, whereas the internal diffusion is the transport into the interior of the pores on the surface.

A different way to model the diffusion is to view it as a transport through a layer or a film of thickness, δ, which possess a certain resistance. This resistance against diffusion is assumed in the model to only be within this layer and the properties, such as concentration and temperature, of the edges of the layer are identical to those in the bulk.

The particles will diffuse from regions with higher concentration to regions with lower concentration. In other words, the driving force for diffusion involving mass is the concentration gradient. The mass transfer of component A in one dimension, z, for a binary system, is given in equation (2.30). The illustrated relationship between the mentioned concentration gradient and the molar flux of A denoted W_A, is known as Fick's First Law, where D_{AB} is the diffusivity of A in B.

$$W_{\mathrm{A_z}} = -D_{\mathrm{AB}} \frac{dC_{\mathrm{A}}}{dz} \tag{2.30}$$

The local mass-transfer coefficient given as $\tilde{k_c}$ is defined as the ratio of the diffusivity (also known as the diffusion coefficient) to the film thickness at a particular point ($\tilde{\delta}$) is given as:

$$\tilde{k_{\mathrm{c}}} = \frac{D_{\mathrm{AB}}}{\tilde{\delta}} \tag{2.31}$$

The expression in equation 2.31 can be generalised to be valid for the entire film, as indicated in figure 2.16.

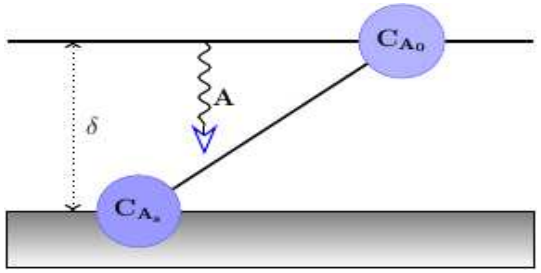

Figure 2.16: Model of a concentration profile in a stagnant film

If the film is thick, the time needed for particle A to travel to the surface will be longer. In other words the mass-transfer coefficient will be small and the mass transfer slow. The external diffusion is then the rate-limiting step for adsorption. When the film is too thin to offer resistance, the internal diffusion determines the reaction rate. The mass transfer can be increased if the particle decreases or if the flow of the fluid passing the surface is increased since both parameters decrease the film thickness. [pp. 543-565] [59]

Adsorption isotherms

An adsorption isotherm is an equation which represents the relationship between the concentration of the adsorbate adsorbed onto a surface at constant temperature and the equilibrium concentration of the adsorbate in a solution or pressure of the adsorbate adsorbed in the gas phase and the equilibrium gas pressure at constant temperature ([12], [pp. 332, 409] [5]).

There are different adsorption isotherm models, which are based on different assumptions such as the Langmuir isotherm, the Freundlich isotherm and the Brunauer-Emmett-Teller (BET) isotherm. These models can be used to predict the adsorption equilibrium. The data from the isotherms is presented as curves, which relate the surface coverage[18] to either the concentration or the pressure.

With respect to adsorption isotherm types there are five. Type I reflects monolayer adsorption and chemisorption (section 2.10.1). Type II deviates from Langmuir, but does indicate monolayer as well. This type of isotherm is observed when the adsorption is physical. Type III explains multilayered adsorption. Both Type IV and Type V are partially similar to Type II and Type III. In other words both Type IV and Type V have the presence of monolayer adsorption and multilayer adsorption. These two types are associated with porous solids where the adsorbate condences in small pores when the pressure,$p < p_0$, where p_0 is the saturation pressure of the material at the temperature of the experiment.
(pp. 409-411] [5],[62])

[18]Fraction of the surface occupied by the adsorbate

Langmuir isotherm

The assumptions of the formation of a monolayer and localised adsorption, which indicates immobilisation, form the basis of the Langmuir isotherm. The adsorption sites are believed to be uniform and there are no interactions between the adsorbed molecules since the adsorption energy is the same for all parts of the surface in addition to being independent of the surface coverage. The Langmuir adsorption model for an adsorption at solid-gas interface is represented in equation (2.32) where θ is the surface coverage, K indicates the rate of adsorption divided by the rate of desorption (k_{ads}/k_{des}), which are equally fast at equilibrium, and p is the equilibrium pressure of the gas phase. The pressure can be substituted for concentration for adsorption from a solution. For adsorption at the solid-liquid interface a dilute concentration is presumed, which is one of the limitations of this isotherm. For instance this model does not apply to the adsorption of polymers.

$$\theta = \frac{Kp}{1 + Kp} \tag{2.32}$$

Looking at the Langmuir adsorption model equation the adsorbed amount is proportional to the pressure when the pressure is low, and the surface coverage increases linearly. Hence, in the Henry law region (θ=Kp) the adsorption behaves ideally. This is another limitation of the Langmuir isotherm (2.17) since few monolayers behave ideally. At high pressure there is a saturation point, where the surface coverage is equal to unity.

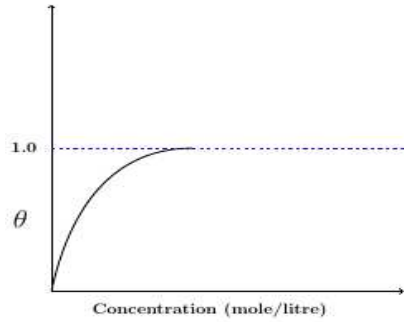

Figure 2.17: Langmuir adsorption isotherm

This model may be applied for chemisorption. [pp. 332-337, 420-422] [5]

Brunauer-Emmett-Teller isotherm

The BET isotherm is also an immobile adsorption model. However, it deviates from the Langmuir adsorption model by assuming the formation of multilayers. In other words there will be no limiting value once the pressure is high. The adsorption and desorption can occur from any layer as long as there is no layer stacked on top of it. It is furthermore pointed out by [5] that additional layers can be stacked without the necessity of the monolayer to be complete or in other words equal to unity. The BET model is depicted in equation (2.33).

$$\theta = \frac{V}{V_{\mathrm{m}}} = \frac{c(\frac{p}{p_0})}{(1-(\frac{p}{p_0}))[1+(c-1)\frac{p}{p_0}]} \tag{2.33}$$

In the equation above V_{m} is represents the volume of gas that could be adsorbed if there is a complete monolayer, V is the sum of the volume of adsorbate held by each site, p_0 is the saturation pressure and in this case c is

a function of the adsorption energy (ε), the energy of evaporation (ε_{v}), the Boltzmann constant (k_{B}) and the temperature (T) as depicted in equation (2.34).

$$c = \exp \frac{\varepsilon - \varepsilon_{\mathrm{v}}}{k_{\mathrm{B}} T} \tag{2.34}$$

After the first layer the desorption energy is the same for all layers, thus also for the adsorption. The model also presumes that a single adsorption energy applies to all surface sites [p. 433] [5]. In other words the isothem allows V_{m} to be extracted from the multilayer adsorption data.

For the volume of the adsorbate to be equal to infinity, the equilibrium pressure has to be equal to the saturation pressure. Due to the assumptions in this adsorption model, the curve obtained is s-shaped as shown in figure 2.18. ([pp. 425-428] [5], [p.312] [63])

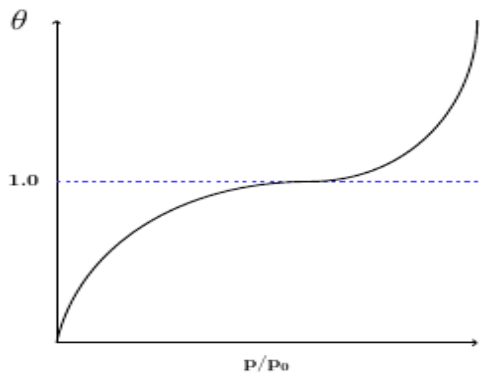

Figure 2.18: BET adsorption isotherm

Freundlich isotherm

The Freundlich model is given in equation (2.35), where n and a are constants with n >0 and c is the concentration.

$$\theta = ac^{\frac{1}{n}} \tag{2.35}$$

This model may be regarded as an empirical isotherm, which assumes Langmuir adsorption at each type of site. When $n = 1$, the isotherm is identical to the lower concentration limit of Langmuir isotherm, thus linear. As $n \to \infty$ unity is approached. Since the model is exponential it may presumed that the surface coverage increases with increased concentration of the adsorbate in the solution. The Freundlich isotherm is illustrated in figure 2.19. [p. 337] [5]

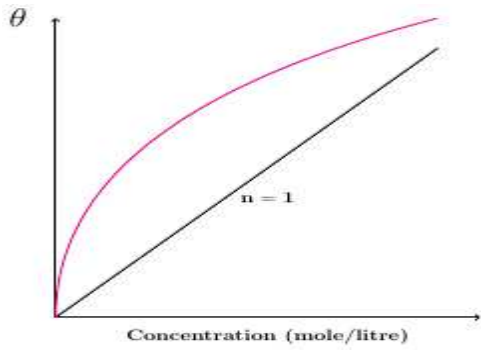

Figure 2.19: Freundlich adsorption isotherm

Estimation of the adsorbed adsorbate

The estimation of the amount of adsorbed adsorbate on a surface at equilibrium is done using equation (2.36):

$$q_{\mathrm{e}} = \frac{(c_0 - c_{\mathrm{e}})V}{m} \tag{2.36}$$

where q_e is the equilibrium concentration of adsorbate adsorbed onto the surface of the adsorbent, c_0 is the initial concentration of the adsorbate, m is the mass of the adsorbent, V is the total volume and c_{e} is the equilibrium concentration of adsorbate in the solution [p. 294] [64].

An introduction to polymers

Polymers are large molecules built up of monomers, or in other words a repetitive chemical unit. These molecules have a wide range of properties that may be caused by their size and their structure. If they can be reheated and obtain different conformations, they are classified as thermoplastics, whereas those polymers that do not possess this ability are thermosets. The polymerisation process can either be step growth, where the chain is slowly built systematically, or chain growth, where the end of the chain is an active site. With respect to the chain growth the active site, which can be negatively charged, positively charged or a free radical, has to be created as an initial step. Figure 2.20 illustrates both the step growth and how the chain propagate in chain growth.

$$M_1 + M_1 \rightarrow M_2$$
$$M_1 + M_2 \rightarrow M_3$$
$$M_2 + M_2 \rightarrow M_4$$
$$M_2 + M_3 \rightarrow M_5$$
etc.

(a) Step growth

$$\sim\sim\sim\sim M^* + M \sim\sim M\text{-}M^*$$
etc.

(b) Chain growth

Figure 2.20: Polymerization process of polymers

Polymers with identical monomers with the exception of the end groups is a homopolymer. Copolymers have different units in the backbone. They can be alternating-, random-, block- or graft copolymers. The chemical structure can be either linear or branched. If the chains are linear a crystalline phase can be formed. [pp. 4-6,32-51] [14]

Microstructure and morphology

The sequence of monomers can be referred to as the microstructure, which resembles the primary structure used in biology. The secondary structure is the local conformations, also regarded as rotational states of the polymeric chain, such as staggered and eclipsed. Morphology or the quaternary structure, when applied to polymers, is the degree of order or study of order. A crystalline region has a high degree of order compared to amorphous[19] regions, hence the number of conformations is low. The morphology is then dependent upon different factors such as the flexibility of the chain, the temperature and the vdW forces.
[pp. 207,220, 237] [14]

Polymeric properties

The molecular weight of a polymer has an important influence on the polymeric properties in addition to the structure. With respect to polymers the molecular weight it distributed, which causes molecular weight averages. The number average molecular weight, $\bar{\mathrm{M}}_{\mathrm{n}}$, is determined according to equation (2.37) and the weight average molecular weight, $\bar{\mathrm{M}}_{\mathrm{w}}$, is obtained from equation (2.38).

$$\bar{\mathrm{M}}_{\mathrm{n}} = \frac{\sum \mathrm{N_x M_x}}{\sum \mathrm{N_x}} \tag{2.37}$$

$$\bar{\mathrm{M}}_{\mathrm{w}} = \frac{\sum \mathrm{N_x M_x^2}}{\sum \mathrm{N_x M_x}} \tag{2.38}$$

[19] Defined as the opposite of crystalline, or in other words lack of order [12]

In the two given equations above, M_x denotes the molecular weight of a molecule corresponding to the degree of polymerisation, x. N_x represents the number of chains with x repeating units. It can be noted that some physical properties are sensitive to a low molecular weight, whereas others are sensitive to a high molecular weight.
([pp. 6, 16-17] [14], [p. 195] [16])

A polymer with surface active properties can be obtained by either grafting hydrophilic chains to a hydrophobic backbone, grafting hydrophobic chains to a hydrophilic backbone, alternating segments or a combination of the mentioned options. The polymer is then able to orient itself according to its environment. [p. 261] [16]

How the different chains affect each other also contribute to the polymeric properties such as temperature and solubility. As mentioned in section 2.1, London vdW forces are always present and will affect the affinity between different segments of a chain.

Solubility or in other words, whether a polymer will dissolve in a solvent or not, is related to thermodynamics. A decrease in the free energy indicates miscibility. If the entropy or the number of conformations available, given in equation (2.7), for the polymer in the solvent increases compared to before contact, the solvent is regarded as good. The segments of the polymer may repel each other or there is an affinity for the solvent. For instance due to functional polar groups in the polymer and a polar solvent. Figure 2.21 depicts how a polymer conducts itself in different solvents. [pp. 237, 307, 331] [14]

(a) Polymer in a good solvent **(b)** Polymer in a bad solvent

Figure 2.21: Illustrations of the behavior of a polymer depending on the solvent

Polymer induced colloid stability

In order to induce colloid stability the particles have to be prevented from the coarsening processes. Polymers have to be adsorbed or grafted on a particle surface in order to be able to stabilise the colloidal system. The adsorption of polymers is a reversible process, which can be affected by for instance temperature and compression of the polymer layer. However, whether a polymer coated surface adds to the attractive vdW forces or disperse the particles depends on the solvent.

In a good solvent, segments of the polymer chain have a higher affinity for the solvent than each other as previously mentioned. The polymer extend its chain as depicted in figure 2.21a. In the presence of another particle with a polymeric layer any segment overlap will reduce the freedom of orientation compared to the freedom that the polymer would posses when the particle is further away. A particle without a polymer coat may also restrict the freedom of orientation. In both cases the free energy will increase, which is not a favourable situation. Thus, the particles remain dispersed.

In the case of a bad solvent the polymers will allow the particles to come closer as illustrated in figure 2.21b. The colloidal system can also be destabilised if the particle surface has enough vacant sites for the polymer to act as a bridge between two particles in a bad solvent.

Depletion stabilisation may occur when the polymer concentration is high in a good solvent, since what can be regarded as depletion forces are weaker than the forces causing dispersion. The dispersed polymers exert an osmotic pressure force in the surroundings of the particles. As the particles

come closer, the region between the particles will be drained of the polymers in order to prevent loss of entropy with the respect to the polymers. Hence, the osmotic pressure between the particles will become smaller than the osmotic pressure "outside of the region "with the two particles. The approaching particles then become attracted to each other. ([pp. 331-332] [14], [pp. 604-614] [5])

Electric charges on a surface can either stabilise or destabilise a colloidal dispersion. If the electric charges counteract the vdW forces, the colloidal stability is known as electrostatic stability. Basically if the electric charges are similar the particles will repel each other, whereas dissimilar charges will cause attraction. There are different factors which influence the effect of the electric charges on the colloidal system such as:

1. the Debye-length, indicated in section 2.8.3
2. the magnitude of the surface potential, ψ_0, which is related to the total charge of the particle, is characterized by the zeta potential (2.8.5)
3. the strength of the vdW attraction, which is a material property represented by the Hamaker constant

With respect to charged polymers, there will be a combined effect of both steric stability and electrostatic stability which is known as electrosteric stability.
[pp. 516, 526, 575] [5]

Application of polymer coated magnetic nanoparticles

There are various polymers that may be applicable for coating of iron oxide MNP. In general polymers containing functional groups, such as carboxylic acids, secondary amino groups, and sulfates, can be grafted to the surface of magnetite. In other words poly-L-lysine, polyamidoamine and polyethyleneimine (PEI), which are all polycations due to the presence of secondary amino groups, NH_2, are thus potentially suitable for the removal of NA.

With respect to biological applications, poly-L-lysine, which is a linear polymer, can increase the number of positive sites on the surface of a cell upon adsorption [65]. Babič et al. [66] found that the poly-L-lysine modified iron MNP provide good colloidal stability and that the effectivity of the polymer increases with the molecular weight with respect to internalization[20] [p. 749].

Polyamidoamine is a polymer that can be linear or dendritic depending on the sequence of amine and amido groups as well as their molar ratio [p. 3901] [68]. The main chain contains tertiary amino groups, but given the right molar ratio at low temperatures, secondary amino groups can be procured. Dendritic polyamidoamine, which has a branched structure, can be used to further functionalize a silica coated surface as performed by Fujiki et al. [69] by means of the divergent method. It was discovered that the branched polyamidoamine propagated from the terminal group of a terminal diamine-type polyoxyethylene already grafted onto the silica surface. Nevertheless, a low density of the initial amino groups was concluded to be

[20]Endocytosis. The process of drawing proteins into the cell [67]

the best option compared to high density due to steric hindrance provided by the polyamidoamine [pp. 359 - 371] [69]. When the steric hindrance becomes too large, the macromolecule will cease to grow. Moreover, the advantage of a dendritic polymer, also known as a dendrimer, is the high density of functional groups. As the shape is globular it can be used to cary drug in its interior [pp. 35-37] [70].

According to [71], PEI does not only have a higher charge density than the two previously mentioned polymers, but it has the highest cationic-charge-density-potential of organic macromolecules in general. Every third atom is an amino group that can be protonated. Furthermore, PEI possesses a good buffer capacity independent of the pH. By comparison to the linear poly-L- lysine, it was found that the PEI network captured DNA more efficiently. It was also noted that even though the short chained PEI gave low cellular toxicity, the efficiency was low as well in contrast to the long chained polymer. Nevertheless, as the chain length increased, so did the toxicity and not only the amount of surface bonded cells [pp. 7298, 7301] [71]. Based on the documented toxicity of PEI, [72] conducted experiments where it was concluded that it is possible to maintain high transfection[21] efficiency at the same time as reducing the toxic effects by optimization of the polymer chain length [p. 3282] [72].

With respect to other areas of application, PEI can for instance be grafted onto a silica surface and be used to adsorb CO_2. The amino groups then react with the CO_2 in post-combustion, as in the experiments conducted by [74].

[21] The cell infection is initiated by using only the nucleic acid of a virus [73]

Adsorption of polymers

How polymers adsorb onto solid surfaces depends on different parameters. In the work conducted by [75] a comparison was made between adsorbing chains with the presence of chemical impurities or an adsorbing surface with chemical impurities and chemically pure systems. It was concluded that in most cases the primary effect of the impurities was the reduction of the total adsorbance. It was, however, observed as well that certain impurity configurations could cause the chains to be stretched away from the surface, thus requiering less surface area. If the impurity content could be tailored the maximization of the adsorbance might be possible.

The adsorption of a polymer from a good solvent onto a metal nanoparticle surface of varying curvatures was studied by means of adsorbing polymethyl methacrylate (PMMA) onto aluminium oxide (Al_2O_3) in the work conducted by [76]. Based on the result the following conclusions were given:

- In the case of a cluster radius much larger than the radius of gyration of the polymer, the adsorption was similar to adsorption on a flat metal surface.

- When the cluster size is similar to the magnitude of the radius of gyration of the polymer, the geometrical constraints force the scaling of the adsorbed monomer densities with the curvature. As a result the thickness of the adsorbed polymer layer became similar to the thickness of the adsorbed layer on a flat surface.

- When the radius of the cluster has the same order of magnitude as the thickness of the adsorbed layer, the curvature is too large to support an energy gradient between the adsorbed layer and the bulk. Hence, the adsorbed polymer will extent its chains out and away from the surface of the cluster in order to decrease the density gradient.

It was also noted that the surface excess was independent of the chain length of the polymer. The model of the coated particle is given in figure 2.22. Two adsorption shells were formed. The layer with the width L had a constant radial distribution of monomers. The layer with the width L_0, was the depletion shell where the concentration of monomers decreased.

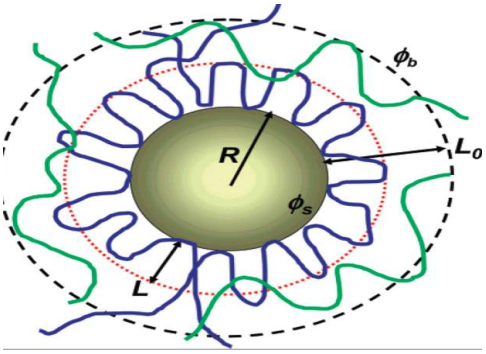

Figure 2.22: Illustration of adsorbed polymer chains onto a spherical nanoparticle

Polyethyleneimine coated iron (II, III) oxide

The amount of PEI adsorbed onto the Fe_3O_4 MNP surface can be systematically controlled by changing the concentration of the polymer during the adsorption process, due to a unique adsorption profile. Smaller aggregates are formed due to the stabilization effect of the polymer. The amount of adsorbed PEI determines the number of available functional groups on the surface of the particle.

When the pH decreases, PEI gets more positive charges. The MNP core, however, becomes negatively charged with an increase in pH (section 2.8.4.1). As a consequence the zeta potential increases for the PEI functionalized MNP as depicted in figure 2.23.

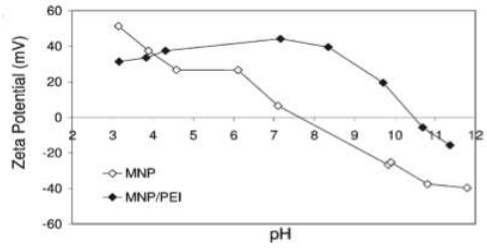

Figure 2.23: Effect of PEI coating of maghemite

For PEI, the experimental parameters that can affect the adsorption onto Fe_{34} MNP are the length and concentration of the polymer in addition to the shape and the dimension of the MNP, as indicated in section 2.8.4. Hence, for optimal coating it is in general recommended to use low molecular weight polymer and low salt concentration. It may be mentioned that any added salt can result in aggregation of the MNP.

Since the PEI has a large number of proton accepting groups, it can be

positively charged over a wide range of pH. With respect to the Le Châtelier's principle, and the definition of pH as given in equation (2.39), the PEI will become more protonated at lower pH as indicated by equation (2.40)

$$[H_3O^+] = 10^{-pH} \tag{2.39}$$

$$[HA] \leftrightarrow [H^+] + [A^-] \tag{2.40}$$

A maximum absorption, or in other words optimization, of PEI onto Fe_3O_4 may take place between pH 6 and pH 8.

([pp. 12248-12249] [77], [p. 7317][78], [p. 6849] [79])

Adsorbing polyethyleneimine

In the work conducted by [77] PEI, with an average molecular weight (Mw) of 25 kDa, was used to functionalize Fe_3O_4 MNP by means of adsorption, for the later removal of copper. A stock of PEI was prepared and used to make new solutions with different concentrations. A specified amount of each solution was then added to co-precipitated Fe_3O_4 MNP. After adjusting the pH to 8, the mixtures were sonicated using a sonication probe and left in a heating oven for the adsorption to be completed. The particles were afterwards separated using a magnetic field.

Health Safety and Environment issues regarding nanoparticles

Since nanoparticles are very small they are able to penetrate cells, HSE risks have to be taken into consideration. Materials made of nanoparticles compose a potential treat to both the health of humans as well as the environment all the way from the production cycle to disposing the products after distribution and utilization. The industry acts in a proactive manner and takes precautions in order to reduce the risks associated with nanoparticles. Some of the safety measures are:

- produce and apply nanoparticles in a closed and controlled environment
- homogenize the nanoparticles in a gaseous or liquid medium
- particularly protect the respiratory system
- retrieve used nanoparticles or pretreat them prior to exposing them to the environment
- if the performance can be maintained, use a less toxic nanoparticle

([80], [81])

Chapter 3

Materials and Methods

The presentation of the sample preparations and experimental techniques in this section reflects the chronological order of the work done. The MNP studied in this thesis as well as the characterisation tests are presented in table 3.1.

Table 3.1: The MNP studied in this thesis and the characterisation tests used

Type of MNP	Characterisation tests
Fe_3O_4	Zeta potential and digital video microscope (DVM)
Fe_3O_4/PEI	Zeta potential
Fe_2O_3	Zeta potential and DVM
Fe_2O_3/PEI	Zeta potential, DVM, thermogravimetric analysis (TGA) and BET

The coating was done by modifying the method used in [77]. Milli-Q water (MQ) was used as solvent for all the prepared solutions and phenylacetic acid (PAA) served as the model acid. A simplified model of the coated nanoparticle is illustrated in figure 3.1.

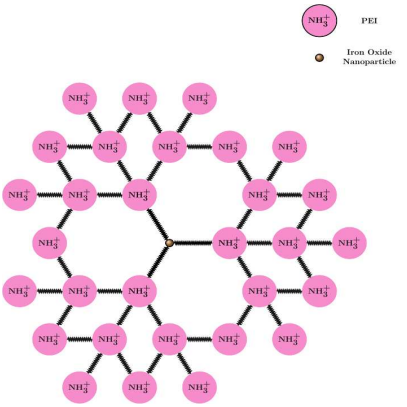

Figure 3.1: Simplified model of PEI coating of the iron oxide MNP

Initially the plan was to use co-precipitated Fe_3O_4 MNP as core for the PEI coating with respect to the adsorption of the model acid. Hence, the experiments began with co-precipitation. Ultra violet (UV) spectroscopy, which was used to test if the PAA could be adsorbed by the PEI coated MNP, concluded the experimental plan.

With the exception of the magnets used for the separation of the Fe_2O_3/ PEI MNP from the supernatant in the mass production, which were of unknown material, all the separations were conducted using Amazing Magnets Grade N40 with the coating NICUNI.

95% confidence intervals have been used to represent the values obtained from the repetitive test from the Zetasizer as well as for the BET. An introduction to the confidence interval is provided in 3.3.1.3. The correla-

tion coefficient is used to indicate how acceptable the data is in the case of linear models. A brief introduction is given in section 3.3.5.1.

Materials

Polyethyleneimine (50 wt%) with a weight average molecular weight of 750.000 and a number average molecular weight of 60.000 was obtained from Sigma-Aldrich, [82]. Iron (II,II) oxide (50-100 nm), iron (III) oxide (<50 nm), phenylacetic acid (99%), 4-ethylbenzoic acid (99%), 97 % reagent grade $FeCl_3$ and hydrochloric acid (37%) were also purchased from Sigma-Aldrich. Anhydrous $FeCl_2$ (99.5 %) was bought from ThermoFisher and sodium hydroxide (>99%) from VWR Chemicals. Synthesised Fe_3O_4 nanoparticles (MAG1) were procured from [83].

Methods and sample preparations

Synthesis of the magnetic iron (II, III) oxide

Co-precipitation, described in section 2.8.1, was chosen as method for the synthesis of the Fe_3O_4 nanoparticles at an inert nitrogen atmosphere at 80 °C. As depicted in equation (3.1), for one batch, 1 M $FeCl_3$ prepared in 20 ml of 0.2 M HCl was blended with 0.5 M $FeCl_2$ prepared in 20 ml of 0.2 M HCl. This mixture was then added dropwise from a burette, during mechanical stirring for five minutes, into a 200 ml solution of 1.5 M NaOH in a three neck flask connected to an Allihn condenser.

$$FeCl_2 + 2\,FeCl_3 + 8\,NaOH \rightarrow Fe_3O_4 + 4\,H_2O + 8NaCl \tag{3.1}$$

The stirring continued for another 20 minutes before cooling the suspension to ambient temperature. The solution was then cleaned with MQ several times in order to remove excess NaOH, using a magnetic field to separate the MNP from the liquid phase. Both batches that were prepared were cleaned until a pH of 8-9 before the produced MNP were transferred into an empty vial with known mass. Any water that was still left was removed using N_2 (g) at 70 °C.

By assuming that only Fe_3O_4 MNP had been produced, the yield could be estimated from equations (3.2) and (3.3) where Mm is the molar mass and m denotes mass.

$$\% \quad \text{yield} = \left(\frac{\text{Actual mass}}{\text{Theoretical mass}}\right) * 100 \tag{3.2}$$

$$\text{Theoretical mass} = m_{FeCl_2} * \left(\frac{Mm_{Fe}}{Mm_{FeCl_2}}\right) + m_{FeCl_3} * \left(\frac{Mm_{Fe}}{Mm_{FeCl_3}}\right) \tag{3.3}$$

An illustration of the experimental setup is shown in figure 3.2. The synthesised MNP were then stored in their solid phase. [84]

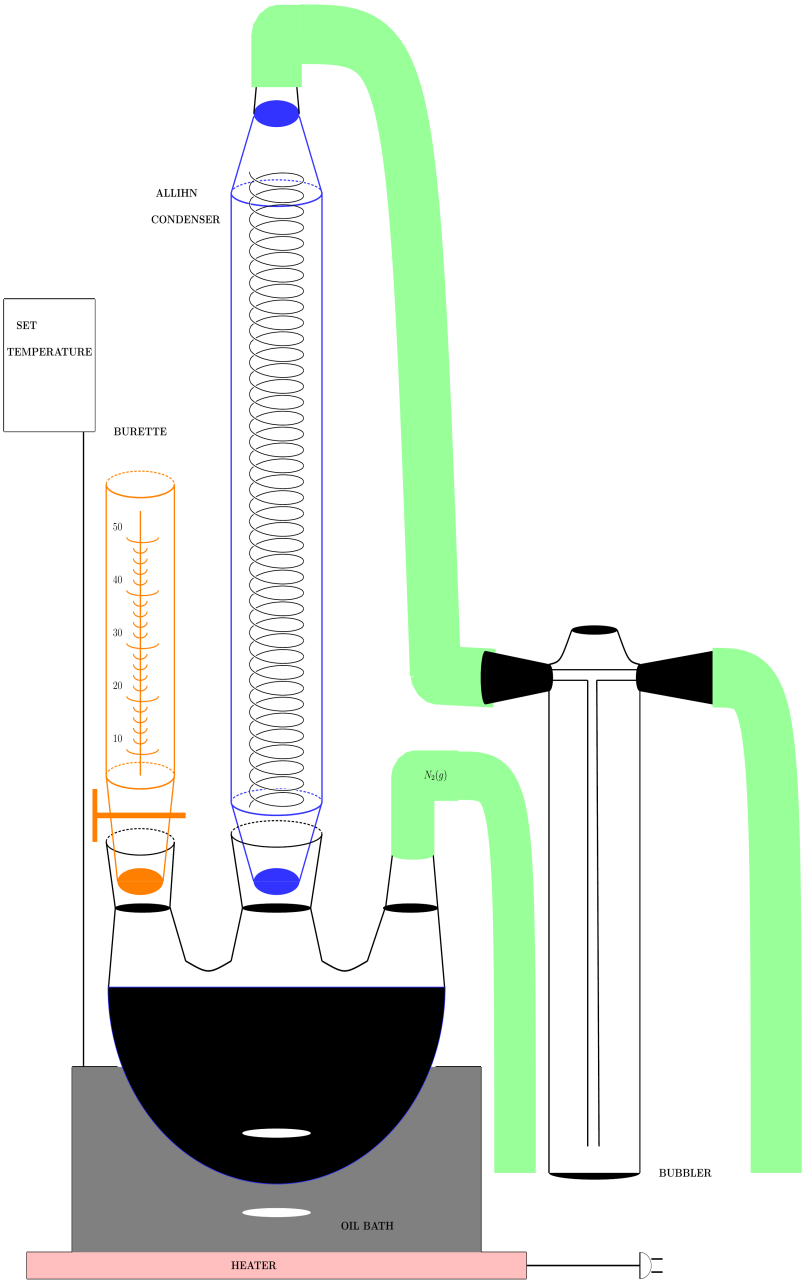

Figure 3.2: Illustration of the synthesis of Fe_3O_4 MNP

Production of polyethyleneimine coated iron (II, III) oxide

Prior to the coating, the zeta potential as function of pH was measured according to the experimental setup in section 3.3.1, both for a stock of PEI with 1 wt% concentration and for the purchased Fe_3O_4 MNP. The coating was only done on the purchased Fe_3O_4 MNP.

Coating of iron (II, III) oxide as function of increased bulk polyethyleneimine concentration

In order to see the effect of the bulk PEI concentration, a stock of PEI with the concentration of 0.33 wt% was prepared using stirring for 30 minutes at 200 rpm. A stock of Fe_3O_4 MNP with the concentration of 1.99 g/L was then prepared and sonicated for 30 minutes.

PEI was added to the Fe_3O_4 MNP suspensions according to table 3.2 once magnetism was ensured. The response to the magnetic field is shown in figure 6.1 in appendix A.

After adding PEI, the suspensions were adjusted to pH 8, with a Mettler Toledo pH meter using small amounts of HCl and NaOH (0.0025 M - 0.025 M), in order to maximize the charge differential between PEI (+ve) and the MNP (-ve) in consistency with [p. 12249] [77]. The suspensions were then shaken overnight using H5 501 digital IKA - WERKE at maximum speed.

Table 3.2: PEI coating of the prepared suspensions of Fe_3O_4 MNP

Sample	Mass stock of Fe_3O_4 MNP (g)	Mass PEI (g)	Mass MQ (g)	Conc. after adding MQ (g/L)
1	2.07	0.00	2.02	1.01
2	2.02	0.02	1.99	1.01
3	2.01	0.04	1.95	1.02
4	2.01	0.32	1.74	1.10
5	2.02	1.03	1.00	1.34
6	2.01	2.03	0.00	1.99

Coating of iron (II, III) oxide as function of constant bulk polyethyleneimine concentration

Based on the conclusion from the 95% confidence intervals for the Fe_3O_4/PEI MNP, given in appendix A, subsection 6.1.2.1, a new coating attempt was made keeping the bulk PEI constant.

The PEI was added directly to the new prepared stocks. The suspensions were adjusted to pH 8 with a Mettler Toledo pH meter using small amounts of HCl and NaOH (0.0025 M - 0.025 M). The suspensions were then shaken overnight using H5 501 digital IKA - WERKE at maximum speed. The suspensions were diluted before running the Zetasizer Nano ZS, due to the concentration range of the instrument (section 3.3.1.2), as shown in table 3.3.

Table 3.3: PEI coating of the prepared suspensions of Fe_3O_4 MNP, new approach

Sample number	Conc. of Fe_3O_4 MNP stock (g/L)	Mass of Fe_3O_4/PEI MNP stock (g)	Mass PEI (g)	Mass MQ (g)
1	4.9	2.01	20.04	5.01
2	9.9	1.00	20.08	5.04
3	24.6	0.42	20.03	5.00
4	44.4	0.21	20.00	5.02
5	99.8	0.11	20.01	5.01

Calcination

An autoclave bomb 4748 was used to calcinate the Fe_3O_4 MNP in an attempt to remove any chemical impurities. An amount of 3.262 g was loaded into the autoclave bomb, which was placed in a Carbolite BWF 11/13 high temperature furnace at room temperature and heated up to 250 °C. The temperature remained constant for three hours at the maximum temperature before cooling down.

Some of the mass of the Fe_3O_4 MNP that was left after the calcination, was dispersed in MQ in order to obtain a concentration of 1.99 g/L (similar to before the calcination) and sonicated for 30 min. A picture was taken using DVM at 10x and compared to the particle size in the picture before calcination. Both pictures are given in appendix A, subsection 6.1.3.

Production of polyethyleneimine coated iron (III) oxide

Since the MNP core had to be changed from Fe_3O_4 MNP to Fe_2O_3 MNP due to the low confidence for the zeta potentials as explained in appendix A, subsection 6.1.2.1, the characterisation tests performed for the original core had to be conducted for the new core:

1. Response to magnetic field
2. Zeta potential as function of pH
3. DVM

A test coating of PEI onto the Fe_2O_3 MNP was conducted using the Zetasizer Nano ZS. A stock of Fe_2O_3 MNP with the concentration of 2.5 g/L (total mass of 50 g) was prepared and sonicated for 10 minutes. The suspension was transferred to a centrifugation tube and centrifuged at 5000 rpm for 20 minutes. The samples were prepared as shown in table 3.4. The samples were then adjusted to pH 8 before shaking overnight as for the PEI coating of the Fe_3O_4 MNP.

Table 3.4: Preparation of the samples for the zeta potential measurements of the Fe_2O_3 MNP and the Fe_2O_3/PEI MNP

Sample number	Volume of Fe_2O_3 MNP supernatant (ml)	Volume of PEI (ml)	Volume of MQ (ml)
1	10	-	10
2	10	10	-

Concentration of the supernatant

Since it had been decided to use the supernatant of the Fe_2O_3 MNP for PEI adsorption (appendix A, subsection 6.1.3), the concentration of the supernatant had to be determined. The subequations (3.4) were used in order to procure this concentration, where the vial with cap is abbreviated to VC.

$$\text{mass}_{\text{ before}} = \text{mass}_{\text{ VC+MNP initially}} - \text{mass}_{\text{ empty VC}} \tag{3.4a}$$

$$\text{mass}_{\text{ after}} = \text{mass}_{\text{ VC+MNP dried}} - \text{mass}_{\text{ empty VC}} \tag{3.4b}$$

$$\text{mass}_{\text{ MQ}} = \text{mass}_{\text{ before}} - \text{mass}_{\text{ after}} \tag{3.4c}$$

$$\text{concentration} = \frac{\text{mass after}}{\text{mass MQ}/1000} \tag{3.4d}$$

Concentration after centrifuging iron (III) oxide with the concentration of 2.5 g/L

The mass of two empty glass vials with cap were determined using a Semi-Crystalline Balance OHAUS Explorer Ex125D, version 2.11/2.12. In order to obtain the most exact values, the vials were cleaned with ethanol prior to the test and only handled with gloves, in order to eliminate any influence by fat.

Two stocks of 2.5 g/L of Fe_2O_3 MNP with a total mass of 50 g were prepared in glass vials and sonicated for at least 10 minutes in a sonication bath. They were then centrifuged at 5000 rpm for 20 minutes. Afterwards 5 ml of the supernatant from each stock were transferred into new glass vials with known mass. The mass of the glass vials with content was noted.

The supernatants were then dried using N_2 g at 70 °C. Once both samples were dry, the glass vials were placed back on the balance in order to note the mass after drying. The calculations are given in appendix C, subsection 6.3.0.1.

Concentration after centrifuging iron (III) oxide with the concentration of 10 g/L

The 2.5 g/L concentration of Fe_2O_3 MNP used for the first coating attempt was too low for the concentration of the supernatant to be determined after the centrifugation as explained in Appendix C, subsection 6.3.0.1. The concentration test was performed again with an increased initial concentration.

The mass of two empty glass vials with cap were determined using a Semi-Crystalline Balance OHAUS Explorer Ex125D, version 2.11/2.12. In order to obtain the most exact values, the vials were cleaned with ethanol prior to the test and only handled with gloves, in order to eliminate any influence by fat.

Two stocks of 10 g/L of Fe_2O_3 MNP with a total mass of 35 g were prepared in glass vials and sonicated for at least 20 minutes in a sonication bath. They were then centrifuged at 5000 rpm for 20 minutes. Afterwards 20 ml of the supernatant from each stock were transferred into new glass vials with known mass. The mass of the glass vials with content was noted. The supernatants were then dried using N_2 g at 70 °C. Once both samples were dry, the glass vials were placed back on the balance in order to note the mass after drying. The calculations are given in appendix C, subsection 6.3.2.1.

Polyethyleneimine concentration affecting the adsorption onto iron (III) oxide

Once the concentration of the supernatant for Fe_2O_3 MNP had been determined, it was of interest to test the effect of the concentration of PEI on the adsorption onto the Fe_2O_3 MNP, as it had been done for the initial core.

Due to the concentration range for the Zetasizer Nano ZS (section 3.3.1.2), five ml of the obtained Fe_2O_3 MNP supernatant with the concentration of 0.88 g/L was diluted by adding 25 ml of MQ. Hence, the concentration used of Fe_2O_3 MNP supernatant for the PEI coating was 0.15 g/L.

In consistency with [77], pH 8 had been chosen for the adsorption of PEI onto Fe_2O_3 MNP. Both the PEI stock and the diluted Fe_2O_3 MNP supernatant was adjusted to pH 8 prior to the coating. With respect to the supernatant the pH adjustment was done with a Mettler Toledo pH meter using small amounts of HCl and NaOH (0.0025 M - 0.025 M) after sonication for one minute. To ensure a homogeneous pH distribution, the IKA MS basic shaker was used. The PEI stock was adjusted while stirring.

Immediately after adding the polymer, sonication was done in an ultrasonication bath for four minutes. During the following hour sonication was repeated four times for about 30 seconds. The particles were then left standing over night in room temperature in order to allow the adsorption to be completed.

The different solutions used for the Zetasizer Nano ZS are presented in table 3.5, where the bulk PEI was procured from equation 3.5 using a PEI stock of 0.509 wt%.

Table 3.5: Preparation of the solutions for adsorption of PEI onto the Fe_2O_3 MNP at pH 8

Sample number	Mass Fe_2O_3 (g)	Mass stock PEI (g)	Mass MQ (g)	Bulk PEI (wt%)
1	2.00	0.00	2.00	0.00
2	2.02	0.02	2.0	0.002
3	2.02	0.06	1.94	0.01
4	2.00	0.26	1.80	0.03
5	2.01	1.01	1.03	0.13
6	2.02	2.02	0	0.26

Mass production of the polyethyleneimine coated iron (III) oxide

Once the concentration of the supernatant of the Fe_2O_3 had been procured and the effect of the concentration of PEI on the adsorption onto Fe_2O_3 MNP had been obtained from the Zetasizer Nano ZS, the mass production of the Fe_2O_3/PEI MNP began.

For one batch 10 parallel stocks of Fe_2O_3 MNP were prepared with the concentration of 10 g/L and the complete mass of 35 g in glass vials. Each stock was then sonicated for at least 20 minutes in a sonication bath. In order to ensure balance in the centrifuge the mass transferred to the centrifugation tube was noted, and an equal mass of MQ was loaded into another centrifugation tube. Two stocks were centrifuged at the same time for 20

minutes at 5000 rpm.

While the first stock was prepared for centrifugation, the other stock remained in the sonication bath. This was done as it, at an early stage in the experiments, was noticed that the dispersed particles sedimented fast and the dispersion was less homogeneous when transferred to the centrifugation tube (appendix C, subsection 6.3.2).

After the centrifugation, 20 ml of the supernatant from each stock was transferred into a new glass vial[1] using a FinTip pipette (5 ml). The supernatant was then adjusted to pH 8 with a Mettler Toledo pH meter using small amounts of HCl and NaOH (0.0025 M - 0.025 M). To ensure a homogeneous pH distribution, the IKA MS basic shaker was used.

A stock of PEI (0.509 wt%) was prepared by loading 0.660 g of PEI into a bottle and adding MQ until a total mass of 64.8 g. The solution was then stirred at 500 rpm for 1 hour before the pH was adjusted to pH 8 with 1M HCl and 0.25 M NaOH also using the Mettler Toledo pH meter.

Based on the effect of the concentration of the bulk PEI on the adsorption onto the MNP, represented in the figure 4.9, an amount of five g of the PEI stock was added to each 20 ml Fe_2O_3 supernatant (0.88 g/L). The bulk PEI was estimated from equation (3.5).

$$\text{Bulk PEI} = \text{Stock solution [wt\%]}(\frac{m_{PEI}}{m_{tot}}) \tag{3.5}$$

In a similar manner, the concentration after coating for the Fe_2O_3 MNP can be determined.

Immediately after adding the polymer, sonication was done in an ul-

[1] MNP stick to plastic, especially when charged

trasonication bath for four minutes. During the following hour sonication was repeated four times for about 30 seconds. The particles were then left standing over night in room temperature in order to allow the adsorption to be completed.

The particles were then separated for three hours using a magnetic field[2]. About 60% -70 % of the supernatant could be removed, depending on the strenth of the magnetic field. The removed liquid volume was replaced with MQ before sonication for one minute.

After the cleaning, the suspensions spent 48 hours on the magnets before drying with N_2 g at 80 °C. This was done, as it at an early stage (section 4.5.1), was noticed that the drying was too time consuming at 70 °C. After the second separation about 90% of the supernatant could be removed.

[2]Uknown material

Separation of the polyethyleneimine coated iron (III) oxide nanoparticles from the supernatant using a magnetic field

Initially for the first batch of mass produced Fe_2O_3/PEI MNP (vials 9-19), three hours of separation using magnets was used prior to cleaning with MQ. In an optimization attempt of losing less MNP when continuing the mass production (batch 4), pictures were taken after three, six and 24 hours respectively in order to look for any great turbidity difference. These pictures are given in appendix D, subsection 6.4. However, since only a small turbidity difference could be detected three hours were kept as separation time prior to the cleaning.

Experimental setup for characterisation methods

Zeta potential

Auto titration

The automatic titrator connected to the Malvern Zetasizer Nano ZS can be used to automatically adjust the pH by adding small amounts of 0.25 M HCl and 0.25 M NaOH to a solution or suspension prior to measuring the zeta potential. A small magnet is used to even distribute the added acid or base. For each time the pH is adjusted, a new value for the zeta potential is obtained.

Concentration range

When testing the zeta potential some requirements exist with respect to the concentration. A detector inside the Zetasizer Nano ZS, which is used to procure the zeta potentials, display a count rate that indicates if the concentration of the sample is within the range of the instrument or not. [p. 6.6] [49]

Confidence interval representation

In order to represent the zeta potential from the curve that is obtained from the Zetasizer Nano ZS software, both the mean and the standard deviation are of interest. Natural distributed data is assumed. For a 95 % confidence interval an analyst will be 95 % confident that the unknown population mean will be captured by the obtained interval [p.345] [85].

There are two ways to estimate the sample standard deviation. If the individual values within a sample (parallel) are unknown, the sample standard deviation can be obtained from the population mean as depicted in equation (3.7). However, if the individual values are known equation (3.8) can be used instead. [86]

The data points will be located far from the mean if the standard deviation value is large and close to the mean if the value is small [p.40] [85]. In other words, when the margin of error is small the accuracy of the measurement is higher.

The estimations are done in excel based upon the following mathematical formulas [pp.30,39] [85]:

$$\bar{\mathrm{x}} = \frac{1}{\mathrm{n}} \sum_{i=1}^{\mathrm{n}} \mathrm{x}_i \tag{3.6}$$

$$\mathrm{s} = \sqrt{\frac{1}{\mathrm{n}-1} \sum_{i=1}^{\mathrm{n}} (\mathrm{x}_i - \bar{\mathrm{x}})^2} \tag{3.7}$$

$$\sigma = \sqrt{\frac{\sum_{i=1}^{\mathrm{m}} \mathrm{s}_i^2}{\mathrm{m}}} \tag{3.8}$$

With respect to one parallel, n, is the number of measurements, the, $\mathrm{x_i}$, indicates the zeta potential of one measurement, the, $\bar{\mathrm{x}}$, represents the mean of all the measurements and, s, is the sample standard deviation. Equation (3.8) is used to get an estimate of the standard deviation for the parallels combined, where, m, is the number of parallels and, $\mathrm{s_i}$, is the standard deviation for each parallel.

In other words, the zeta potential will be represented as a range of values

as shown in equation (3.9):

$$\text{estimate} \pm \text{margin of error} \tag{3.9}$$

where the estimate of the zeta potential of population (each pH value) is the mean, equation (3.6), of the parallels and the margin of error is represented as the standard deviation of the parallels combined. The margin of error for a 95 % confidence interval [pp.344-345] [85] is calculated from:

$$\text{margin of error} = 1.960(\frac{\text{s}}{\sqrt{\text{m}}}) \tag{3.10}$$

It can be observed from equation (3.10), that the margin of error is dependent upon the amount of samples. Hence, in order to reduce the margin of error the sample size (m) can be increased. Since the mean is not a resistant measure, outliers can have a large influence on the confidence interval. [pp. 347-350] [85]

If a test is performed for the population mean, whether the true mean has been determined or not can be decided using a hypothesis test. If the confidence intervals do not overlap, then the true mean cannot be in both confidence intervals. One of them has to be rejected. However, there are two types of error that results from incorrect decisions.
[pp. 370-390] [85]

Execution of the Zetasizer Nano ZS

Parameters and cells used for the measurement of the zeta potential

The zeta potential was measured at 25 °C using the Helmholz-Smoluchowski model, the equilibration time was set to 120 seconds. The different parameters used are provided in table 3.6

Table 3.6: Parameters for the analysis of the zeta potential

Parameters	**PEI**	**Fe_2O_3 & Fe_3O_4 MNP**	**Fe_3O_4/PEI MNP**	**Fe_2O_3/PEI MNP**
Refractive index	Polystyrene Latex	Graphene Oxide	Polystyrene Latex	Polystyrene Latex
Time delay (s)	60	10	30	30
Measurements	5	3	5	3
Maximum runs	50	100	100	100
pH range	7-11	4-9	8	7-9

Two different cells were used in order to measure the zeta potential. An illustration of the disposable folded capillary cell is depicted in figure 3.3a. The reusable Dip cell with a cuvette made of quartz, is shown in figure 3.3b).

When the sample was loaded into the quartz cuvette, it was tilted 45 °. The same angle was used when inserting the Dip cell in order to avoid air bubbles. The cell was cleaned before it was used each time in 0.0025 M HCl in an ultrasonication bath.

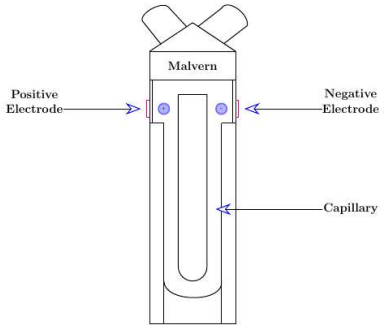

(a) Capillary cell

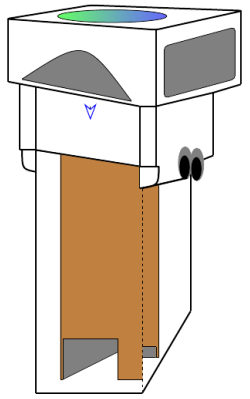

(b) Dip cell

Figure 3.3: Illustration of the different cell types used for the Zetasizer

Zeta potential for the iron oxide nanoparticles

In order to find the isoelectric point for the naked MNP core it was decided to run the Zetasizer Nano ZS for both the purchased MNP and the synthesised MNP. The zeta potential for the Fe_3O_4 MNP obtained from [83]

(denoted MAG1 MNP), was determined from auto titration using the disposable capillary cell.

When determining the zeta potential the Dip cell was used for the purchased MNP as well as for the synthesised Fe_3O_4 MNP in addition to the Fe_3O_4/PEI MNP and Fe_2O_3/PEI MNP. The pH was manually adjusted using a Mettler Toledo pH meter by adding small amounts of HCl and NaOH (0.0025 M - 0.025 M) after sonicating the suspensions for 1-2 minutes. The measurements were conducted with the parameters given in section 3.3.2.1.

It was decided to superimpose all the obtained zeta potentials as function of pH in order to see of the isoelectric point occured at the same pH value.

Zeta potential for polyethyleneimine

Since the isoelectric point for all the tested uncoated nanoparticles, with exception of the purchased Fe_3O_4 MNP, had been observed at pH 7 as presented in the results (section 4.2.1), it was of interest to test how the electrokinetic mobility of PEI would change from this pH. A solution of PEI with the concentration of 1 wt% was prepared. The measurements were conducted with the parameters given in section 3.3.2.1.

The disposable folded capillary cell was used when measuring the zeta potential, and the pH was adjusted using the titrator. Between each test the cell was cleaned with 96 % ethanol and MQ as the electrodes became black quite fast.

Using the zeta potential to test optimal pH for polyethyleneimine coating of iron (III) oxide

The choice of pH 8 for the PEI adsorption was based on [77] for the initial Fe_3O_4 MNP, however, it was also pointed out in [77] that maximum adsorption could take place between pH 6 and pH 8. In order to test if pH 8 was still the optimal pH for the adsorption of PEI after changing the MNP to Fe_2O_3 MNP, additional zeta potentials were tested for pH 7 and 9 for the coated and uncoated particles and superimposed with the data from pH 8 (sample 6, section 4.4.1).

Since the Fe_2O_3 MNP had the isoelectric point at pH 6 as shown in section 4.2.1, this pH was excluded. pH 9 was included, though, in order to see what would happen when the Fe_2O_3 MNP had more negative charges, but PEI less positive charges.

The solutions prepared for the optimization test are given in table 3.7. Equal amounts of PEI and Fe_2O_3 MNP were used in order to be at the saturation limit. The coating was done according to section 3.2.5.

With respect to the instabillity of the naked MNP when suspended in water, it of interest to compare the obtained 95% confidence intervals for the uncoated Fe_2O_3 MNP from this optimization test, to the 95% confidence intervals that was initially obtained for the uncoated Fe_2O_3 MNP. The result obtained is presented in appendix B section 6.2.

Table 3.7: Preparation of the solutions for the optimization test of PEI adsorption onto the Fe_2O_3 MNP

Sample number	Mass Fe_2O_3 (g)	Mass stock PEI (g)	Mass MQ (g)	Bulk PEI (wt%)
Blank pH 7	2.02	0	2.02	0.00
Coated pH 7	2.00	2.01	0	0.26
Blank pH 8	2.00	0	2.00	0.00
Coated pH 8	2.02	2.02	0	0.26
Blank pH 9	2.02	0	2.01	0.00
Coated pH 9	2.00	2.01	0.00	0.26

Digital Video Microscope

The Nikon Eclipse ME600 fitted with a CoolSNAP camera by Media Cybernetics with the installed software Image-Pro-Plus 5.0 was used in order to take digital pictures. A drop of the system to be studied was placed on a glass disk after the focal plane was found.

With respect to comparison, pictures were taken prior to any treatment for both Fe_3O_4 MNP and Fe_2O_3 MNP. In order to test the effect of centrifugation and coating on the Fe_2O_3 MNP with respect to size and polydispersity, additional pictures were taken.

The pictures of the Fe_2O_3 MNP with the initial concentration of 2.5 g/L were taken prior to any optimization adjustments. Hence, these are presented in appendix C, subsection 6.3.1.

The pictures taken of the Fe_2O_3 MNP with the initial concentration of 10 g/L are presented in the results, since these were taken of mass produced Fe_2O_3/PEI MNP.

Thermogravimetric Analysis

TGA was performed using TA Instruments Q600 SDT Thermogravimetric Analyzer with DSC in order to determine the mass of PEI compared to the mass of Fe_2O_3 MNP. In other words, TGA could determine whether PEI had been adsorbed or not in addition to how good the adsorption was.

When running the instrument the decrease in mass was measured as function of time in a controlled atmosphere provided by N_2 g (100 ml/min). The Fe_2O_3/PEI MNP were loaded into one of the alumina pans used and the temperature was allowed to increase from 10 °C to 800 °C, using fast ramp, where it remained for three minutes before cooling down to room temperature. As the instrument measures the mass exactly, it was no need to use a balance prior to running the test.

Gas adsorption

As the nanoparticles have a large surface compared to their volume, it is important to determine the specific surface area, which is the total area (A_{tot}) accessible to adsorption for a unit mass of solid (m_{tot}). The specific surface area of the Fe_2O_3/PEI coated MNP was obtained using the BET method. The determination of using the BET isotherm is consistent with [5], which points out that the BET isotherm is the standard equation for obtaining the specific area from gas adsorption data [p. 413].

This method assumes that the data fits the BET isotherm and estimates the amount of adsorbed nitrogen gas on the magnetic nanoparticle surface given a known mass of particles at known pressure. The BET value is defined as the specific area of a surface and is shown in equation (3.11).

$$BET_{\text{surface area}} = A_{\text{sp}} = \frac{A_{\text{tot}}}{m_{\text{tot}}} = \frac{3}{\rho R_{\text{s}}} \tag{3.11}$$

Using software the specific surface area can be obtained from equation (3.12) where σ^0 is the area of surface occupied per molecule and the molar volume of the adsorbing gas (N_2 g) is 22.414 cm^3 /mole given the volume of the adsorbents in a monolayer, V_{m}.

$$A_{\text{sp}} = \frac{V_{\text{m}} N_{\text{A}} \sigma^0}{22.414} \tag{3.12}$$

[pp. 8, 334,409, 431] [5]

Correlation coefficient

Correlation is a dimensionless measurement, which indicates how good the linear model is. It is a number between -1 and 1, where values close to 0 indicates a weak linear relationship. Perfect correlation occurs at $\pm$ 1. [pp. 103-105] [85].

Execution of gas adsorption

Two parallels of Fe_2O_3/PEI MNP were conducted. The MNP were loaded into a sample tube with known mass. After obtaining an exact value for the mass of particles, the sample was degassed over night at room temperature using the Micromeritics Vac Prep 061 Sample Degas System as shown in figure 3.4.

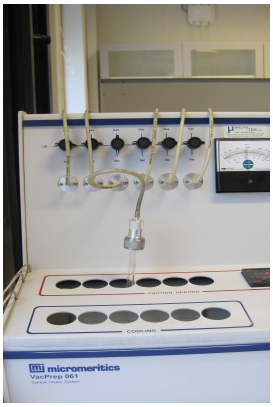

Figure 3.4: Degassing the pores of the sample

When the sample had reached a preasure of 150 mTorr it was moved to the Micromeritics Tri Star 3000 Surface Area and Porosity Analyzer. Liquid nitrogen was placed underneath the sample tube during the analysis (figure 3.5).

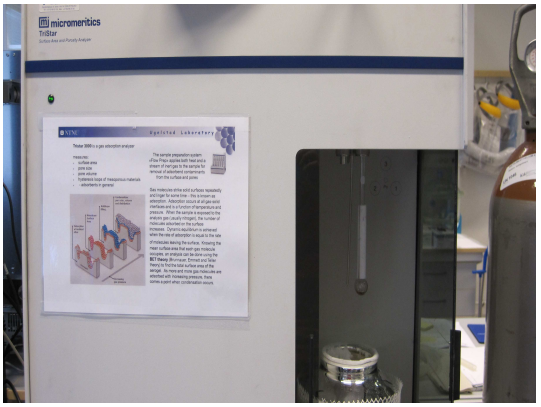

Figure 3.5: Running the gas adsorption

The mass of sample was typed into the created file in order to obtain BET. The mass was measured after the test as well, due to the potential loss of particles during the test. For both parallels that were run, a small decrease in particle mass was detected. Hence, the BET was recalculated by the software.

Ultra Violet spectroscopy and the removal of the model naphthenic acid

The UV-visible spectroscopy is a technique, which measures the energy absorbed when the valence electrons are excited to a higher energy level. Due to this electronic excitation, changes in the electronic, vibrational and rotational energy levels of the molecule are induced. The excitation can be between bonding and anti-bonding orbitals as well as between non-bonding and anti-bonding ones, since the anti-bonding orbitals have the highest energy level. For benzene the maximum absorbance occurs at 255 nm [87]. Since this is the aromatic ring present in PAA a change in the spectre is expected to appear close to this wavelength.

Shimadzu UV-2401PC Recording Spectrophotometer with UVProbe Ver. 2.10 was used to procure calibration curves and to perform test adsorptions using Fe_2O_3/ PEI MNP. The baseline was set using MQ in order to remove any background noise. The most diluted sample was loaded first into the quartz cuvette, after loading MQ again. If the concentration was too high (outside of the linear range), the sample was diluted using MQ. During the analysis energy is absorbed. Using the Beer - Lambert equation, given in section 3.3.6.1, the amount of adsorbed acid could be estimated by means of surface excess as shown in section 3.3.6.2.

As indicated in equation (2.2), the NA are dissociated at a high pH and hence distributed in the water phase. At a low pH most acids are in the oil phase as they remain undissociated. Reinsel et al. [13] suggested that below pH 5 most naphthenic acids are undissociated and thus in the oil phase.

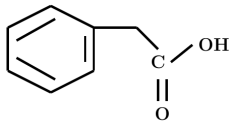

(a) Undissociated state

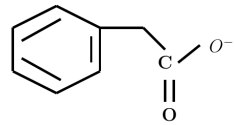

(b) Dissociated state

Figure 3.6: Phenylacetic acid as model NA

Absorbance and Beer - Lambert equation

The spectre obtained is a plot of the wavelength of the light absorbed against the absorbance, where the wavelength of the maximum absorbance is given as $\lambda_{\max}$.

Generally the absorbance of a detected compound is proportional to the concentration in accordance with Beer-Lambert equation (3.13), where A is the absorbance, c is the concentration of the solute in the sample, ϵ is the molar absorptivity and l is the length of the light path in cm through the sample.

$$A = \epsilon cl \tag{3.13}$$

The intensity of the light of the reference beam is denoted I_0 whereas the intensity of the light after the radiation has passed through the sample is I. The logarithm of the ratio of these intensities is another way to depict the absorbance as indicated in equation (3.14).

$$A = log(\frac{I_0}{I}) \tag{3.14}$$

It may be noted that the Beer-Lambert law has its limitations. [pp. 119-121, 126] [88]

Surface excess

The surface excess dentoted, Γ, can be defined as the ratio between the amount of moles of an adsorbed component and the area of the interface as given in equation (3.15). Another way to depict the surface excess is the difference of the adsorbed component (the solute on the surface) and the solute in the bulk. The surface excess can experimentally be obtained from the concentration difference of the adsorbate in the bulk initially (c_0) and the equlibrium concentration (c_e) for a known the BET value and the bulk volume, V.

$$\Gamma = \frac{V(c_0 - c_\mathrm{e})}{\mathrm{Surface\ area}} = \frac{V \triangle c}{\mathrm{BET\ mass}} \tag{3.15}$$

[pp. 324-326] [5]

Calibration curve of phenylacetic acid, pH 8

A stock solution of 1.5 g/L PAA was prepared and the pH adjusted to 8. At this pH the acid is negatively charged. The UV absorption was measured at wavelength range 400-200 nm. Pure MQ was loaded as blank in order to get the baseline, thus removing background noise. The range of concentrations used, 0.01 g/L - 0.87 g/L, made from the stock and the corresponding max absorbances are located in table 6.7 in appendix F.

Test adsorption of phenylacetic acid, pH 8

In order to test if the prepared Fe_2O_3/PEI MNP could be used to adsorb PAA, two different methods were attempted and compared to the effect of the uncoated core. All the tests were done in room temperature.

First a stock of PAA with the concentration of 1.5 g/L was prepared. The solution was then stirred at 600 rpm for 1 hour and adjusted to pH 8. The amount of Fe_2O_3/PEI MNP needed for the test adsorption was determined using the average BET value of 62.5 m^2/g in order to ensure 95 % confidence (section 4.6). It was assumed a surface execss of 1 mg/m^2 and a concentration difference of 0.5 g/L for PAA as in [89] due to the similarities of the MNP core. The prepared suspensions for the test adsorptions are provided in table 3.8.

Table 3.8: Test adsorption of PAA at pH 8

Method	**Mass Fe_2O_3/PEI MNP (g)**	**Mass Fe_2O_3 MNP (g)**	**Mass PAA (g)**
Sonication	0.0452	-	5.0079
Shaking	0.0542	-	5.0022
Shaking	-	0.053	5.187

With respect to using shaking as a method, the PAA solution was added to the Fe_2O_3/PEI MNP and Fe_2O_3 MNP in separate glass vials. The shaking was done using H5 501 digital IKA - WERKE at 300 rpm overnight. The following day (the tests were done separately) the suspension was placed on a magnet for separation.

As for sonication as a method, the sonication was done in a sonication bath for five minutes immediately after adding the PAA solution to the Fe_2O_3 MNP in a glass vial. During the following hour sonication was repeated four times for about 30 s. The suspension was then left overnight without further treatment. The following day the suspension was placed on a magnet for separation.

For both methods once the separation was complete, the supernatant was loaded into a quartz cuvette in order for the UV absorbance to be measured. If the concentration of PAA was too high (not in the linear range), the supernatant was diluted with MQ. The initial bulk concentration could then be estimated from equation (3.16).

$$c_1 = c_2(\frac{m_1 + m_{\text{MQ}}}{m_1}) \tag{3.16}$$

Calibration curve of phenylacetic acid, pH 4.5

Due to the negligible adsorption of PAA at pH 8, another test adsorption at a pH close to the pK_A was performed. Hence, a new calibration curve was needed. The choice was made due to the affinity of PAA (section 4.7.2). For PAA pK_A is 4.31 at 25 °C [90]. A stock of PAA with the concentration of 0.15 g/L was made and adjusted to pH 4.5. The UV absorption was measured at wavelength range 400-200 nm. The range of concentrations used, 0.04 g/L - 0.14 g/L, made from the stock and the corresponding max absorbances are located in table 6.9 in appendix F.

Test adsorption of phenylacetic acid, pH 4.5

Since the sonication gave a slightly better result than the shacking at pH 8, the test adsorption at pH 4.5 (table 3.9) was done using sonication for five minutes immediately after adding the PAA solution to the Fe_2O_3/PEI MNP. During the following hour sonication was repeated four times for about 30 s. The test adsorption was done in room temperature. The amount of Fe_2O_3/PEI MNP needed, remained equal to the amount used for the test adsorption of PAA at pH 8. If the concentration was outside the linear range, the supernatant was diluted with MQ.

Table 3.9: Test adsorption of PAA at pH 4.5

Method	**Mass Fe_2O_3/PEI MNP (g)**	**Mass PAA (g)**
Sonication	0.0454	5.0163

Calibration curve for 4-ethylbenzoic acid, pH 4.5

Since the affinity for the model acid towards the water affects the amount adsorbed onto the coated MNP, a test adsorption using 4-ethylbenzoic acid (EBA) was attempted. A stock with the concentration of 0.17 g/L was prepared using stirring at 700 rpm for more than four hours. The solution was then adjusted to pH 4.5 in order to obtain a calibration curve close to the pK_A for EBA, which is 4.35 [91]. The UV absorption was measured at wavelength range 400-200 nm. As for PAA the peak was close to the maximum absorbance for benzene as mentioned in section 3.3.6. The range of concentrations used, 0.01 g/L - 0.03 g/L, made from the stock and the corresponding max absorbances are located in table 6.10 in appendix F.

Test adsorption of 4-ethylbenzoic acid

The test samples used for the test adsorption is given in table 3.10. Immediately after adding EBA to the Fe_2O_3/PEI MNP, sonication was done for five minutes as for the PAA at pH 4.5. During the following hour sonication was repeated four times for about 30 s. The test adsorption was done

in room temperature. The amount of Fe_2O_3/PEI MNP needed, remained equal to the amount used for the test adsorption of PAA at pH 8. If the concentration was outside the linear range, the supernatant was diluted with MQ.

Table 3.10: Test adsorption of EBA at pH 4.5

Method	**Mass Fe_2O_3/PEI MNP (g)**	**Mass EBA (g)**
Sonication	0.0513	5.0378

Chapter 4

Results and Discussion

This chapter aims to present the main results from the chemical analysis as well as the adsorption of the model NA. The presentation is organized according to the very structure of the experiments, starting with the yield from the co-precipitation. However, the main results related to the original Fe_3O_4 MNP and the results from the optimization steps related to the Fe_2O_3/PEI MNP have been presented in the appendices.

For all pH adjustments severeal measurements were performed in order to ensure that the pH remained in the following interval: pH $\pm$ 0.05. Hence, the pH values are presented as whole numbers whenever used, as the effect on the system from the lower boundary to the upper boundary is not expected to be significant.

Co-precipitation of magnetic iron (II, III) oxide

Using co-precipitation the first synthesised batch had a yield of 37 %, whereas the second batch had a somewhat higher yield of 44 %. These values are low compared to the work done by [89] where the yield of co-precipitated Fe_3O_4 were 72% and 109 % for batch one and two respectively.

The low yield for both batches was mainly due to loosing a lot of the obtained MNP during the cleaning procedure with MQ. The separation of the obtained MNP from the water was done only using a magnetic field. In the experiments performed by [89], a rotavapor (LaboroTA 4003, Heidolph) was used to reduce the amount of MQ in the suspension.

Perhaps less MNP had been lost if centrifugation could have been used after testing the magnetism with an external field. The excess NaOH might then have been removed together with the supernatant as the “cake ”at the bottom of a centrifugation tube would have been re-dispersed with MQ a few times. Another possible way to reduce the loss of the MNP could be to add HCl and neutralize the NaOH. Yet another parameter that could have decreased the loss of the MNP, is time. The MNP could have been left on the magnet overnight between each cleaning. However, this is a time consuming method if several cleanings are necessary.

Due to the low yield, it was decided to use the purchased Fe_3O_4 MNP as core for the PEI coating.

Zeta potential for the pH estimation

Since the pH has an important effect on the PEI adsorption onto the iron oxide MNP the zeta potential was measured for a range of pH values for both uncoated MNP (- ve) and the polymer (+ ve).

Surface charge for uncoated iron oxide as function of pH

The zeta potential as function of pH for both purchased iron oxide MNP and synthesised iron oxide MNP (section 2.8.1) were measured for comparison, including the MNP obtained from the work done by [83]. By superimposing the zeta potentials, it can be observed in figure 4.1 that the isoelectric point occurs at about pH 6-7, with the exception of the purchased Fe_3O_4 MNP. The deviation may be due to different batches or impurities.

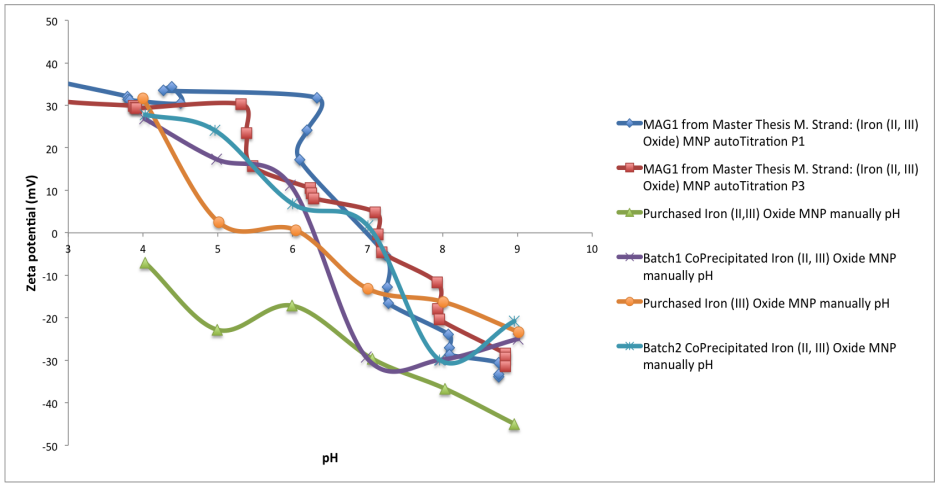

Figure 4.1: Zeta potential as function of pH for the iron oxide MNP

A note has to be made regarding the auto titration of the MAG1 from

[83], which was conducted as part of the training of the Zetasizer NanoZS. Since this method was no longer possible for the other iron oxide MNP, then it was concluded after performing the test that the time that has past since they were co-precipitated has had an effect on the size since they were uncoated. In other words the magnetism was lower for the MAG1 MNP, than for the new co-precipitated Fe_3O_4 MNP (Batch1 and Batch2) and the purchased MNP. Hence, it was decided to adjust the pH manually for the latter MNP.

Surface charge of polyethyleneimine as function of pH

As indicated in figure 4.2 the highest zeta potential values were noticed at pH 7 and pH 8 for PEI (1 wt% solution). As the pH increased, the zeta potential decreased and became negative somewhere between pH 10 and pH 11. Due to the basic environment the PEI then changed from positive to neutral.

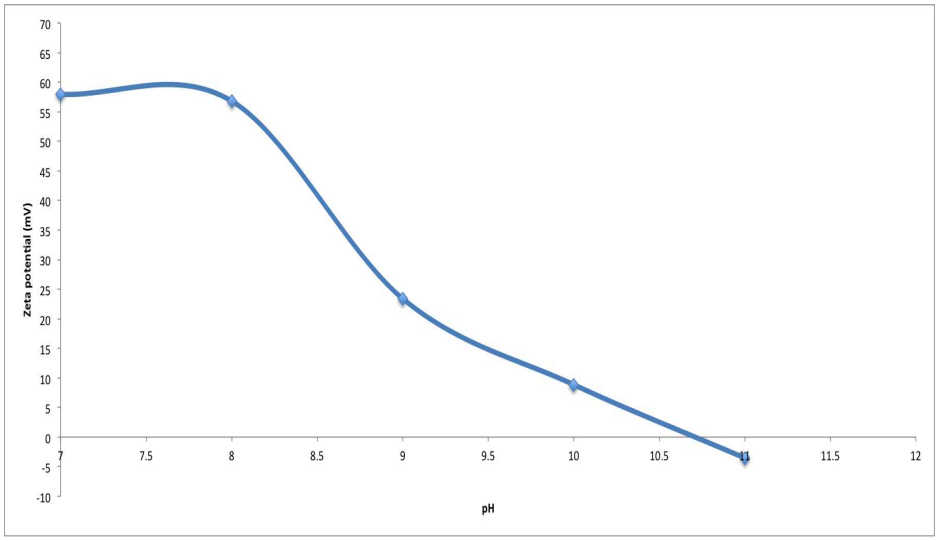

Figure 4.2: Zeta potential as function of pH for PEI

The 95 % confidence intervals for the zeta potential of PEI as function of pH is given in table 4.1. The largest margin of error was obtained for pH 8. The true zeta potential may then be as high as 64.3 mV or as low as 49.3 mV. This indicates that in the worst case for pH, the zeta potential is lower than the worst case for pH 7 (54.5 mV). Nonetheless, both pH 7 and pH 8 are consistent with [77], which found that the optimal pH for the adsorption of PEI onto Fe_3O_4 MNP is in the range from pH 6 to pH 8 (section 2.12.3).

Table 4.1: 95 % confidence intervals of the zeta potential as function of pH for PEI

pH 7	pH 8	pH 9	pH 10	pH 11
58.0 $\pm$3.5	56.8 $\pm$7.5	23.4 $\pm$0.9	8.9 $\pm$1.0	-3.5 $\pm$1.1

Summary of the development of the coating procedure

A summary of the methods involved when developing the coating procedure for the PEI functionalized iron oxide MNP is provided by means of figure 4.3 and 4.4. These figures serve two purposes: Presenting the main results without too many details and a visualization of the thought process involved in order to start mass production. All the main results from this part have been provided in the appendices.

As previously mentioned, the Fe_3O_4 MNP were used initially as core for the PEI functionalization, however, due to the low confidence of capturing the true zeta potential as indicated both in figure 6.2 and in the tables provided in appendix A, subsection 6.1.2, the Fe_3O_4 MNP were replaced by the Fe_2O_3 MNP, which are in a more oxidized state [32]. The picture taken of the dispersed Fe_3O_4 MNP, using DVM, is shown in figure 6.3 in the appendix B. It was also decided to use centrifugation in order to remove any MNP large enough to affect the result from the Zetasizer Nano ZS. The characterization tests conducted on the original Fe_3O_4 MNP are presented in figure 4.3. The parameters used for the zeta potential in addition to the model are given in section 3.3.2.1.

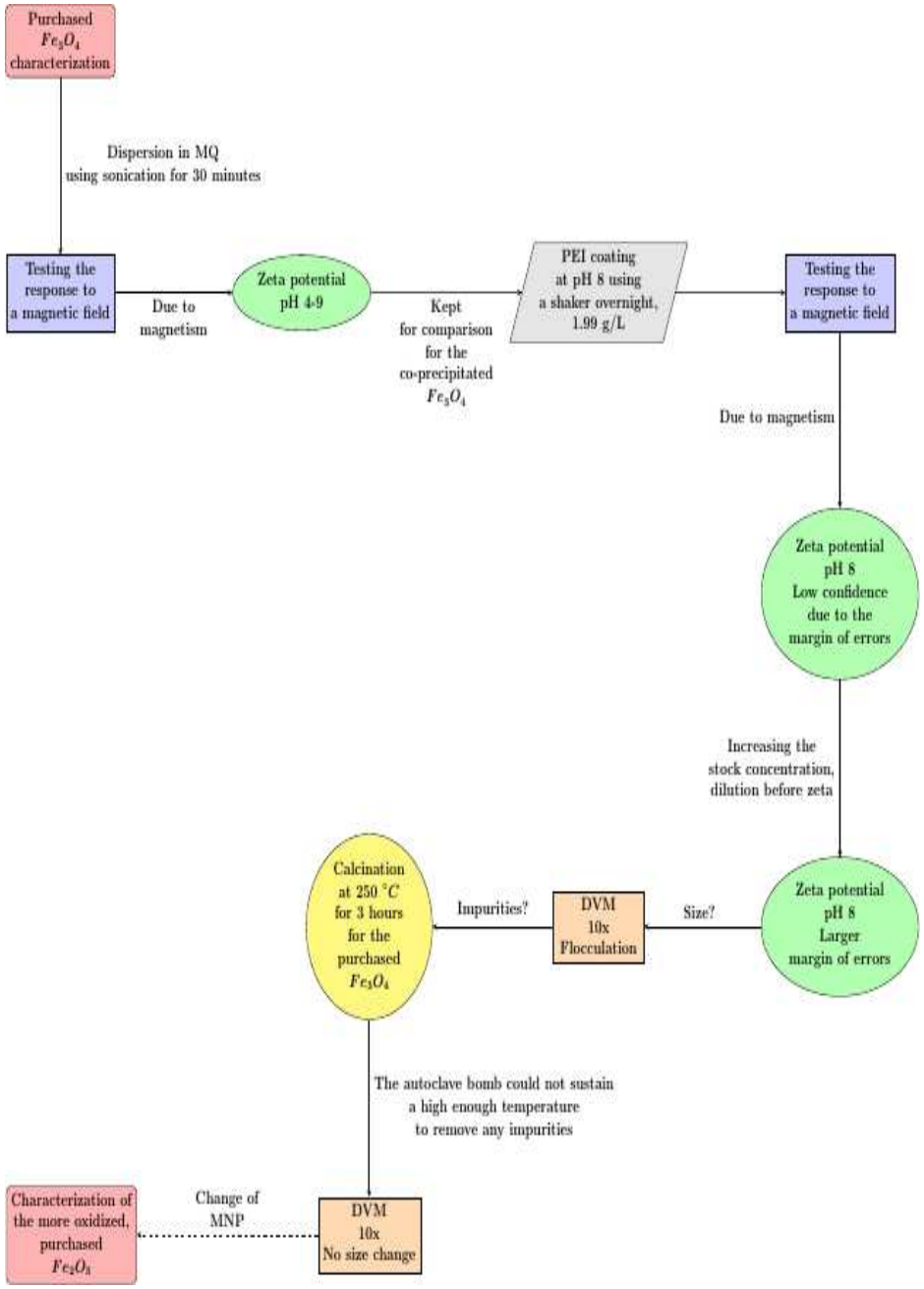

Figure 4.3: Characterization of the Fe_3O_4 MNP for PEI coating

The steps taken using Fe_2O_3 MNP until mass production of the Fe_2O_3/PEI MNP could be conducted are depicted in figure 4.4. Since the supernatant of the Fe_2O_3 MNP was used for PEI adsorption, the concentration of the supernatant had to be determined. As mentioned in section 3.3.3, pictures were taken using DVM in order to see the effect of the different steps taken in order to improve the method.
Based on these results from the DVM and the difference in the turbidity in appendix C, subsection 6.3.2, an initial concentration of 10 g/L was used for Fe_2O_3 MNP with a complete mass of 35 g in addition to the improved sonication procedure with respect to optimizing the parameters in the mass production of Fe_2O_3/PEI MNP.

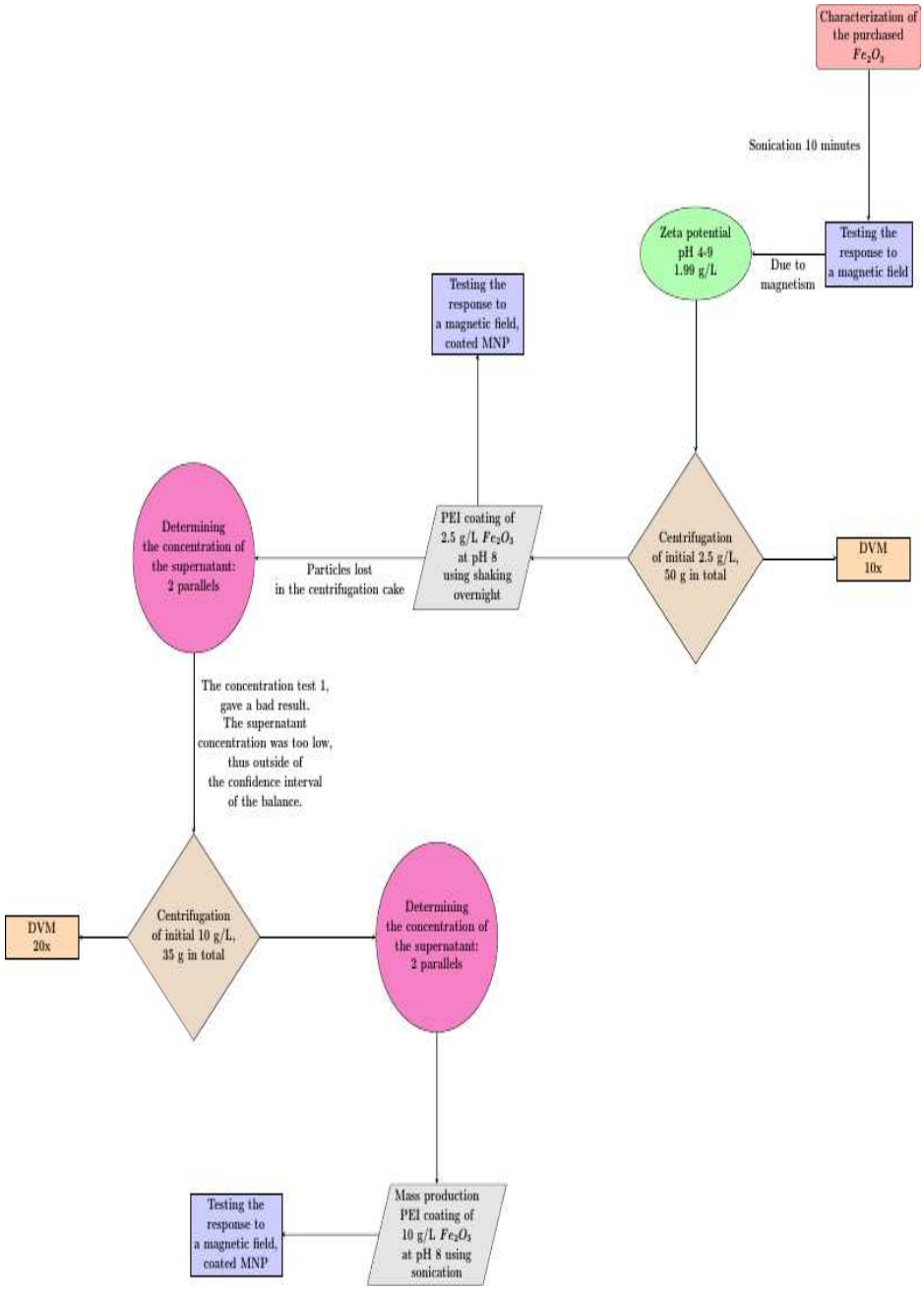

Figure 4.4: Characterization of the Fe_2O_3 MNP for PEI coating

Characterisation of iron (III) oxide

Magnetism

In order to be able to use the purchased Fe_2O_3 MNP, magnetism had to be ensured. The response of the uncoated particles with the concentration of 2.5 g/L, which was immediate, is shown in figure 4.5.

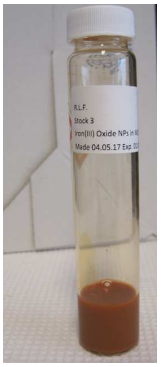

(a) Without magnet

(b) With magnet

Figure 4.5: Purchased Fe_2O_3 MNP

Digital video microscope of iron (III) oxide

For Fe_2O_3 MNP with the concentration of 2.5 g/L a picture was also taken at 10x for comparison to the Fe_3O_4 MNP given in figure 6.3. The image is shown in figure 4.6. The degree of polydispersity seemed to be lower than for the Fe_3O_4, which may be the result of different production methods.
In order to get an impression of the size and the distribution of the uncoated Fe_2O_3 MNP (2.5 g/L) before any treatment was conducted, a picture was taken using DVM at 10x. The particles seemed both smaller and less poly-

dispersed than the purchased Fe_3O_4 MNP (figure 6.3) given in appendix B, subsection 6.1.3.

The actual size of the Fe_2O_3 MNP can be estimated from dynamic light scattering (DLS). Due to the time frame, however, this was not done.

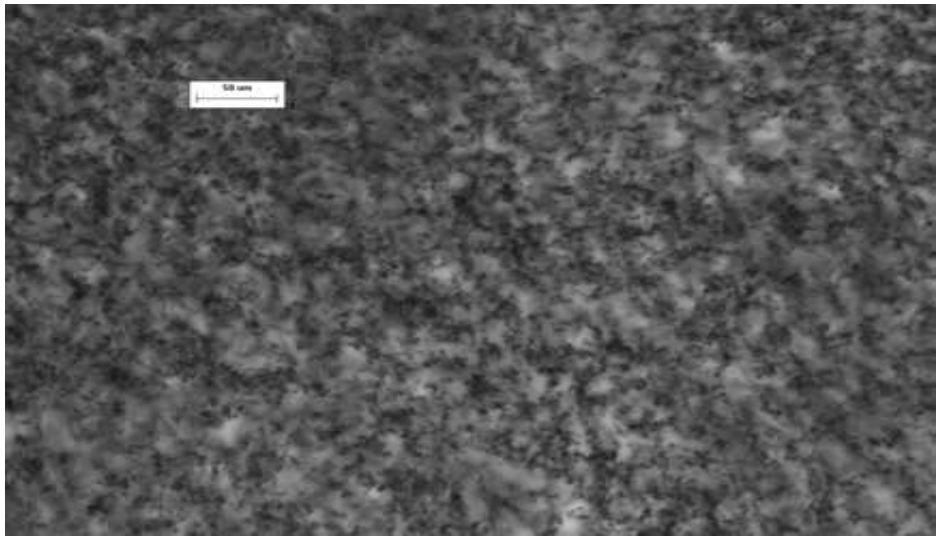

Figure 4.6: Particle size of Fe_2O_3 MNP

Effect of centrifuging iron (III) oxide after procedure improvements

A magnification of 20x was needed in order to capture the image given in figure 4.7 of the supernatant with the concentration of 0.88 g/L. The calculations yielding this concentration are located in the appendix C, subsection 6.3.2.1.

The better dispersion and the smaller particle size may be due to improving the homogeneity of the suspension, by allowing the particles to sonicate for as long as possible before transferring the content to the centrifugation tube. Decreasing the total mass of the initial concentration (10 g/L) to 35 g, may also have had a positive effect as less particles were left behind during the transfer to the centrifugation tube. Pictures supporting this hypothesis are given in the appendix C, subsection 6.3.2.

In the image presented it is possible to see small particles separated from each other. The polydispersity is low compared to the polydisperisty and size distribution depicted both in figure 4.6 and in figure 6.5, which was expected after performing the centrifugation under optimal conditions.

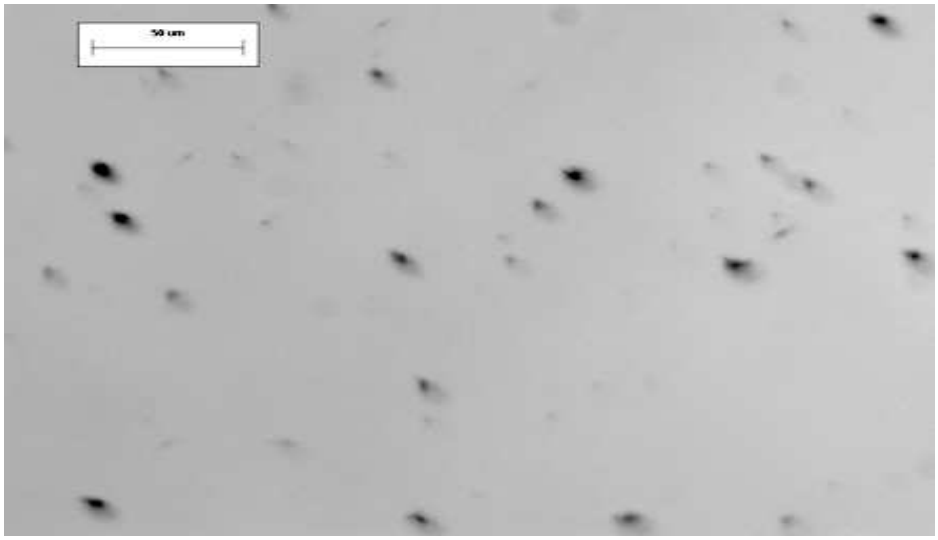

Figure 4.7: Particle size of the supernatant of the Fe_2O_3 MNP with the concentration of 0.88 g/L

Effect of the polyethyleneimine coating of iron (III) oxide

Magnetism

After coating of the Fe_2O_3 MNP (0.88 g/L) the magnetism was intact as shown in figure 4.8. Once the vial was placed on the magnet, the MNP became attracted to the magnetic field in less than one minute. The magnet had been moved up and down the outside of the vial once in order to get a better picture of the response.

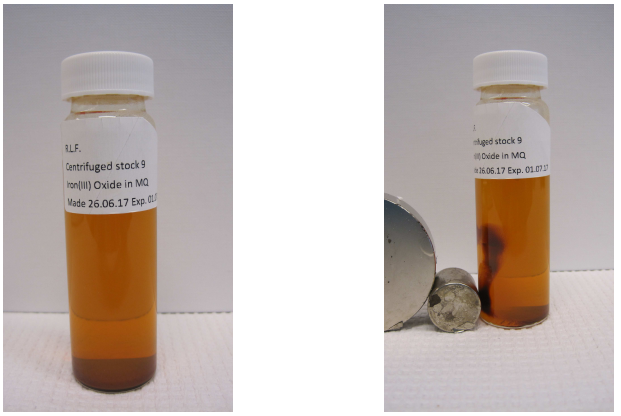

(a) Without magnet **(b)** With magnet

Figure 4.8: Response to external magnetic field after coating

Effect of the concentration of polyethylenemine

When the effect of the bulk PEI was to be determined a stock of PEI was used with the concentration of 0.509 wt% at pH 8. The adsorption onto Fe_2O_3 MNP reached the saturation limit quite fast, as depicted in figure 4.9. Increasing the concentration of PEI would cause no further adsorption possibly due to the steric hindrance provided by the polymer.

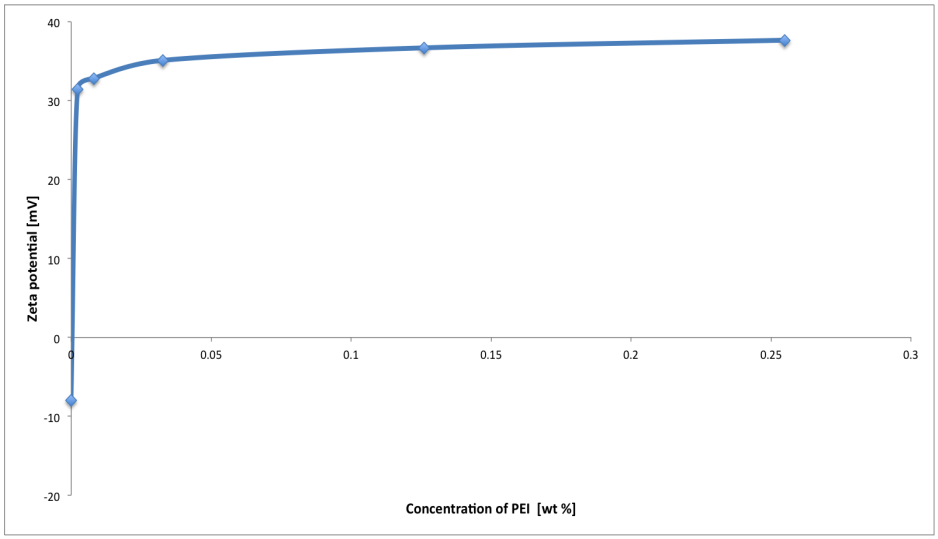

Figure 4.9: Adsorption limit of PEI at pH 8

The margin of error is small as shown in table 4.2, thus there is a high confidence that the true zeta potential has been captured for each pH. A clear difference is observed when comparing these 95% confidence intervals to the 95% confidence intervals given in table 6.1 in appendix A.

Table 4.2: 95% confidence interval for the zeta potential for the Fe_2O_3/PEI MNP

Bulk BEI (wt%)	**95% confidence interval**
0.00	-8.0 $\pm$4.4
0.002	31.5 $\pm$1.1
0.01	32.8 $\pm$0.6
0.03	35.1 $\pm$0.4
0.12	36.7 $\pm$0.6
0.25	37.7 $\pm$1.0

There are several parameters that can have an influence on this higher confidence. A summary of the parameters are given in table 4.3 along with a suggested effect on the system.

Table 4.3: Parameters affecting the higher confidence and possible explanation

Parameter	**Suggested explanation**
Change of MNP	Fe_2O_3 MNP are more oxidized than Fe_3O_4 MNP
Decreased total mass of Fe_2O_3 MNP suspension	Volume smaller than centrifugation tube. Hence, more small MNP could be a part of the supernatant.
Sonication during coating	Better dispersion
Optimized centrifugation	Low polydispersity

Zeta potential for pH optimization

As indicated in figure 4.10 pH 9 would not have been the best choice for the coating, since the zeta potential is below +30 mV. In other words, the MNP are in the unstable region where the vdW attractive forces are greater than the electrostatic repulsion. The MNP will coalescence in consistency with the theory in section 2.8.5.

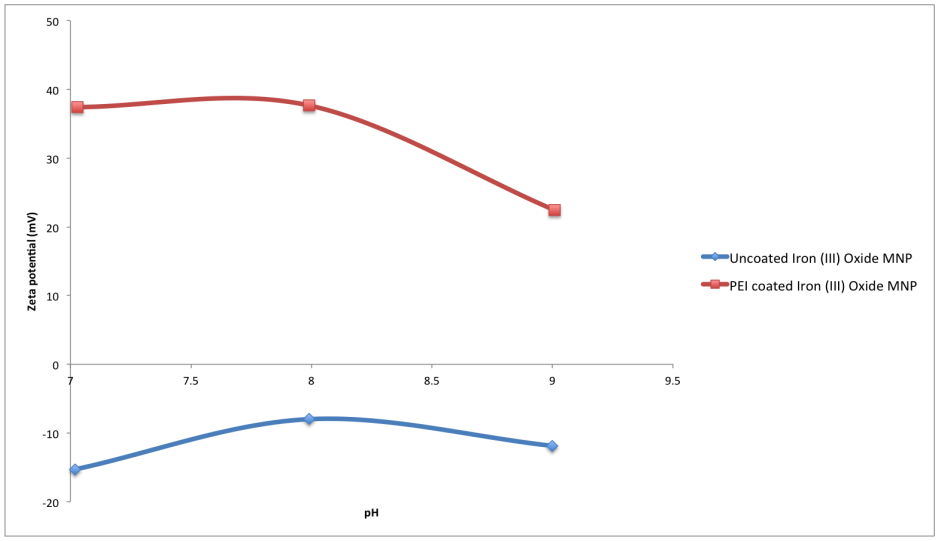

Figure 4.10: The effect of pH on the adsorption of PEI

Only a small difference between pH 7 and pH 8 can be observed after the coating, though with respect to the margin of error given in table 4.4, pH 8 was kept at the optimal value.

Table 4.4: 95% confidence intervals of the zeta potential as function of pH for Fe_2O_3/PEI MNP

pH 7	pH 8	pH 9
37.4 $\pm$3.5	37.7 $\pm$1.0	22.4 $\pm$0.6

By comparing figures 4.1 and 4.10 it is also observed that the zeta potentials for the uncoated Fe_2O_3 MNP deviate. The 95 % confidence intervals of the experimental zeta potentials for the uncoated Fe_2O_3 MNP, which also indicate this instability, are given in tables in the appendix A subsection 6.2. The deviation may be caused by different stocks being tested or that the system is not too far from the isoelectric point and simply displays the expected instability.

Additionally, since the 95% confidence intervals for pH 9 did not overlap, the instability of the system itself when suspending the Fe_2O_3 MNP in MQ may have been detected as explained in Appendix A, subsection 6.2.

Perhaps future tests such as TGA can verify whether pH 8 actually is the optimal pH for PEI adsorption onto Fe_2O_3 MNP or if pH 7 is better.

Mass production of polyethyleneimine coated iron (III) oxide

Separation of the polyethyleneimine coated iron (III) oxide nanoparticles from the supernatant using a magnetic field

Initially the second separation for the first batch of the mass produced Fe_2O_3/PEI MNP was allowed 24 hours on the magnets yielding the turbidity as shown in figure 4.11a. About 40 % of the supernatant volume could be removed with a pipette. Four of the vials containing Fe_2O_3/PEI MNP were dried using N_2 g. Since three days were necessary in order to remove the rest of the MQ even after increasing the temperature to 80 ° C from 70 ° C, the other vials with Fe_2O_3/PEI MNP were allowed 48 hours of separation when placed back on the magnets.

As indicated in figure 4.11b more particles had been attracted by the magnet after 48 hours, thus as much as 90 % of the supernatant could then be removed before drying the particles. The drying was then done after approximately five hours as opposed to three days.

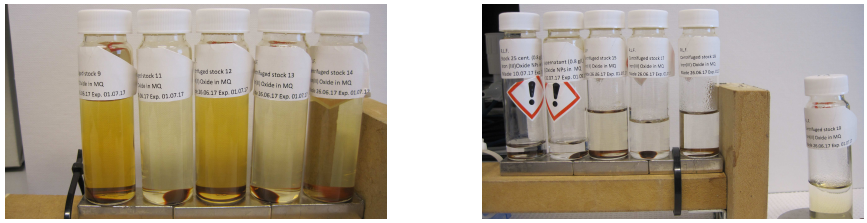

(a) After 24 hours **(b)** After 48 hours

Figure 4.11: Separation using a magnetic field

Another interesting result was also detected. When gathering the Fe_2O_3/PEI MNP for the TGA, the mass obtained from three vials was noted to be 0.035 g. This indicated that an average mass of 0.011 g could be retrived from one vial.

After the separation time on the magnets had been increased to 48 hours, the average from one vial was determined again. This time the mass from one vial was 0.014. This indicated that by increasing the time, more supernatant could be removed without loosing any MNP and the coating procedure became more efficient since the one batch could be dried in one day compared to one week[1].

[1] About five vials could be dried simultaneously.

Digital video microscope

For comparison a picture was taken after the PEI coating of the Fe_{23} MNP, before drying, at 20x. However, due to poor quality this image had to be discarded later. Hence, additional pictures were taken of redispersed Fe_2O_3/PEI MNP at 20x. Two of the pictures taken of the redispersed Fe_2O_3/PEI MNP (0.88 g/L) are shown in figure 4.12. It is clearly indicated that the polymer acts as a flocculant, since the floccs is so easily observed particularly in figure 4.12b. The size is large compared to the size indicated in figure 4.7. Furthermore, as the sizes range from a few µm to nearly 50 µm when superimposing the two random samples taken from the suspension, it can be conluded that there is a high degree of polydispersity in the system.

(a) Random drop 1 of redispersed Fe_2O_3/PEI MNP

(b) Random drop 2 of redispersed Fe_2O_3/PEI MNP

Figure 4.12: Size distribution, 20x

Thermogravimetric Analysis

For a sample of 26.22 mg the composition with respect to mass for the Fe_2O_3/PEI MNP was 6 wt%, as idicated in figure 4.13. The result is based on the inspection of the curve, which is displayed from left to right.

Initially, between 0 ° C and 100 ° C, any remaining water was burned off. By inspecting the y-axis of the graph the mass of water is 2 wt%. The PEI then started to decompose at about 100 ° C until about 400 ° C where there a change in the slope can be detected and the core began to decompose.

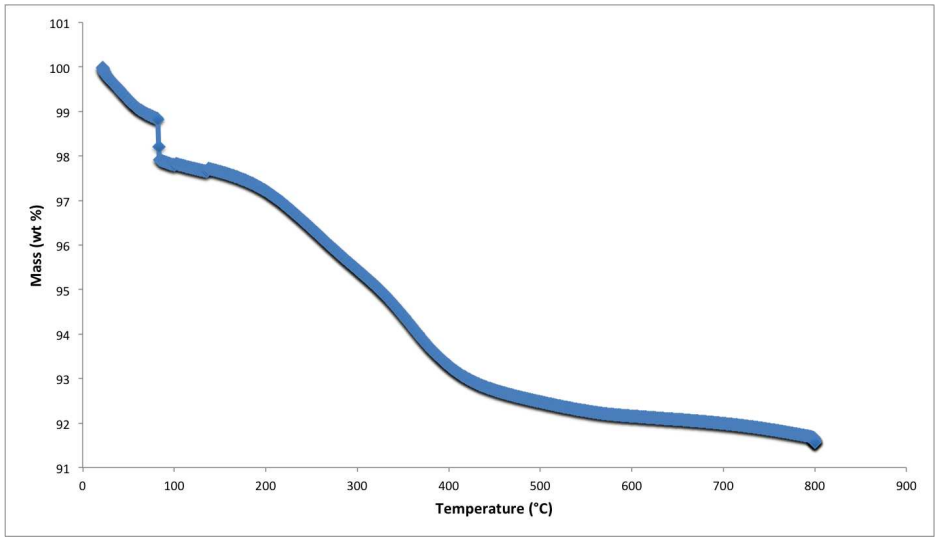

Figure 4.13: Decrease in particle mass with time

The functionalization of the Fe_2O_3 MNP by PEI was also indicated by the change in color of the dry powder. In figure 4.14 a black metallic colour is observed as opposed to the brown colour of the uncoated Fe_2O_3 MNP as shown in the suspension in figure 4.5a.

Figure 4.14: Solid state of Fe_2O_3/PEI MNP

Gas adsorption for polyethyleneimine coated iron (III) oxide

For both parallels the correlation coefficient is close to 1, which indicates that there is a positive linear association. The correlation also depicts how acceptable the obtained values are (3.3.5.1).

Table 4.5: BET surface area, its correlation coefficient, R, and the cross-sectional area for Fe_2O_3/PEI MNP

Parallel	Mass Fe_2O_3/PEI MNP (g)	BET surface area (m^2/g)	Correlation	Molecular cross-sectional area (nm^2)
1	0.0428	65.7 $\pm$0.2	0.99	0.16
2	0.0896	59.3 $\pm$0.2	0.99	0.16

Based on the parallels there is 95% confidence that the true BET, which was used in the estimation of the amount of Fe_2O_3/PEI MNP needed, is 62.5 m^2/g due to the low margin of error: 62.5 ± 0.2.

Figure 6.11 in the appendix E section 6.5 shows that both monolayer adsorption and monolayer adsorption were present.

Surface excess of polyethyleneimine on the surface of iron (III) oxide

Based on the mass of PEI from TGA and the BET value for the Fe_2O_3/PEI MNP, the surface excess of the polymer could be determined by combining equation (3.15) and equation (3.11). The amount of PEI adsorbed onto Fe_2O_3 MNP was 0.92 mg/m^2. Whether the adsorption could be maximized by means of detecting and removing potential chemical impurities in consistency with [p. 8652][75], is beyond the scope of this thesis.

Removal of model naphthenic acid using polyethyleneimine coated iron (III) oxide

Separation of the polyethyleneimine coated iron (III) oxide nanoparticles in a phenylacetic acid solution

After shaking the Fe_2O_3/PEI MNP were separated from the 1.5 g/L PAA solution using a magnet. The response to the magetic field was instantaneous. It can be observed in figure 4.15a that the particles are located on the right hand side at the bottom. This was a consecuence of the response not being uniform, hence the magnet was placed on the side of the vial first before placing it underneath. No turbidity of the supernatant was observed.

With respect to the sonication the reponse was uniform when placed on the magnet as indicated in figure 4.15b. The attraction to the magnetic field was immediately for the sonication as well.

(a) Magnetic response for shaking

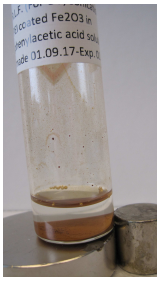

(b) Magnetic response for sonication

Figure 4.15: Comparison of the responses to the same magnetic field for Fe_2O_3/PEI MNP

Separation of iron (III) oxide nanoparticles in a phenylacetic acid solution

The uncoated Fe_2O_3 nanoparticles was separated from the PAA solution (1.5 g/L) using a magnetic field as shown in figure 4.16. The separation occured within one minute.

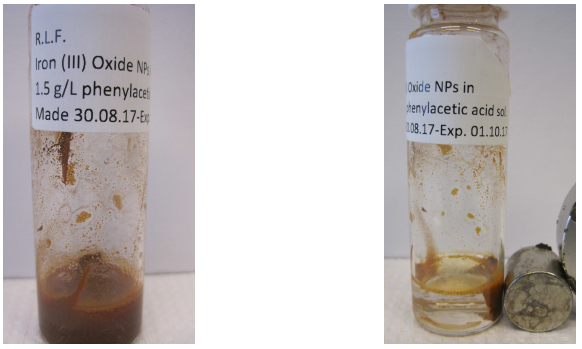

(a) Without magnet **(b)** With magnet

Figure 4.16: Response to the magnetic field for Fe_2O_3

Calibration curve for phenylacetic acid, pH 8

The calibration curve for PAA at pH 8, shown in figure 4.17, was used for the the estimation of the supernatant in the test adsorption. Since the squared value of the correlation coefficient is high, the linear model is representative. The linear function is given in equation (4.1).

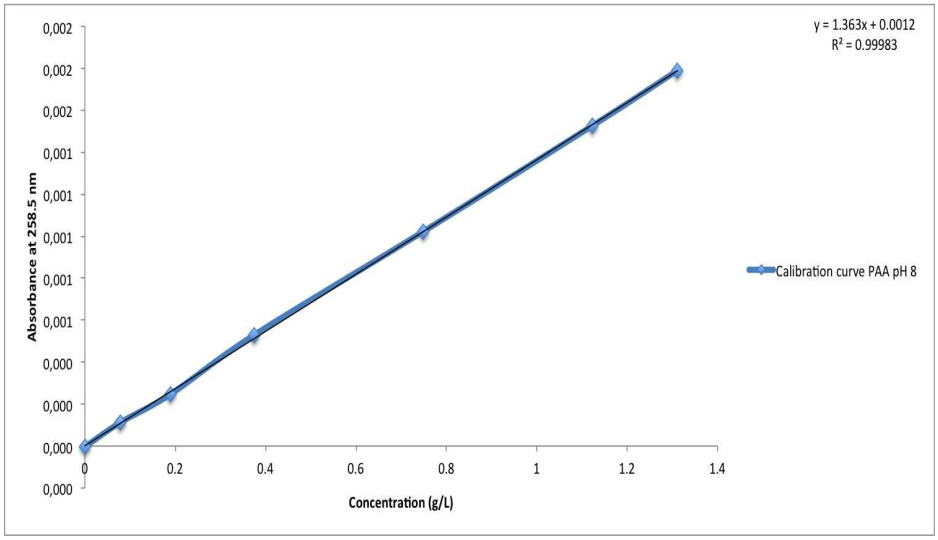

Figure 4.17: Calibration curve for PAA at pH 8

$$A = 1.363c + 0.0012 \tag{4.1}$$

Test adsorption for phenylacetic acid, pH 8

For the three test adsorptions that were conducted on the supernatant after separating the Fe_2O_3/PEI MNP from the solution, equation (4.1) was used to estimate the unknown concentrations as the UV provided the maximum absorbance at 258.5 nm.

Given table 3.8, the values for the surface excess were procured by combining equations (3.15) and (3.11). The equilibrium concentration, q_e, was procured from equation (2.36). Since the supernatant had to be diluted, the values for the bulk was estimated using equation (3.16).

Table 4.6 provides the results after the test adsorption at pH 8 using the value from balance for the known stock 3 of PAA with the concentration 1.5 g/L.

Table 4.6: Surface excess and equilibrium concentration of PAA given the concentration difference, pH 8

Sample MNP	**Abs. at 259 nm**	$\mathbf{C_e}$ **diluted (g/L)**	$\mathbf{C_e}$ **(g/L)**	$\mathbf{\triangle C}$ **(g/L)**	**Surface excess** $\mathbf{(mg/m^2)}$	$\mathbf{q_e}$
Sonicat. Fe_2O_3/PEI	0.82849	0.61	1.52	-0.02	-0.03	-0.002
Shaking Fe_2O_3/PEI	0.79446	0.58	1.54	-0.04	-0.06	-0.004
Shaking Fe_2O_3	0.83124	0.61	1.56	-0.06	-	-0.01

Since stock 3 of PAA with a concentration of 1.5 g/L also had been loaded, the first step in figuring out the negative results was to check if the absorbance would give 1.5 g/L using the procured calibration curve.

$$1.363c = 0.59265 - 0.0012 \rightarrow c = 0.4339 \rightarrow 1.5637$$

Table 4.7 shows the values obtained when the calibration curve was used to estimate the bulk concentration (1.5637 g/L).

Table 4.7: Surface excess and equilibrium concentration of PAA given the concentration difference, pH 8

Sample MNP	**Abs. at 259 nm**	$\mathbf{C_e}$ **diluted (g/L)**	$\mathbf{C_e}$ **(g/L)**	$\triangle$**C (g) /L**	**Surface excess** $\mathbf{(mg/m^2)}$	$\mathbf{q_e}$
Sonicat. Fe_2O_3/PEI	0.82849	0.61	1.52	0.05	0.08	0.01
Shaking Fe_2O_3/PEI	0.79446	0.58	1.54	0.03	0.04	0.002
Shaking Fe_2O_3	0.83124	0.61	1.56	-0.01	-	0.01

In case there were any chemical impurities present in PAA that could affect the adsorption, it was decided to measure the zeta potentials as function of pH. See appendix F, subsection 6.6.2.

It was concluded, however, that since PAA initially has a high affinity for water, PAA when in dissociated state could remain dissolved in the water and not attach itself to the Fe_2O_3/PEI MNP surface. Hence, another test

adsorption was of interest at a lower pH in order to decrease the affinity for water.

Calibration curve for phenylacetic acid at pH 4.5

Due to the negligible adsorption of PAA at pH 8, another test adsorption at a pH close to the pK_A was performed. The new calibration curve, which was obtained from the prepared solutions, given in table 6.9 in appendix F, is shown in figure 4.18. Since the squared value of the correlation coefficient is high, the linear model is representative. The linear function is given in equation (4.2).

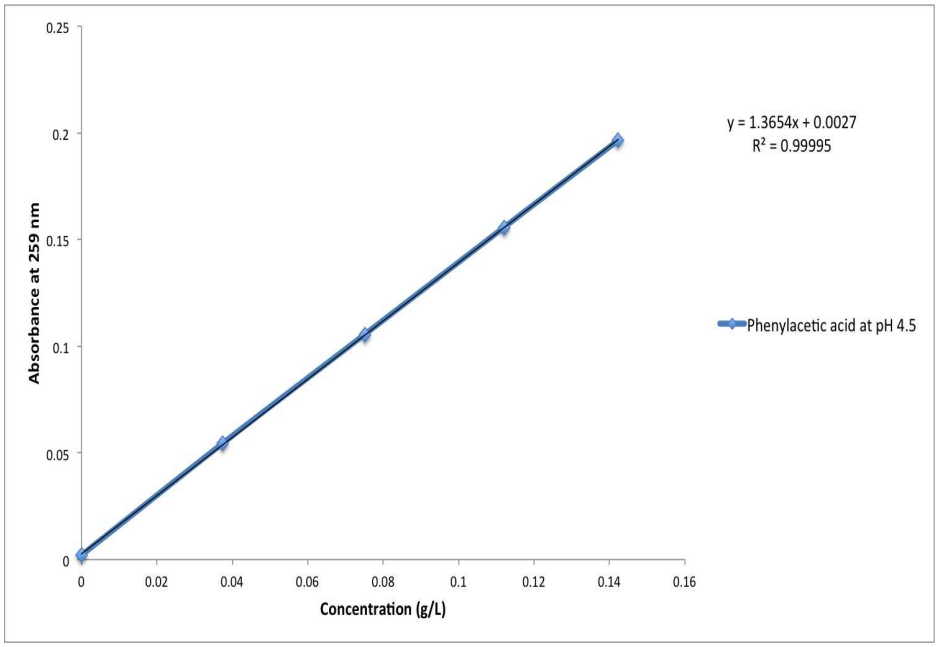

Figure 4.18: Calibration curve for PAA at pH 4.5

$$A = 1.3654c + 0.0027 \tag{4.2}$$

Test adsorption of phenylacetic acid at pH 4.5

As indicated in figure 4.19, the separation time needed at pH 4.5 is longer than for pH 8 where the response was immediately.

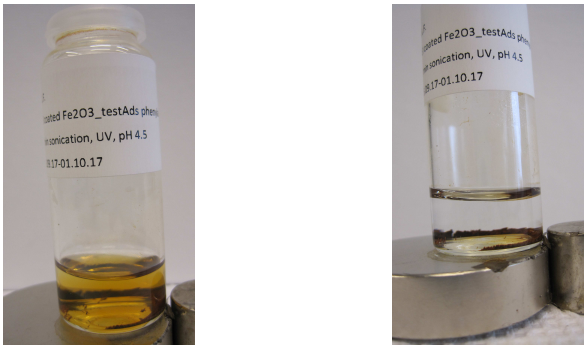

(a) 2 hours **(b)** 3 days

Figure 4.19: Response to the magnetic field

As for pH 8 the concentration difference has been estimated using both the value from the balance and the calibration curve for the known concentration. A deviation was present again, however, at the pH close to the $\mathrm{pK_A}$ an adsorption was detected. The surface excess was determined to be 0.28 mg/m^2.

Table 4.8 shows the results using the value obtained from the balance for the known bulk concentration of stock: 0.15 g/L

Table 4.8: Surface excess and equilibrium concentration of PAA given the concentration difference, pH 4.5

Sample MNP	**Abs. at 259 nm**	$\mathbf{C_e}$ **diluted (g/L)**	$\mathbf{C_e}$ **(g/L)**	$\mathbf{\triangle C}$ **(g/L)**	**Surface excess** $\mathbf{(mg/m^2)}$	$\mathbf{q_e}$
Sonicat. Fe_2O_3/PEI	0.15913	0.12	1.34	0.16	0.28	0.02

$$1.36654c = 0.15553 - 0.0027 \rightarrow c = 0.1119 \rightarrow 1.4346$$

Table 4.9 shows the results when the concentration difference was estimated based on the bulk concentration obtained from the calibration curve: 1.4346 g/L. The surface excess was determined to be 0.16 mg/m^2.

Table 4.9: Surface excess and equilibrium concentration of PAA given the concentration difference, pH 4.5

Sample MNP	**Abs. at 259 nm**	$\mathbf{C_e}$ **diluted (g/L)**	$\mathbf{C_e}$ **(g/L)**	$\mathbf{\triangle C}$ **(g/L)**	**Surface excess** $\mathbf{(mg/m^2)}$	$\mathbf{q_e}$
Sonicat. Fe_2O_3/PEI	0.15913	0.11	1.34	0.09	0.16	0.01

The low values for the surface excess of PAA can be due to a low amount of adsorption sites, since the surface excess of PAA had been calculated to be 0.9 mg/m^2 based on the gas adsorption and TGA. In consistency with the theory in sections 2.12.2 and 2.12.3, it was concluded that chain

length of the PEI is of importance for an optimal adsorption onto the Fe_2O_3 MNP surface for the later removal of PAA. However, just in case the affinity of the PAA was too high, it was decided to run a test adsorbtion EBA for comparison.

Calibration curve of 4-ethylbenzoic acid at pH 4.5

Since the affinity for the model acid towards the water affects the amount adsorbed onto the coated MNP, a test adsorption using 4-ethylbenzoic acid (EBA) was attempted. The calibration curve obtained from the prepared solutions, given in table 6.10 in appendix F, is shown in figure 4.20. Since the squared value of the correlation coefficient is high, the linear model is representative. The linear function is given in equation (4.3).

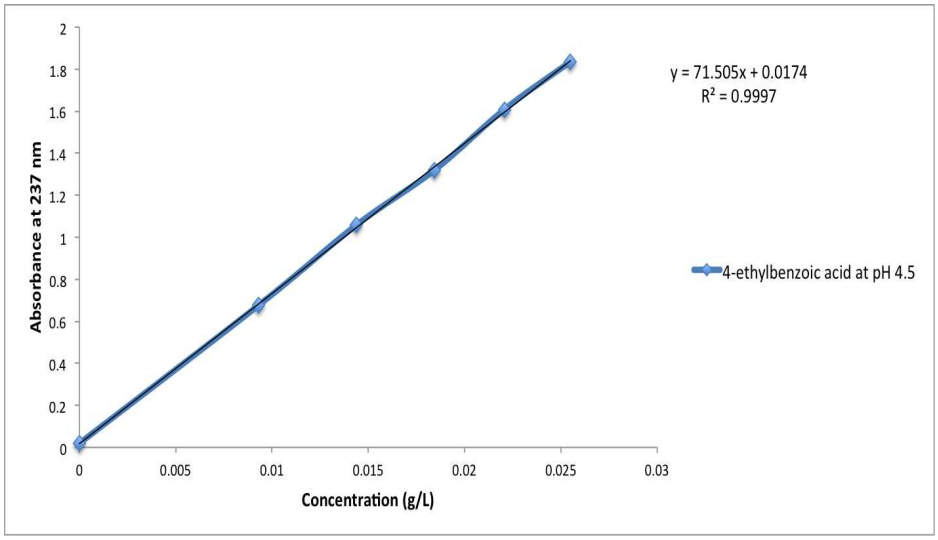

Figure 4.20: Calibration curve for PAA at pH 4.5

$$A = 71.5c + 0.0174 \tag{4.3}$$

Test adsorption of 4-ethylbenzoic acid at pH 4.5

The separation of the Fe_2O_3/PEI MNP from the model acid, EBA, was allowed 5 days on the magnet. The decision was based on the amount of time needed for dissolving EBA in MQ when preparing the 0.17 g/L solution (section 3.3.6.7). At the time of running the UV, there was still some turbidity as indicated in figure 4.21. Thus, the UV may not be representative as the supernatant can have been contaminated.

Since noise was observed in the spectre for the supernatant, a plot was made where the result from the supernatant was superimposed with the other obtained specters. The plot is given in figure 6.13 in appendix F. A similar noise was observed for the undiluted stock, whereas both the diluted supernatant and the diluted stock displayed one single maximum absorbance. It was thus concluded that the noise was the result of the limit of the UV instrument and not a detected contamination.

Figure 4.21: Separation of Fe_2O_3/PEI MNP from the 4-EBA solution

Table 4.10 shows the results when the concentration difference is estimated from the known concentration value from the balance: 0.17 g/L

Table 4.10: Surface excess and equilibrium concentration of EBA given the concentration difference, pH 4.5

Sample MNP	**Abs. at 237 nm**	$\mathbf{C_e}$ **diluted (g/L)**	$\mathbf{C_e}$ **(g/L)**	$\triangle\mathbf{C}$ **(g/L)**	**Surface excess** $(\mathbf{mg/m^2})$	$\mathbf{q_e}$
Sonicat. Fe_2O_3/PEI	0.7879	0.01	0.15	0.02	0.03	0.002

$$71.5c = 1.5273 - 0.0211 \rightarrow c = 0.0211 \rightarrow 0.175$$

Table 4.11 shows the results using the calibration curve to estimate the known concentration (0.175 g/L) and hence the concentration difference.

Table 4.11: Surface excess and equilibrium concentration of EBA given the concentration difference, pH 4.5

Sample MNP	**Abs. at 237 nm**	$\mathbf{C_e}$ **diluted (g/L)**	$\mathbf{C_e}$ **(g/L)**	$\triangle\mathbf{C}$ **(g/L)**	**Surface excess** $(\mathbf{mg/m^2})$	$\mathbf{q_e}$
Sonicat. Fe_2O_3/PEI	0.7879	0.01	0.15	0.02	0.04	0.002

According to the surface excess value for EBA, the adsorption is negligible. It can be concluded, that using EBA is less suitable for test adsorption both due to the separation time needed in addition to the negligible adsorption that may be the result of MNP contamination.

Chapter 5

Conclusion and Recommendations

Conclusion

Since the NA causes several problems, the removal of these acids is imperative. The main objective of this thesis has been to test how effective the PEI coated iron oxide MNP are to remove PAA from the water phase, which has served as the model NA. Hence, the adsorption of PEI onto the MNP surface and the amount of adsorption sites are important.

In order to be able to successfully adsorb PEI onto the iron oxide MNP various characterisation experiments were conducted and optimized.

According to the TGA the Fe_2O_3 MNP did adsorb PEI, which was the main step in order to remove the model NA from water provided the magnetism remained intact. The surface excess was determined to be 0.9 m^2/g.

The adsorption pH was chosen to be pH 8 based on the optimization for adsorbing PEI onto the Fe_3O_4 MNP. Since the isoelectric point for the Fe_2O_3 MNP was indicated at pH 6, and PEI increases its amount of positive

charges when the pH decreases, pH 7 could possibly be a better adsorption pH in the case of the Fe_2O_3 MNP core. However, the 95% condifence intervals were overlapping for pH 7 and pH 8.

In the test adsorption of the model acid, PAA, at pH 8 no adsorption was detected. As the model acid has a high affinity for water, which is enhanced when the pH increases, the test adsorption was performed again close to the pK_A for PAA. The value for the surface excess indicated that the adsorption of the model acid had occured, though in small amounts. Two different values were calculated. When bulk PAA prior to the adsorption was estimated from the calibration curve, then surface excess was estimated to be 0.16 mg/m^2, whereas 0.28 mg/m^2 was procured using the value from the balance.

The DVM of the redispersed Fe_2O_3/PEI MNP indicated high agglomeration. Since the polymer is supposed to provide steric hindrance for the flocculation of MNP, the coating was not optimal.

The low pH seemed to be the optimal pH for adsorption, however, another model acid, EBA was tested for adsorption in case the initial model acid had a too high affinity. No adsorption was detected, though due to the difficulty of separating the coated particles from the EBA solution there may have been a contamination.

According to previous research of adsorbing PEI onto a MNP core, it is the polymer that determines the number of available functional groups on the particle surface and a low molecular weight is recommended in order to avoid flocculation as the surface excess is independent of the chain length.

Based on the findings it is put forward by the operator to optimize the

number of adsorption sites of PEI by using a shorter chain length, while keeping the optimal pH close to $pK_A$for the adsorption of PAA. An additional possible optimization variable for the adsorption of PEI onto Fe_2O_3 MNP is pH 7. It is also suggested to use a transmission electron microscope in order to get an understanding of the layer of PEI coating the Fe_2O_3 MNP.

Recommendations

With respect to future work if it is possible to obtain an optimized adsorption of both PEI onto Fe_2O_3 MNP and thus the removal of PAA, it would be of interest to develop a recycling method for a possible up-scaling of using Fe_2O_3/PEI MNP to adsorb NA in produced water and hence reduce corrosion. It is suggested to runpH 7 and pH 8 in parallels for the adsorption of PEI with a lower molecular weight.

Bibliography

[1] J. A. Mouljin, M. Makkee, A. E. V. Diepen, *Chemical Process Technology* (John Wiley & Sons, 2013), second edn.

[2] B. Academica, Crude oil, http://academic.eb.com/levels/collegiate/article/28047 (2017). Accessed: 2017-02-07.

[3] L. J. Shi, B. X. Shen, G. Q. Wang, Removal of Naphthenic Acids from Beijian Crude Oil by Forming Ionic Liquids, *Energy & Fuels*, http://pubs.acs.org/doi/pdf/10.1021/ef800497p (2008).

[4] T. Fan, J. Wang, J. S. Buckley, Evaluating Crude Oils by SARA Analysis, *SPE Journal*, https://www.onepetro.org/download/conference-paper/SPE-75228-MS?id=conference-paper%2FSPE-75228-MS (2002).

[5] P. C. Hiemenz, R. Rajagopalan, *Principles of Colloid and Surface Chemistry* (CRC Press, Boca Raton, 1997), third edn.

[6] R. L. Fyllingsnes, TKP4520 lab project report rheological analysis of

the strength of wax-oil gels in relation to shut-in of a pipeline (2016). Unpublished paper, Norwegian University of Science and Technology: Department of Chemical Engineering, Trondheim.

[7] S. Kokal, Crude-Oil Emulsions: A State-Of-The-Art Review, *SPE Journal*, https://www.onepetro.org/download/journal-paper/SPE-77497-PA?id=journal-paper%2FSPE-77497-PA (2005).

[8] G. E.Oliveira, C. R. E. Mansur, E. F. Lucas, G. Conz*á*lez, W. F. de Souza, The Effect of Asphaltenes, Naphthenic Acids, and Polymeric Inhibitors on the Pour Point of Paraffins Solutions, Journal of Dispersion Science and Technology, http://www.tandfonline.com/doi/pdf/10.1080/01932690601107526?needAccess=true (2007).

[9] T.-P. Fan, Characterization of Naphthenic Acids in Petroleum by Fast Atom Bombardment Mass Spectrometry, *Energy & Fuels*, http://pubs.acs.org/doi/abs/10.1021/ef00027a003 (1991).

[10] W. K. Seifert, R. M. Teeter, Identification of Polycyclic Naphthenic, Mono- and Diaromatic Crude Oil Carboxylic Acids, *Analytical Chemistry*, http://pubs.acs.org/doi/abs/10.1021/ac60284a004 (1970).

[11] T. Baugh, K. Grande, H. Mediaas, J. Vindstad, N. Wolf, The Discovery of High-Molecular-Weight Naphthenic Acids (ARN Acid) Responsible for Calcium Naphthenate Deposits, *SPE Journal*, https://www.onepetro.org/conference-paper/SPE-93011-MS?sort=

&start=0&q=93011&from_year=&peer_reviewed=&published_between=&fromSearchResults=true&to_year=&rows=10# (2005).

[12] J. Daintith, ed., *Oxford Dictionary of Chemistry* (Oxford University Press, 2004), fifth edn.

[13] M. A. Reinsel, J. J. Borkowski, J. T. Sears, Partition Coefficients for Acetic, Propionic, and Butytic Acids in a Crude Oil/Water System, *Journal of chemical and engineering data*, http://pubs.acs.org/doi/abs/10.1021/je00015a026 (1994).

[14] P. C. Painter, M. M. Coleman, *Fundamentals of polymer science. An introductory text* (CRC Press LLC, Boca Raton, 2000), second edn.

[15] M. J. Lawrence, G. D. Rees, Microemulsion-based media as novel drug delivery systems, *Advanced Drug Delivery Reviews*, http://www.sciencedirect.com/science/article/pii/S0169409X00001034 (2000).

[16] K. Holmberg, B. Jönsson, B. Kronberg, B. Lindman, *Surfactants and Polymers in Aqueous Solution* (John Wiley & Sons, 2002).

[17] S. S. Ltd, Organic deposits, http://www.scaledsolutions.com/index.php?page=Performance%20Tests&subpage=Organic%20Deposits (2016). Accessed: 2017-02-07.

[18] E. L. Nordgård, A.-M. D. Hanneseth, J. Sjöblom, Inhibition of Calcium Naphthenate. Experimental Methods to Study the Effect of Commercially Available Naphthenate Inhibitors, *Journal of Dispersion Science and Technology*, http://www.tandfonline.com/doi/pdf/10.1080/01932690903212891?needAccess=true (2010).

[19] G. Rosseau, H. Zhou, C. Hurtevent, Calcium Carbonate and Naphthenate Mixed Scale in Deep-Offshore Fields, *SPE Journal*, https://www.onepetro.org/download/conference-paper/SPE-68307-MS?id=conference-paper%2FSPE-68307-MS (2001).

[20] Schlumberger, Oilfield glossary, http://www.glossary.oilfield.slb.com/Terms/w/water_cut.aspx (2017). Accessed: 2017-02-07.

[21] M. Turner, P. Smith, Controls on Soap Scale Formation, Including Naphthenate Soaps-Drivers and Mitigation, *SPE Journal*, https://www.onepetro.org/download/conference-paper/SPE-94339-MS?id=conference-paper%2FSPE-94339-MS (2005).

[22] P. P. Alvisi, V. F. Lins, An overview of naphthenic acid corrosion in a vacuum distillation plant, *Engineering Failure Analisis*, http://www.sciencedirect.com/science/article/pii/S1350630711000720 (2011).

[23] ExxonMobil, Kearl, http://crd.exxonmobil.com/crudeoil/download/KEARL.pdf (2016). Accessed: 2016-11-02.

[24] O. Yèpez, Influence of different sulfur compounds on corrosion due to naphthenic acid, *Fuel*, http://www.sciencedirect.com/science/article/pii/S0016236104002200 (2004).

[25] A. Zhang, Q. Ma, K. Wang, X. Liu, P. Shuler, Y. Tang, Naphthenic acid removal from crude oil through catalytic decarboxylation on magnesium oxide, *Applied Catalysis*, http://www.sciencedirect.com/science/article/pii/S0926860X06000792 (2006).

[26] S. Sugiyama, K. Sato, S. Yamasaki, K. Kawashiro, H. Hayashi, Ketones from carboxylic acids over supported magnesium oxide and related catalysts, *Catalysis Letters*, https://link.springer.com/content/pdf/10.1007%2FBF00764227.pdf (1992).

[27] V. V. Rogers, M. Wickstrom, K. Liber, M. KacKinnon, Acute and Subchronic Mammalian Toxicity of Nanpthenic Acids from Oil Sands Tailings, *Toxicological Sciences*, https://academic.oup.com/toxsci/article-lookup/doi/10.1093/toxsci/66.2.347 (2002).

[28] R. G. Bossert, THE METALLIC SOAPS, *Journal of Chemical Education*, http://pubs.acs.org/doi/pdf/10.1021/ed027p10 (1950).

[29] B. Issa, I. M. Obaidat, B. A. Albiss, Y. Haik, Magnetic Nanoparticles: Surface Effects and Properties Related to Biomedicine Applications, *Internataional Journal of Molecular Science*, http://www.mdpi.com/1422-0067/14/11/21266/htm (2013).

[30] B.D.Cullity, C. Graham, *Introduction to Magnetic Materials* (John Whiley & Sons, 2009), second edn.

[31] A. P. Guimarães, *Principles of Nanomagnetism* (Springer, Dordrecht, 2009).

[32] A.-H. Lu, E.L.Salabas, F. Schüth, Magnetic nanoparticles: Synthesis, Protection, Functionalization, and Application, *Angewandte Chemie: International edition*, http://onlinelibrary.wiley.com/doi/10.1002/anie.200602866/full (2007).

[33] Y.-W. Jun, J.-W. Seo, J. Cheon, Nanoscalling Lalls of Magnetic Nanoparticles and Their Applicabilities in Biomedical Sciences, *American Ceramic Society*, http://pubs.acs.org/doi/abs/10.1021/ar700121f (2007).

[34] S. A. Majetich, M. Sachan, Magnetostatic interactions in magnetic nanoparticle assemblies: energy, time and length scales, *Journal of Physics D: Applied Physics*, http://iopscience.iop.org/article/10.1088/0022-3727/39/21/R02/meta (2006).

[35] T. Hyeon, S. S. Lee, J. Park, Y. Chung, H. B. Na, Synthesis of Highly Crystalline and Monodisperse Maghemite Nanocrystallites without a Size-Selection Process, *Journal of the American Chemical Society*, http://pubs.acs.org/doi/abs/10.1021/ja016812s (2001).

[36] J. Mendez-Garza, B. Wang, A. Madeira, C. D. Giorgio, G. Bossis, Synthesis and Surface Modification of Spindle-Type Magnetic Nanoparticles: Gold Coating and PEG Functionalization, *Journal of Biomaterials and Nanobiotechnology*, https://www.researchgate.net/publication/243459170_Synthesis_and_Surface_Modification_of_Spindle-Type_Magnetic_Nanoparticles_Gold_Coating_and_PEG_Functionalization (2013).

[37] S. Sun, H. Zeng, Size-Controlled Synthesis of Magnetite Nanoparticles, *Journal of American Chemical Society*, http://pubs.acs.org/doi/pdf/10.1021/ja026501x (2002).

[38] W. Fu, H. Yang, M. Li, M. Li, N. Yang, G. Zou, Anatase TiO_2

nanolayer coating on cobalt ferrite nanoparticles for magnetic photocatalyst, *Materials Letters*, http://www.sciencedirect.com/science/article/pii/S0167577X05006178 (2005).

[39] E. V. Shevchenko, D. V. Talapin, A. L. Rogach, A. Kornowski, M. Haase, H. Weller, Colloidal Synthesis and Self-Assembly of $CoPt_3$ Nanocrystals, *Journal of American Chemical Society*, http://pubs.acs.org/doi/pdf/10.1021/ja025976l (2002).

[40] T. Jaumann, E. Ibrahim, S. Hampel, D. Maier, A. Leonhardt, B. Büchner, The Synthesis of Superparamagnetic Cobalt Nanoparticles Encapsulated in Carbon Through High-pressure CVD, *Chemical Vapour Deposition*, http://onlinelibrary.wiley.com/doi/10.1002/cvde.201207020/full (2013).

[41] A. J. Rondinone, A. C. S. Samia, Z. J. Zhang, Superparamagnetic Relaxation and Magnetic Anistropy Energy Distribution in $CoFe_2O_4$, Journal of Physical Chemistry B, http://pubs.acs.org/doi/abs/10.1021/jp9912307 (1999).

[42] I. O. Sosa, C. Noguez, R. G. Barrera, Optical Properties of Metal Nanoparticles with Arbitrary Shapes, *Journal of Physical Chemistry B*, http://pubs.acs.org/doi/pdf/10.1021/jp0274076 (2003).

[43] R. J. Hill, J. R. Craig, G. Gibbs, Systematics of the Spinel Structure Type, *Physics and Chemistry of Minerals*, https://link.springer.com/content/pdf/10.1007%2FBF00307535.pdf (1979).

[44] J. Noh, O. I. Osman, S. G. Aziz, P. Winget, J.-L. B. $\acute{e}das$, Magnetite Fe_3O_4 (111) Surfaces: Impact of Defects on Structure, Stability and Electronic Properties, *Chemistry of Materials*, http://repository.kaust.edu.sa/kaust/handle/10754/565799 (2015).

[45] Z.-X. Sun, F.-W. Su, W. Forsling, P.-O. Samskog, Surface Characteristics of Magnetite in Aqueous Suspension, *Journal of Colloid and Interface Science*, https://doi.org/10.1006/jcis.1997.5239 (1998).

[46] S. Aldrich, Iron (iii) oxide, http://www.sigmaaldrich.com/catalog/product/aldrich/544884?lang=en&region=NO (2017).

[47] J. Tuček, L. Machala, S. Ono, A. Namai, M. Yoshikiyo, K. Imoto, H. Tokoro, S. ichi Ohkoshi, R. Zbořil, Zeta-Fe_2O_3-A new stable polymorph in iron (iii) oxide family, Scientific Reports, https://www.ncbi.nlm.nih.gov/pmc/articles/PMC4606832/ (2015).

[48] nanoComposix europe, Zeta potential, http://nanocomposix.eu/products/zeta-potential-nanoparticle-analysis (2017). Accessed: 2017-02-20.

[49] M. I. Ltd., Zetasizer Nano Series User Manual, http://www.biophysics.bioc.cam.ac.uk/files/Zetasizer_Nano_user_manual_Man0317-1.1.pdf (2004). Accessed: 2017-03-08.

[50] Malvern, ZETASIZER NANO Series, http://www.malvern.com/Assets/MRK1839.pdf (None). Accessed:2017-02-21.

[51] W. Wu, Q. He, C. Jiang, Magnetic Iron Oxide Nanoparticles: Synthesis and Surface Functionalization Strategies, *Nanoscale Res Lett* , https://link.springer.com/article/10.1007/s11671-008-9174-9 (2008).

[52] M. Kakihana, "Sol-Gel" Preparation of High Temperature Superconducting Oxides, *Journal of Sol-Gel Science and Technology*, https://link.springer.com/content/pdf/10.1007%2FBF00402588.pdf (1996).

[53] Y. Lu, Y. Yin, B. T. Mayers, Y. Xia, Modifying the Surface Properties of Superparamagnetic Iron Oxide Nanoparticles through A Sol-Gel Approach, *Nano Letters*, http://pubs.acs.org/doi/pdf/10.1021/nl015681q (2002).

[54] Y.-H. Deng, C.-C. Wang, J.-H. Hu, W.-L. Yang, S.-K. Fu, Investigation of formation of silica-coated magnetite nanoparticles via sol-gel approach, *Colloids and surfaces A: Physiochemical and engineering aspects*, http://www.sciencedirect.com/science/article/pii/S0927775705002438 (2005).

[55] X. Zhang, H. Niu, Y. Pan, Y. Shi, Y. Cai, Modifying the surface of Fe_3O_4/SiO_2 magnetic nanoparticles with C_{18}/NH_2 mixed group to get an efficient sorbent for anionic organic pollutants, *Journal of Colloid and Interface Science*, http://www.sciencedirect.com/science/article/pii/S0021979711007491 (2011).

[56] G. Rayner-Canham, T. Overton, *Descriptive Inorganic Chemistry* (W.H. Freeman and Company, 2002), third edn.

[57] D. A. Dougherty, Spin Control in Organic Molecules, *Acc.Chem. Res*, http://pubs.acs.org/doi/pdf/10.1021/ar00003a005 (1991).

[58] I. Chorkendorff, J. Niemantsverdriet, *Concepts of Modern Catalysis and Kinetics* (John Wiley & Sons, 2006).

[59] H. S. Fogler, *Elements of Chemical Reaction Engineering* (Prentice-Hall International, 1992), second edn.

[60] J. E. Brady, *General Chemistry - Principles and Structure* (Tapir Norsk Akademisk Forlag/ John Wiley & Sons, 2000).

[61] D. Maniu, V. Chis, M. Baia, F. Toderas, S. Astilean, Density functional theory investigation of p-aminothiophenol molecules adsorbed on gold nanoparticles, Journal of orthoelectronics and advanced materials, https://www.researchgate.net/profile/Vasile_Chis2/publication/228526147_Density_functional_theory_investigation_of_p-aminothiophenol_molecules_adsorbed_on_gold_nanoparticles/links/0912f50d5a68e8beec000000.pdf (2007).

[62] C. Learning, Adsorption Isotherm, http://www.chemistrylearning.com/adsorption-isotherm/ (2017).

[63] S. Brunauer, P. Emmett, E. Teller, Adsorption of Gasses in Multimolecular Layers, *Journal of American Chemical Society*, http://pubs.acs.org/doi/pdf/10.1021/ja01269a023 (1938).

[64] J. Wang, S. Zheng, Y. Shao, J. Liu, Z. Xu, D. Zhu, Amino-functionalized Fe_3O_4@SiO_2 core-shell magnetic nanomaterials as a

novel adsorbent for aqueous heavy metals removal, *Journal of Colloid and Interface Science*, http://dx.doi.org/10.1016/j.jcis.2010.05.010 (2010).

[65] G. Sitterley, Poly-lysine, http://www.sigmaaldrich.com/technical-documents/articles/biofiles/poly-lysine.html (2008). Accessed: 2016-11-02.

[66] M. Babič, D. Horák, M. Trchová, P. Jendelová, K. Glogarová, P. Lesný, V. Herynek, M. Hájek, E. Syková, Poly(L-lysine)-Modified Iron Oxide Nanoparticles for Stem Cell Labeling, *Bioconjugate Chem.*, http://pubs.acs.org/doi/pdf/10.1021/bc700410z (2008).

[67] M. Marsh, H. T. McMahon, The Structural Era of Endocytosis, Science, http://science.sciencemag.org/content/285/5425/215.full (1999).

[68] E. Mohammadifar, A. N. Kharat, M. Adeli, Polyamidoamine and polyglycerol; their linear, dendritic and linear-dendritic architectures as anticancer drug delivery systems, *Journal of Material Chemistry B*, http://pubs.rsc.org/en/content/articlepdf/2015/tb/c4tb02133a (2015).

[69] K. Fujiki, M. Sakamoto, T. Sato, N. Tsubokawa, POST-GRAFTING OF HYPERBRANCHED DENDRITIC POLYMER FROM TERMINAL AMINO GROUPS OF POLYMER CHAINS GRAFTED ONTO SILICA SURFACE, *Journal of Macromulecular Science, Part A*, http://www.tandfonline.com/doi/pdf/10.1081/MA-100101098?needAccess=true (2007).

[70] E. R. Gillies, J. M. Fréchet, Dendrimes and dendritic polymers in drug delivery, *Elsevier*, http://www.sciencedirect.com/science/article/pii/S1359644604032763 (2005).

[71] O. Boussif, F. Lezoualc'h, M. A. Zanta, M. D. Mergny, D. Scherman, B. Demeneix, J.-P. Behr, A versatile vector for gene and oligonucleotide transfer into cells in culture and in vivo: Polyethylenemine, *Proc. Natl. Acad. Sci.*, http://www.pnas.org/content/92/16/7297.short (1995).

[72] T. Xia, M. Kovochich, M. Liong, H. Meng, S. Kabehie, S. George, J. I. Zink, A. E. Nel, Polyethyleneimine Coating Enhances the Cellular Uptake of Mesoporous Silica Nanoparticles and Allows Safe Delivery of siRNA and DNA, *American Chemical Society*, http://pubs.acs.org/doi/abs/10.1021/nn900918w (2009).

[73] B. Academica, Transfection, http://academic.eb.com/levels/collegiate/article/103739 (2017). Accessed: 2017-02-07.

[74] W. Zhang, H. Liu, C. Sun, T. C. Drage, C. E. Snape, Capturing CO_2 from ambient air using polyethyleneimine-slica adsorbent in fluidized beds, *Chemical Engineering Science*, http://www.sciencedirect.com/science/article/pii/S0009250914002280 (2014).

[75] R. Zajac, A. Chakrabarti, ffects of chemical impurities on the adsorption of polymer chains from a semidilute solution, The Journal of Chemical Physics, http://aip.scitation.org/doi/pdf/10.1063/1.475016 (1997).

[76] E. Hershkovits, A. Tannenbaum, R. Tannenbaum, Polymer adsorption on curved surfaces: A geometric approach, J Phys Chem C Nanomater Interfaces, https://www.ncbi.nlm.nih.gov/pmc/articles/PMC3663076/ (2007).

[77] I. Y. Goon, C. Zhang, M. Lim, J. J. Gooding, R. Amal, Controlled Fabrication of Polyethyleneimine-Functionalized Magnetic Nanoparticles for the Sequestration and Quantification of Free Cu^{2+}, *American Chemical Society*, http://pubs.acs.org/doi/pdf/10.1021/la101196r (2010).

[78] M. Arsianti, M. Lim, C. P. Marquis, R. Amal, Assembly of Polyethyleneimine-Based Magnetic Iron Oxide Vectors: Insights into Gene Delivery, *American Chemical Society*, http://pubs.acs.org/doi/pdf/10.1021/la9041919 (2010).

[79] D. I. Gittins, F. Caruso, Tailoring the Polyelectrolyte Coating of Metal Nanoparticles, *Journal of Physical Chemistry*, http://pubs.acs.org/doi/pdf/10.1021/jp0111665 (2001).

[80] H. Vedam, NanoSafety Policy Overview, *Nanoscience*, http://ieeexplore.ieee.org/stamp/stamp.jsp?arnumber=6111988 (2011).

[81] E. M. Amarfio, S. Mohammed, Environmental and Health Impacts of Nanoparticles Application in Our Oil Industry, *Society of Petroleum Engineers International*, https://www.onepetro.org/download/conference-paper/SPE-172427-MS?id=conference-paper%2FSPE-172427-MS (2014).

[82] S. Aldrich, Poly(ethyleneimine) solution, http://www.sigmaaldrich.com/catalog/product/aldrich/181978?lang=en&region=NO (2017).

[83] M. Strand, Amino-Functionalized Magnetic Nanoparticles for Extraction of Naphthenic Acids, Master's thesis, NTNU (2016).

[84] C. Zhang, *et al.*, Silica-and alkoxysilane-Coated Ultrasmall Superparamagnetic Iron Oxide Particles:A Promising Tool To Label Cells for Magnetic Resonance Imaging, *Langmuir*, http://pubs.acs.org/doi/pdf/10.1021/la061879k (2007).

[85] D. S. Moore, G. P. McCabe, B. A. Craig, *Introduction to the Practice of STATISTICS* (W.H. Freeman and Company, New York, 2012), 7th edn.

[86] Computing the Standard Deviation of Sample Means, https://www.utdallas.edu/~metin/Ba3352/qch9-10.pdf (None). Accessed:2017-03-08.

[87] SMIMADZU, The Relationship Between UV-VIS Absorption and Structure of Organic Compounds, http://www.shimadzu.com/an/uv/support/uv/ap/apl.html (2017).

[88] J. Mohan, *Organic Spectroscopy. Principles and Applications* (Apha Science International Ltd., 2004), second edn.

[89] M. Ronander, Magnetic Nanoparticles for Extraction of Naphthenic Acids from Model Oil, Master's thesis, NTNU (2015).

[90] G. Aylward, T. Findlay, *SI Chemical Data* (John Wiley & Sons Australia, 2008), 6th edn.

[91] C. Book, 4-ethylbenzoic acid, https://www.chemicalbook.com/ProductMSDSDetailCB3153435_EN.htm (2017).

Chapter 6

Appendices

Appendix A: Main results from iron (II, III) oxide and the polyethyleneimine coated iron (II, III) oxide nanoparticles

Magnetism of iron (II, III) oxide

When comparing figure 6.1a to 6.1b it can be observed that the Fe_3O_4 MNP aligned themselves to the external magnet. The response was immediate.

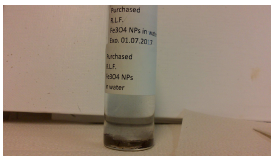

(a) Without magnet

(b) With magnet

Figure 6.1: Response to the magnetic field used for Fe_3O_4 MNP

Zeta potentials and 95 % confidence intervals for polyethyleneimine coated iron (II, III) oxide

The parameters used for the zeta potential measurements are provided in section 3.3.2.1.

Coating of iron (II, III) oxide as function of increased bulk polyethyleneimine concentration

Figure 6.2 depicts the adsorption profile of PEI when the bulk PEI concentration increased. It can be observed that as the bulk concentration of PEI increased, the adsorption onto the Fe_3O_4 MNP increased until the saturation limit was reached. Increasing the concentration of PEI would cause no further adsorption possibly due to the steric hindrance provided by the polymer.

While running the Zetasizer Nano ZS, sedimentation was observed in the cuvette for both parallels that were tested for each of the prepared samples. The large particles causing the sedimentation gave a strong turbidity, which made it difficult to look for bubbles in the horizontal cell.

The error bars in figure 6.2 visualise the margin of error in both positive and negative directions. A large margin of error is observed for the value of the true zeta potential for the Fe_3O_4/PEI MNP. The exact values for the margin of error are given in table 6.1. Due to the large 95% confidence intervals, there is a low confidence for capturing the true zeta potential in consistency with section 3.3.1.3.

Since the margin of error is affected by the number of samples, it was

decided to prepare new stocks of Fe_3O_4 MNP and add a constant mass of PEI.

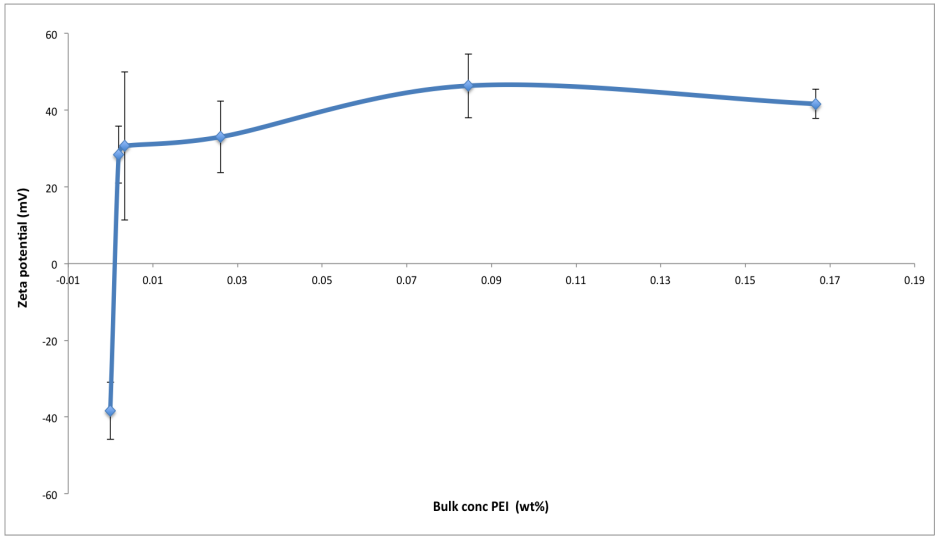

Figure 6.2: Zeta potential of Fe_3O_4/PEI MNP as function of bulk PEI (wt %) at pH 8

Table 6.1: 95% confidence interval for the zeta potentials for the Fe_3O_4/PEI MNP with increased bulk PEI

Bulk BEI (wt%)	**95% confidence interval**
0	-38.4 $\pm$7.4
0.002	28.4 $\pm$7.5
0.003	30.6 $\pm$19.3
0.03	33.02 $\pm$9.4
0.09	46.4 $\pm$8.3
0.17	41.6 $\pm$3.8

Coating of iron (II, III) oxide as function of constant bulk polyethyleneimine concentration

All the run parallels gave similar deviating zeta potential values, as for the Fe_3O_4/PEI MNP with an increased bulk PEI wt% concentration, with the exception of parallel two for sample three as shown in table 6.2. The last parallel had to be discarded due to very deviating values (60 mV and 104 mV). Hence, sample three does not contribute to the 95% confidence interval: 32.3 ± 6.9 mV. If the outliers from sample three had been included, the effect on the confidence interval would have been high as the mean is not a resistant measure as mentioned in section 3.3.1.3.

The low confidence could be affected by the presence of chemical impurities. Hence, before discarding the Fe_3O_4 MNP as core for the PEI adsorption and changing to the more oxidized Fe_2O_3 MNP, it was decided to test if calcination could remove possible impurities and use DVM for comparison.

Table 6.2: Zeta potentials for the Fe_3O_4/PEI MNP with constant PEI

Sample number	Zeta potential (mV) Parallel 1	Zeta potential (mV) Parallel 2
1	34.01	37.96
2	38.78	36.6
3	37.92	-
4	21.34	33.68
5	32.42	20.92

Digital video microscope for iron (II, III) oxide

In order to look at the size of the Fe_3O_4 MNP with the concentration 1.99 g/L that had been used in the first coating attempt at pH 8, a picture was taken at 10x using DVM. Flocculation was indicated in addition to polydispersity as shown in figure 6.3. For co-precipitated MNP, polydispersity can be present as mentioned in section 2.8.1.

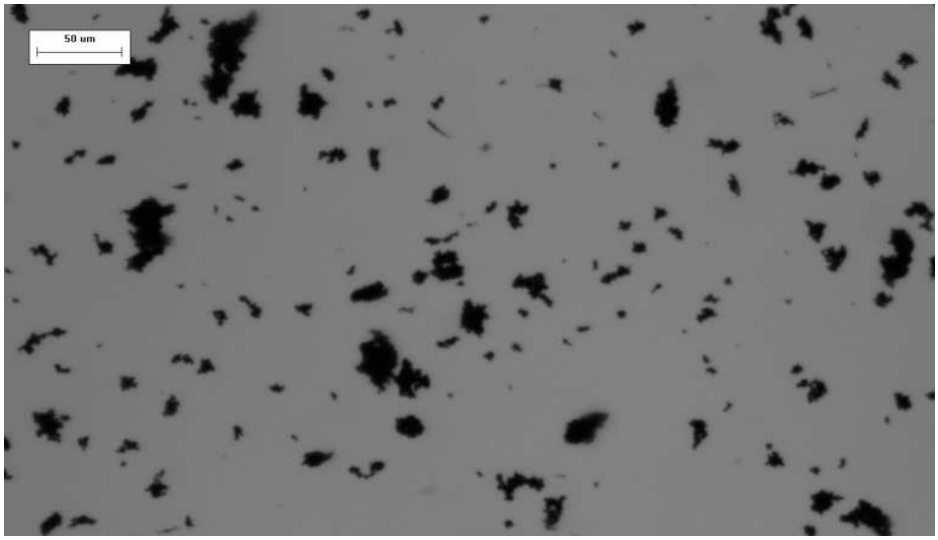

Figure 6.3: Particle size of Fe_3O_4 MNP, 1.99 g/L

Calcination was performed due to possible impurities. The mass after calcination was noted to be 3.4 g.

After conducting the calcination the size of the particles had not decreased. The same degree of polydispersity is also observed. The picture taken after the calcination is shown in figure 6.4. It was thus decided to use centrifugation in order to remove any MNP large enough to affect the result from the Zetasizer Nano ZS, when changing the type of MNP.

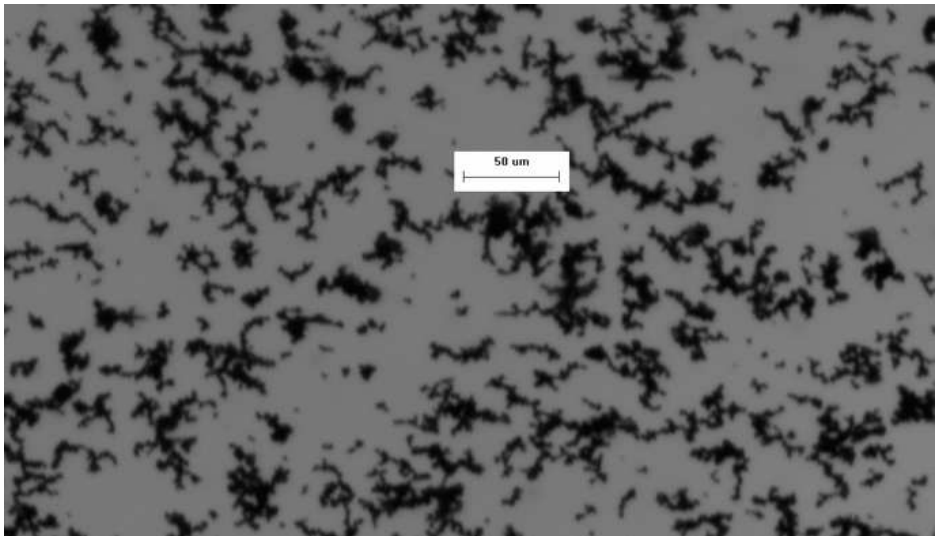

Figure 6.4: Particle size after calcinating Fe_3O_4 MNP, 1.99 g/L

A note can be made that if calcination is to be used later, then perhaps coating these particles with PEI and running the Zetasizer Nano ZS could have been a better characterisation method in order to look for the removal of impurities.

Appendix B: 95% confidence intervals comparison for iron (III) oxide

A comparison between the 95% confidence intervals for the uncoated Fe_2O_3 MNP was made after the zeta test for optimal pH had been conducted, in order to get an understanding of the instability of the naked core when suspended in water. It can be observed that the values in table 6.3 overlap with the values from table 6.4 with respect to pH 7 and 8. However, for pH 9 they are not overlapping. It can be concluded that either the true mean was not captured in the 95% confidence interval the first time the zeta potential was measured or the last time, in consistency with section 3.3.1.3. However, with respect to the margin of error it is assumed that the true zeta potential at pH 9 is in the interval:
-11.9 ± 0.5.

In any case the instabilility of the suspended naked core Fe_2O_3 MNP has been detected.

Table 6.3: 95% confidence intervals of the zeta potential as function of pH for Fe_2O_3 MNP from the optimization test, pH 7-9

pH 7	**pH 8**	**pH 9**
-15.3 ± 6.1	-8 ± 4.4	-11.9 ± 0.5

Table 6.4: 95% confidence intervals of the zeta potential as function of pH for Fe_2O_3 MNP, pH 7-9

pH 7	**pH 8**	**pH 9**
-13.1 $\pm$3.5	-16.2 $\pm$9.9	-23.4 $\pm$6.9

Appendix C: Optimization of the coating procedure for iron (III) oxide before mass production

Supernantant concentration after centrifuging iron (III) oxide with the concentration of 2.5 g/L

The calculated values have been obtained using the subequations (3.4), presented in section 3.2.4, for the concentration test for 2.5 g/L of Fe_2O_3 MNP are given in table 6.5. The vial with cap is abbreviated to VC.

It can be observed that the two concentrations deviate, where the second concentration is negative. Hence, it was decided to increase the concentration in order to inside of the confidence interval of the balance.

Table 6.5: Estimation of the concentration after the centrifugation, 2.5 g/L

Sample number	Mass empty VC (g)	Mass VC and supern. (g)	Mass VC and Fe_2O_3 MNP (s) (g)	Mass MQ (g)	Conc. after cent. (g/L)
1	36.62	42.82	36.63	6.19	0.92
2	36.62	42.56	36.63	5.93	-0.069

Digital video microscope for iron (III) oxide 2.5 g/L

As explained in 3.3.3, the idea behind the different pictures was to see the effect of the different steps taken in the optimization of the coating procedure for the Fe_2O_3 MNP.

The image presented in figure 6.5 was taken at 10x of the supernatant of the Fe_2O_3 MNP with the inital concentration of 2.5 g/L at pH 8. The concentration of the supernatant was unknown, as the concentration was too low to be detected by the balance, as previously mentioned.

The number of particles had decreased compared to how the system initially looked as shown in figure 4.6. However, some of the particles were larger. Perhaps this is just an indication of the polydispersity in the system. It is possible to detect a diameter close to 50 µm for the largest particle in the picture, though the image is dark.

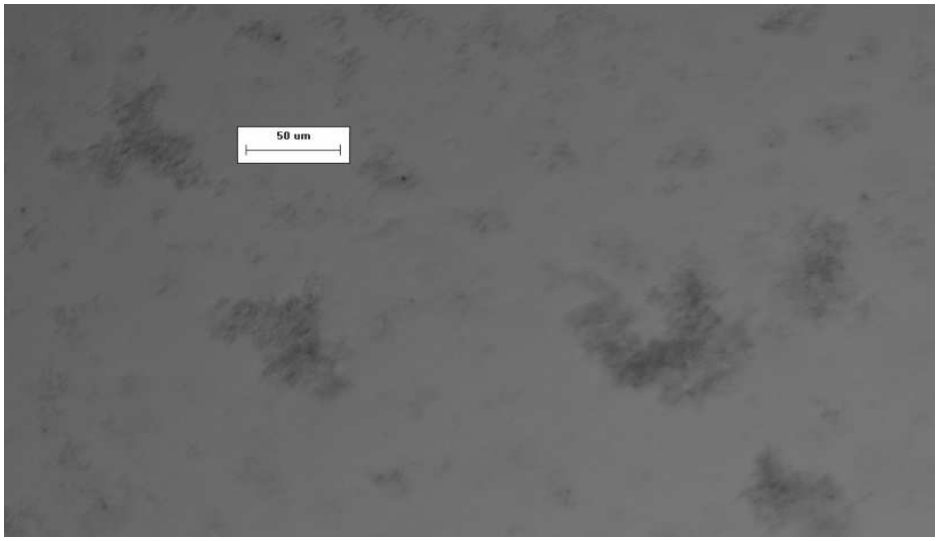

Figure 6.5: Particle size in the supernatant of Fe_2O_3 MNP, initial concentration 2.5 g/L

Another picture was taken at 20x in order to get a better estimate of the size of the largest particles observed. By comparing the scale of 50 µm to the particle it can be noticed, in figure 6.6, that the size is approximately 60 µm.

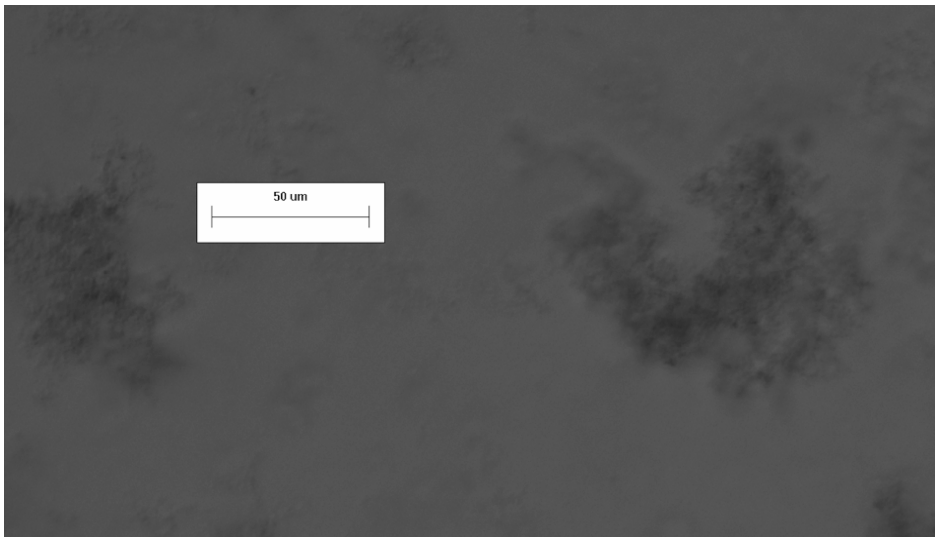

Figure 6.6: Particle size in the supernatant of Fe_2O_3 MNP 20x

Figure 6.7 illustrates the particle size after the coating. The particle size of the Fe_2O_3 MNP is larger than in figure 6.5, which may imply bridging caused by PEI. Moreover, the polydispersity is lower. This may indicate the stabilization effect of PEI in the system.

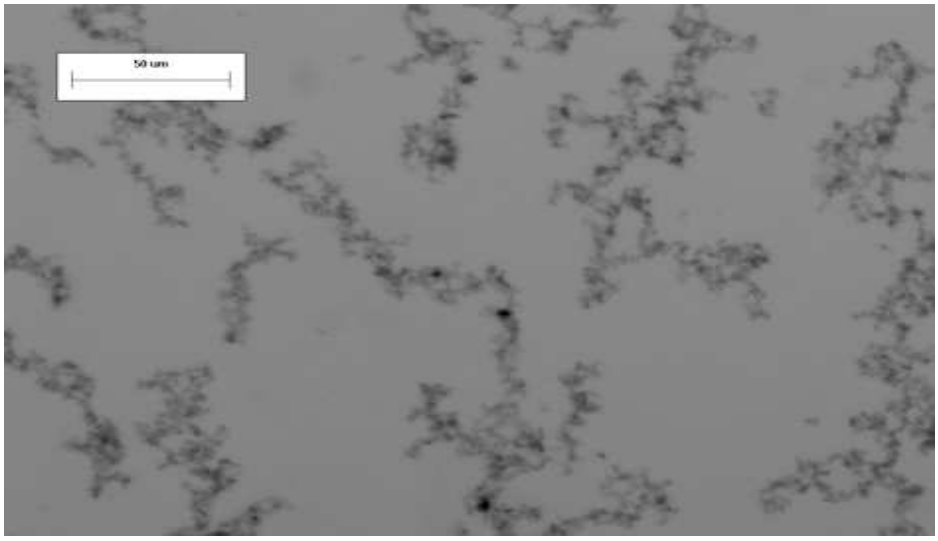

Figure 6.7: Particle size of Fe_2O_3/PEI MNP, initial concentration 2.5 g/L

Turbidity comparison of supernatant

The photo in figure 6.8a was taken as a first attempt to get the concentration after centrifugating 10 g/L when the total mass was 50 g, whereas the photo in figure 6.8b was taken when the total mass was decreased to 35 g. When the total mass was 50 g some of the dispersion remained in the original glass vial due to the volume capacity of the centrifugation tube.

When comparing the turbidities it can be observed that the homogeneity of the suspension, prior to centrifugation was lower for the total mass of 50 g. When the suspension was transferred into a smaller volume, it was not possible to ensure the transfer of equally sized particles. In other words, when particles are left behind small MNP that could contribute to the supernatant concentration had an equally big chance of staying in the original glass vials as large floccs.

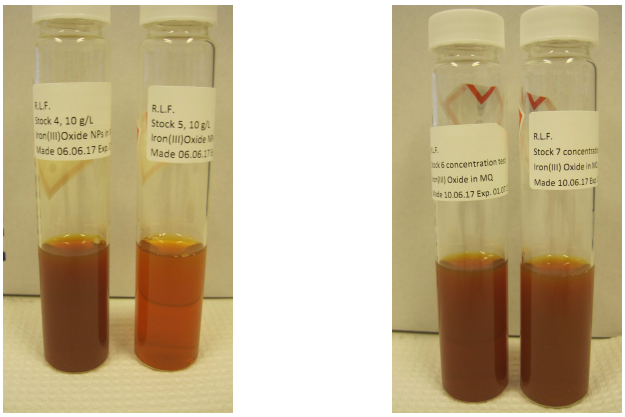

(a) Total mass of 50 g **(b)** Total mass of 35 g

Figure 6.8: Effect from reducing the total mass

One of the pictures taken after the centrifugation of the mass produced

Fe_2O_3/PEI MNP, where an equal turbidity is displayed, is shown in figure 6.9.

Figure 6.9: Turbidity of the supernatant for the mass produced Fe_2O_3/PEI MNP

Moreover, the trubidity of these parallels is similar to the turbidity shown in figure 6.8b. Hence, it can be concluded that reducing the total mass, when preparing the stocks of Fe_2O_3 MNP, is important for the homogeneity of the supernatant.

Supernantant concentration after centrifuging iron (III) oxide with the concentration of 10 g/L

The calculated values have been obtained using the subequations (3.4) presented in section 3.2.4, for the concentration test for 10 g/L of Fe_2O_3 MNP are given in table 6.6. The vial with cap is abbreviated to VC.

Table 6.6: Estimation of the concentration after the centrifugation, 10 g/L

Sample number	Mass empty VC (g)	Mass VC and supern. (g)	Mass VC and Fe_2O_3 MNP (s) (g)	Mass MQ (g)	Conc. after cent. (g/L)
1	36.39	61.51	36.42	25.10	0.88
2	36.70	61.57	36.72	24.85	0.87

Appendix D: Separation of the polyethyleneimine coated iron (III) oxide nanoparticles from the supernatant using a magnetic field

Pictures were taken at three different times in order to compare the turbidity and see if it was necessary to allow the separation for the mass produced particles, prior to cleaning with MQ, to continue for a longer period of time. A comparison of the pictures are given in figure 6.10. No particular turbidity difference could be observed. Due to the equal turbidity, it was concluded that three hours prior to cleaning was enough in order for the process not to be too time consuming.

(a) After 3 hours

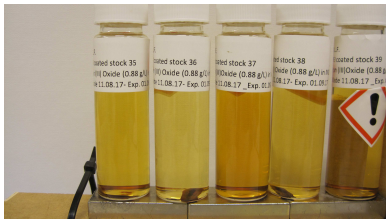

(b) After 6 hours

(c) After 24 hours

Figure 6.10: Separation of Fe_2O_3/PEI MNP from the supernatant using a magnetic field

Appendix E: BET isotherm

As depicted in figure 6.11, both the adsorption and the desorption follows the s-shape mentioned in section 2.10.3.2. A flat region is observed to the left, which may indicate the presence of a monolayer that is followed by multilayered adsorption in consistency with 2.10.3. It is concluded that this might be a Type V isotherm.

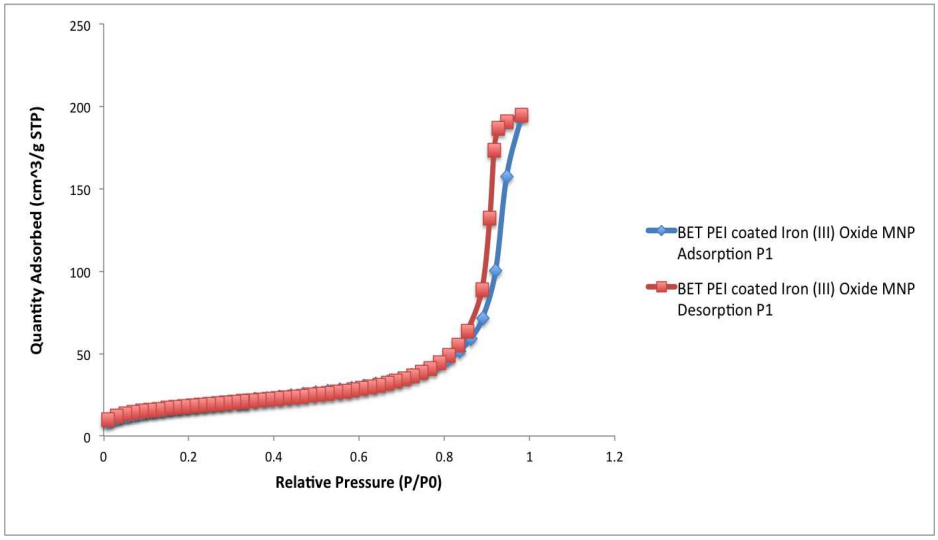

Figure 6.11: BET isotherm type 1 for parallel 1

Appendix F: Removal of the model naphthenic acid using polyethyleneimine coated iron (III) oxide nanoparticles

Concentrations and absorbance for the calibration curve for phenylacetic acid at pH 8

The concentrations used for the calibration curve at pH 8 with the corresponding max absorbances at 258.5 nm are given in table 6.7.

Table 6.7: Concentrations and maximum absorbance of PAA in water, pH 8

Sample	Stock of PAA (g)	MQ (g)	Conc. (g/L)	Abs. at 258.5 nm
1	3.52	0.51	0.87	0.11
2	3.01	1.01	0.86	0.25
3	2.00	2.01	0.49	0.53
4	1.00	3.013	0.25	1.02
5	0.51	3.53	0.13	1.53
6	0.21	3.83	0.01	1.79
Blank	0	1	0	0.00

Appendix Zeta potential for phenylacetic acid as function of pH

Since the adsorption of PAA was negligible at pH 8 it was decided to test the zeta potential as function of pH. A positive value is observed in the plot below pH 6 in figure 6.12.

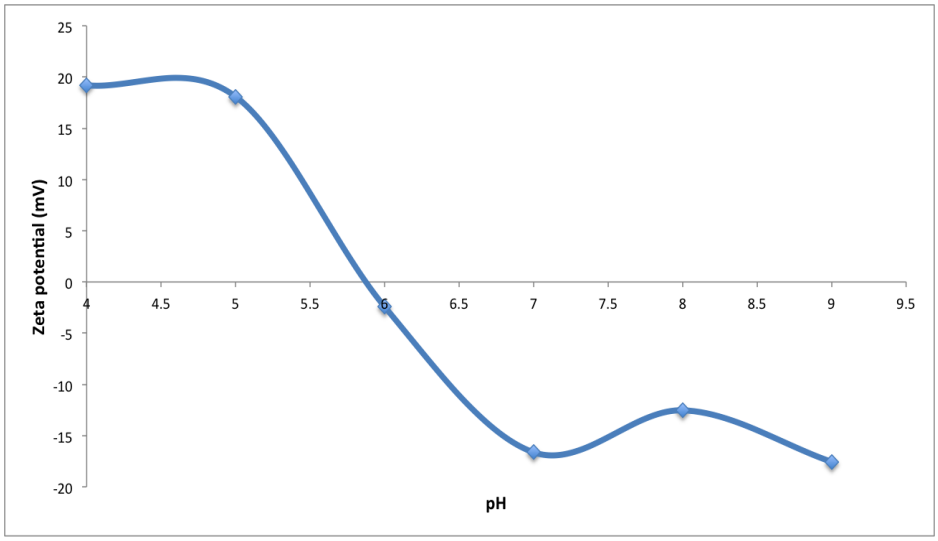

Figure 6.12: Zeta potential of PAA as function of pH

There is a large margin of error that may explain the postive zeta potential, however, the margin of error is small for pH 4. This may be caused by the presence of chemical impurities. Chemical impurities can influence adsorption as mentioned in section 2.12.2. The extent to which chemical impurities could have had affect on the adsorption of PAA, whether present in the adsorbate or the adsorbent, however, is beyond the scope of this thesis.

Table 6.8: 95% confidence intervals of the zeta potential as function of pH for PAA

pH	95% confidence interval
4	19.2 $\pm$0.8
5	18.1 $\pm$8.3
6	-2.4 $\pm$3.3
7	-16.6 $\pm$3.5
8	-12.5$\pm$1.3
9	-17.6$\pm$1.6

Concentrations and absorbance for the calibration curve for phenylacetic acid at pH 4.5

Table 6.9 shows the concentrations and the corresponding absorbances used for the calibration curve at pH 4.5 for PAA.

Table 6.9: Concentrations and maximum absorbance of PAA in water, pH 4.5

Sample	Stock of PAA (g)	MQ (g)	Conc. (g/L)	Abs. at 258.5 nm
1	3.82	0.21	0.14	0.20
2	3.01	1.02	0.11	0.16
3	2.02	2.02	0.08	0.11
4	1.00	3.01	0.04	0.06
Blank	0	1	0	0.00

Concentrations and absorbance for the calibration curve for 4-ethylbenzoic acid at pH 4.5

Table 6.10 shows the concentrations and the corresponding adsorbances used for the calibration curve at pH 4.5 for EBA. Since sample six had the highest concentration, it was loaded last. Sample five was an outlier and was removed in order to obtain a linear curve.

Table 6.10: Concentrations and maximum absorbance of EBA in water, pH 4.5

Sample	Mass stock of EBA (g)	Mass MQ (g)	Conc. (g/L)	Abs. at 237 nm
6	0.61	3.43	0.03	1. 84
1	0.53	3.52	0.02	1.61
2	0.43	3.65	0.02	1.32
3	0.34	3.71	0.02	1.06
4	0.22	3.81	0.01	0.07
Blank	0	1	0	0.02

Absorbance spectre for 4-ethylbenzoic acid

Since there seemed to be noise present for the undiluted supernatant, a plot of the spectre obtained was superimposed with the spectre for the undiluted stock of EBA. A similar noise was indicated as shown in figure 6.13. The diluted supernatant was also superimposed as well as the diluted stock. A peak is clearly indicated for both dilutions. It is concluded that the noise indicated the limit of the instrument.

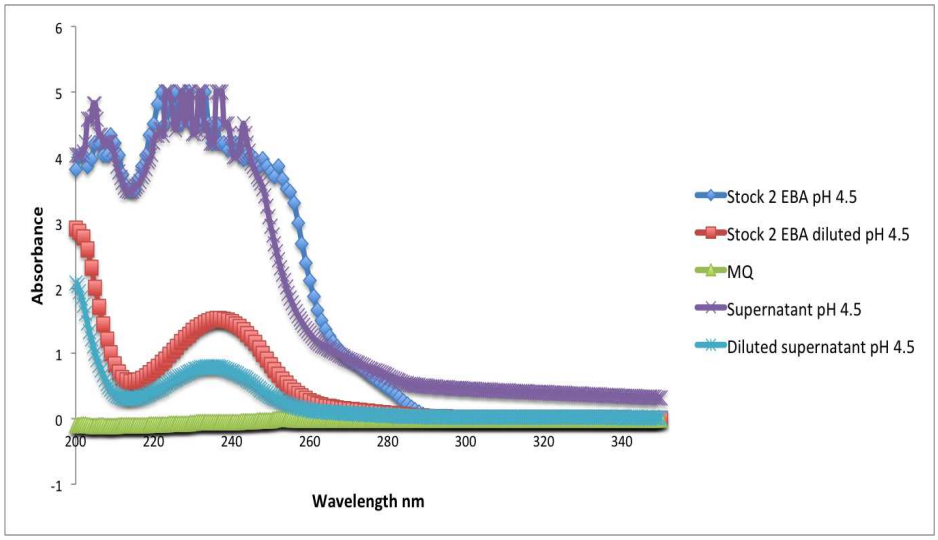

Figure 6.13: Comparison of the absorbances before and after test adsorption